This is to certify that the

dissertation entitled

The Synthesis, Characterization and Reactivity of Iron-Sulfur and Molybdenum-Iron-Sulfur Complexes with Phnoxide Terminal Ligands

presented by

Walter Edward Cleland, Jr.

has been accepted towards fulfillment
of the requirements for

Ph.D. degree in Chemistry

Carl H. Brubaker Jr.
Major professor

Date July 2, 1984

THE SYNTHESIS, CHARACTERIZATION AND REACTIVITY OF IRON-SULFUR AND MOLYBDENUM-IRON-SULFUR COMPLEXES WITH PHENOXIDE TERMINAL LIGANDS

By

Walter Edward Cleland, Jr.

A DISSERTATION

Submitted to
Michigan State University
in partial fulfillment of the requirements
for the degree of

DOCTOR OF PHILOSOPHY

Department of Chemistry

1984

ABSTRACT

THE SYNTHESIS, CHARACTERIZATION AND REACTIVITY OF IRON-SULFUR AND MOLYBDENUM-IRON-SULFUR COMPLEXES WITH PHENOXIDE TERMINAL LIGANDS

By

Walter Edward Cleland, Jr.

The phenoxide-ligated tetranuclear iron-sulfur clusters $[Fe_4S_4(OAr)_4]^{2-}$ (Ar=Ph, p-Tol) have been synthesized by reaction of $[Fe_4S_4Cl_4]^{2-}$ or $[Fe_4S_4(SR)_4]^{2-}$ with NaOAr or HOAr, respectively. The X-ray crystal structure of $(Et_4N)_2[Fe_4S_4(OPh)_4]$ has been determined and shows a short Fe-O distance (mean 1.865(17)Å). Optical spectral features of these complexes are blue shifted compared to corresponding bands in the arenethiolate complexes, while the magnetic properties remain essentially unchanged. Isotropically shifted phenyl proton resonances are observed in the ^1H NMR spectra. These shifts are approximately twice as large as corresponding shifts observed for the arenethiolate analogs. The ^{57}Fe Mossbauer spectrum has been obtained and consists of a single quadrupole doublet. Electrochemical data show that substitution of thiophenoxide by phenoxide results in negative shifts for the first and second reduction potentials of the $[Fe_4S_4]^{2+}$

core. The phenoxide complexes react with electrophiles such as acyl halides and thiophenol to yield the halide and thiophenoxide substituted iron-sulfur tetramers, respectively.

The binuclear iron-sulfur clusters $[Fe_2S_2(OAr)_4]^{2-}$ (Ar= Ph, p-Tol, p-C_6H_4Cl) have been prepared by direct synthesis and by reaction of $[Fe_2S_2Cl_4]^{2-}$ with NaOAr. The crystal structure of $(Bu_4N)_2[Fe_2S_2(OPh)_4]$ has been determined. The results of a variety of other physical measurements including optical, ^1H NMR and ^{57}Fe Mossbauer spectroscopy, electrochemistry and magnetic susceptibility are reported. Ligand exchange reactions with electrophiles are also discussed.

The phenoxide-ligated "double cubane" complex $[Mo_2Fe_6S_8(SEt)_3(OPh)_6]^{3-}$ has been synthesized by reaction of $[Mo_2Fe_6S_8(SEt)_9]^{3-}$ with PhOH. Electronic and ^1H NMR spectroscopy, electrochemistry and magnetic susceptibility data are reported. Ligand exchange reactions with electrophiles are discussed.

General effects of phenoxide ligation to iron and the biological implications for tyrosyl coordination to iron-sulfur and molybdenum-iron-sulfur centers are discussed.

To My Family:

Alice, Walter and Rebecca

ACKNOWLEDGMENTS

I would like to express my sincere appreciation to Professor Bruce A. Averill for his advice and guidance throughout the course of this work. His insights concerning synthetic inorganic chemistry and the interpretation of physical data have been invaluable.

I would like to thank the following individuals for their contributions to this work: Dr. E. Munck and Dr. T. A. Kent for obtaining the ^{57}Fe Mossbauer spectra; Professor G. C. DeFotis and D. A. Holtman for assistance in obtaining variable temperature magnetic susceptibility data on $(Et_4N)_2[Fe_4S_4(OPh)_4]$; Professor James A. Ibers, Dr. M. Sabat and Professor E. Sinn for the crystal structures of $(Et_4N)_2[Fe_4S_4(OPh)_4]$ and $(Bu_4N_2[Fe_2S_2(OPh)_4]$.

I would like to thank Craig Silvis, Paul Lamberty, Jim Davis, Mark Antonio, Susan Kauzlarich and my other coworkers for their friendship and advice on various matters throughout my graduate career.

I would like to acknowledge the Department of Chemistry for providing a teaching assistantship, and special thanks to Professors Brubaker, Eick, Chang and Allison for serving on my Committee. I would also like to acknowledge the University of Virginia for support during my last year.

Special thanks to Mrs. P. Warstler for her expert typing of this dissertation and to J. Kotarski, B. Draper, and L. Ruiz for their work on the graphics.

TABLE OF CONTENTS

LIST OF TABLES

LIST OF FIGURES

LIST OF ABBREVIATIONS

Solvents:

MeCN	= acetonitrile
EtCN	= propionitrile
MeOH	= methanol
i-PrOH	= isopropanol
Et_2O	= diethyl ether
THF	= tetrahydrofuran
DMF	= N,N,-dimethylformamide
DMA	= N,N,-dimethylacetamide
DMSO	= dimethylsulfoxide
NMP	= N-methylpyrrolidinone

Reagents:

PhCOCl	= benzoyl chloride
PhOH	= phenol
PhSH	= thiophenol
p-TolOH	= para-cresol
p-ClC_6H_4OH	= para-chlorophenol

Miscellaneous:

Et_4N^+	= tetraethylammonium
Me_4N^+	= tetramethylammonium

Bu_4N^+	= tetra-n-butylammonium
p-Tol	= para-tolyl
p-C_6H_4Cl	= para-chlorophenyl
Ph	= phenyl
Et	= ethyl
Me	= methyl
BM	= Bohr magneton
SCE	= saturated calomel electrode
MCD	= magnetic circular dichroism
EPR	= electron paramagnetic resonance
ATP	= adenosine triphosphate
TMS	= tetramethylsilane
S_2-o-xylyl	= ortho-xylyldithiolate

INTRODUCTION

Metalloproteins and metalloenzymes are biomolecules that contain metal ions in integral stoichiometries. These metal ions are often the site of electron transfer or catalysis and are therefore termed 'active sites'[1]. These biomolecules are essentially elaborate coordination complexes, which often possess unusual structural and physical properties. For this reason, metallobiomolecules have received increased attention by inorganic and physical chemists, which has led to the emergence of the interdisciplinary field of bioinorganic chemistry.

One aspect of this field involves the "synthesis of relatively low molecular weight complexes, which, ideally, are obtainable in the crystalline form and approach or duplicate the biological unit in terms of composition, ligand types, structure and oxidation levels"[2]. Here the thesis is that synthetic metal complexes, termed 'synthetic analogues', can approximate or 'model' the properties of the related biomolecule and thus yield useful information concerning its biological structure and function.

Possibly the most significant success of this approach has occurred in the area of the non-heme iron-sulfur proteins[3-5], which contain as their active site iron and

acid labile sulfur in Fe_nS_m units where n = 1, m = 0 or n = m = 2, 3, or 4 as shown in Figure 1. In addition, evidence for an Fe_3S_4 center in inactive aconitase has recently been reported[3b]. Synthetic analogues of the one, two and four iron sites have now been prepared and structurally and physically characterized[4]. These complexes usually contain alkyl or aryl thiolate terminal ligands in place of cysteinyl residues in the protein and have proven to be credible structural and electronic models of the protein active sites.

The metalloenzyme nitrogenase, which performs the difficult and useful function of reducing dinitrogen to ammonia for use in biosynthesis, was first isolated in 1960[6] but remained relatively obscure to chemists until the mid-1970's. Nitrogenase is found only in prokaryotic microorganisms. These microorganisms can either form symbiotic associations with higher plant life or live independently; varieties are known that grow either aerobically or anaerobically. Studies of the enzyme show that it possesses several properties that have stimulated a now keen interest by inorganic chemists. For example, nitrogenase fixes dinitrogen under extremely mild conditions (ambient temperature and pressure) compared to the industrial process (450°C and 200-300 atm). Therefore, a long-range goal of research in this area is the development of a catalytic system for dinitrogen reduction based on the metal centers of

Figure 1. Schematic of four types of Fe-S centers that occur in non-heme iron sulfur proteins.

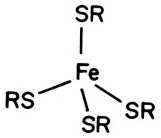

[Fe-4S]

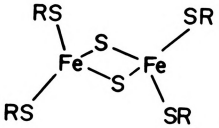

[2Fe-2S]

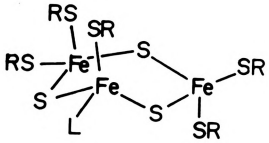

[3Fe-3S]

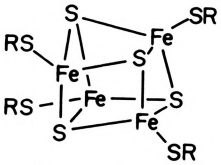

[4Fe-4S]

Figure 1

nitrogenase. In addition, the presence of novel metal-sulfur clusters[7] with peculiar physical properties offers a particularly challenging problem to the inorganic chemist.

Nitrogenase consists of two oxygen-sensitive proteins: the iron protein (Fe protein), containing iron and acid labile sulfur; and the molybdenum-iron protein (MoFe protein), containing molybdenum, iron and acid labile sulfur. Both proteins are essential for activity in the presence of an external reductant and MgATP. The exact mechanism of dinitrogen reduction remains as yet unknown, but available evidence[8,9] suggests the pathway of electron flow shown schematically in Figure 2. Electron transfer is from external reductant (not shown), usually reduced ferredoxin or dithionite, to a $(MgATP)_2$ complex of the Fe protein, to the MoFe protein to substrate. Thus, it is the MoFe protein which actually reduces the substrate.

The iron protein has a molecular weight of $\sim$60,000 and contains four iron atoms and four sulfides per molecule. Cluster displacement and transfer techniques together with EPR results have shown that the iron and sulfide comprise a single 4Fe-4S cluster[10,17]. Evidence that the Fe protein binds two moles of MgATP[11] and that hydrolysis of ATP is only observed during transfer of electrons to the MoFe protein[12] seems to indicate that the function of the protein is to act as a transducer, coupling the energy released by ATP hydrolysis to electron transfer.

Figure 2. Hypothetical view of electron transfer through the nitrogenase system. Electron transfer within the enzyme is from the 4Fe-4S cluster of the Fe protein $(MgATP)_2$ complex to the P-clusters to FeMo-co to substrate.

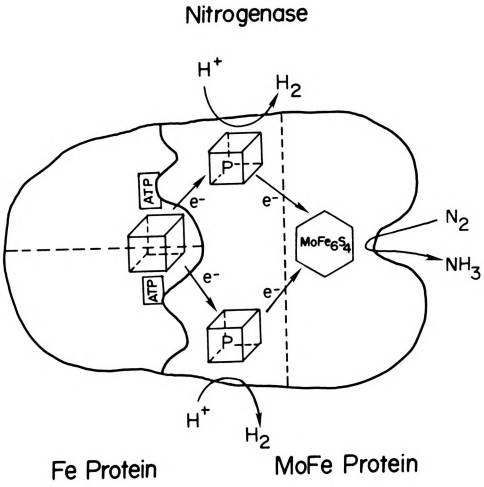
Nitrogenase
H+
H2
P
ATP
e-
e-
MoFe6S8
N2
NH3
H
ATP
e-
e-
P
H+
H2
Fe Protein
MoFe Protein

Figure 2

The MoFe protein has a molecular weight of ~220,000 and contains two Mo atoms, 32 ± 2 Fe atoms and 32 ± 2 [=] per molecule. It contains two types of metal-sulfur clusters[7,13-16]: a soluble, low molecular weight iron-molybdenum cofactor (FeMo-co) of unknown structure, and a variant of the normal 4Fe-4S clusters termed the P-clusters.

Approximately half of the iron and acid-labile sulfur present in the MoFe protein constitute four 4Fe-4S clusters that can be removed from the protein in addition to FeMo-co. This has been shown in three ways: by cluster displacement experiments using fluorinated thiols and ^{19}F NMR spectroscopy for identification of Fe-S clusters[17,18]; by cluster transfer techniques using low molecular weight apoferrodoxins to accept displaced Fe-S clusters followed by reduction and EPR quantitation[19]; and by quantitation of the EPR spectra of the MoFe protein in partially denaturing solvents[20].

The ^{57}Fe Mossbauer spectra of the MoFe protein as isolated can be separated into a magnetic portion due to FeMo-co centers and a diamagnetic portion. The diamagnetic portion consists of two quadrupole doublets in a 3:1 ratio[14,21,22]. Parameters of the less intense doublet (ΔEq = 3.02 mm/s, δ = 0.69 mm/s) are typical of high spin Fe^{2+} in a tetrahedral sulfur environment, and the species responsible has thus been called component Fe^{2+}. The more intense doublet has δ= 0.64 mm/s, which is in the range for Fe^{2+},

but has an unusually small quadrupole splitting, $\Delta Eq = 0.81$ mm/s; this iron has been termed component D. These two components behave as if they were diamagnetic in strong magnetic fields. It has been suggested that the only way to explain the apparent diamagnetism of the iron atoms of components Fe^{2+} and D is that they exist in spin coupled units, termed the P-clusters[14]. Further evidence[13,14,-23-26], including combined EPR, Mossbauer and MCD measurements on dye-oxidized MoFe protein has led to the conclusion that the P-clusters are a variant of the normal 4Fe-4S cluster in the all ferrous $(Fe_4S_4)^0$ oxidation state.

Several suggestions have been made as to the means by which the protein could differentiate three of the iron atoms from the fourth in a 4Fe-4S core. The first, and most obvious, is to exchange an oxygen or nitrogen donor terminal ligand for the cysteinyl mercaptide common to 'normal' clusters. Since ferrous iron has a low affinity for saturated amine ligands[27], tyrosyl phenolate or glutamate or asparate carboxylate seem to be the most reasonable choices. Schematic representations of these models are depicted in Figure 3. The other possibilities include the addition of a fifth ligand to three of the iron atoms or protein imposed distortions of the 4Fe-4S cubane core from its normal geometry. At present, no evidence is available to determine which if any of these possibilities is correct.

Figure 3. Possible models for the P cluster involving oxygen ligation at three vertices of a 4Fe-4S core.

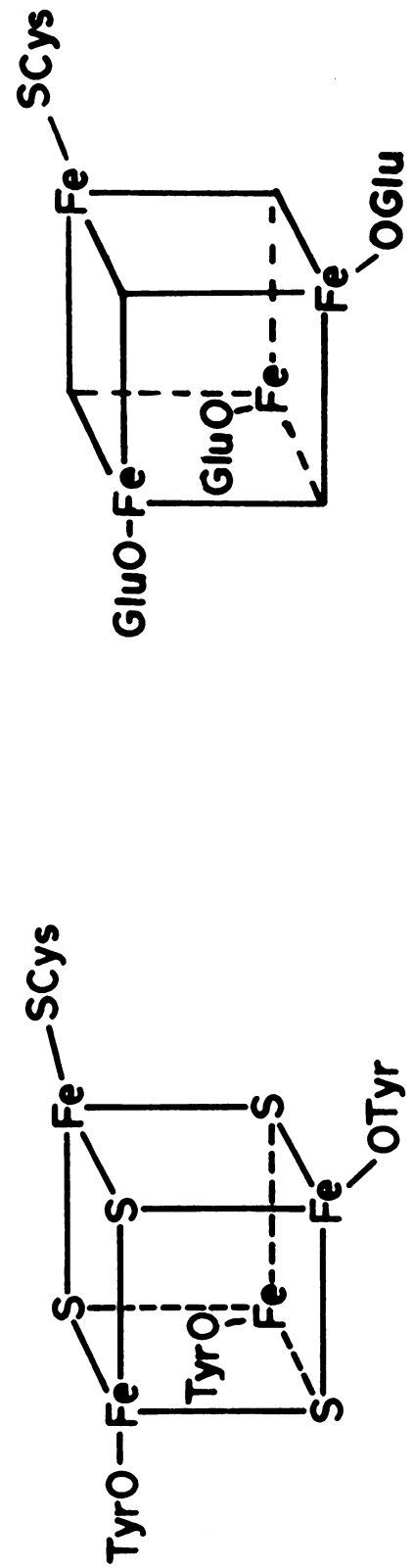
SCys
Fe
OGlu
Fe
GluO-Fe
GluO
Fe
SCys
Fe
S
OTyr
S
Fe
S
Fe
TyrO
TyrO—Fe
Fe
S

Figure 3

Because of the limited data available on the P-clusters, efforts to apply the synthetic analogue approach have been few. To date, no synthetic clusters with oxygen or nitrogen terminal ligands have been isolated. Johnson and Holm[28], however, have generated in solution the $[Fe_4S_4(OAc)_4]^{2-}$ ion and reported briefly on some of its properties. Recently, the complexes $[Fe_4S_4(SC_6H_4\text{-}\underline{o}\text{-}OH)_4]^{2-}$ [30] and $[Fe_4S_4(SPh)_2(S_2CNEt_2)_2]^{2-}$ [29], which contain one and two five-coordinate iron sites, respectively, have been prepared.

The other half of the iron and sulfide and all of the molybdenum present in the MoFe protein comprise two identical iron-molybdenum cofactor units. This cofactor[31-34] can be removed from the protein and exhibits spectroscopic properties very similar to those of the MoFe protein from which it came. Analytical data[32b] show the presence of six to seven iron atoms and approximately 8 or 9 sulfides per molybdenum. The low temperature (6 - 20 K) EPR spectrum[22,35] shows an axial signal with g-values 2.0, 3.8, and 4.3, which has been attributed to one of the two Kramer's doublets of a S = 3/2 spin system. Isolated FeMo-co exhibits a complex magnetic ^{57}Fe Mossbauer spectrum nearly identical to the magnetic portion of the Mossbauer spectrum of the MoFe protein. Detailed analysis[20,36] of this spectrum indicates the presence of spin coupled S = 3/2 units containing $\sim$6 iron atoms each. In addition, ^{57}Fe

ENDOR experiments[37a] on ^{57}Fe enriched MoFe protein indicate the presence of no fewer than six nonequivalent iron sites within the S = 3/2 centers. ^{95}Mo ENDOR experiments on ^{95}Mo enriched MoFe-protein suggest that the molybdenum is a diamagnetic even-electron ion with even formal valency. Molybdenum and iron K-edge extended X-ray absorption fine structure spectroscopy (EXAFS) have provided the only structural information available to date on FeMo-co. Molybdenum K-edge results indicate 4 S atoms at ∿2.35 Å, 2-3 Fe atoms at 2.72 Å and 1-2 additional S atoms at ∿2.47 Å as nearest neighbors to Mo[38-42]. Iron K-edge results indicate an average of 1.3±1.0 O (or N) atoms at 1.8 Å, 3.4±1.6 S atoms at 2.25 Å, 2.3±0.9 Fe atoms at 2.66 Å and 0.41±0.1 Mo at 2.76 Å from Fe[44]. Combined EPR, ^{57}Fe Mossbauer and EXAFS results clearly indicate a novel cluster type of structure for FeMo-co. Several speculative structural models have been proposed for FeMo-co based on the data outlined above. These models are shown in Figure 4. It should be emphasized that these are speculative models, and no synthetic compounds with these specific structures have been prepared.

Because it is believed that FeMo-co is the site of dinitrogen binding and reduction[7,16,45-48] and because of the relative lack of known complexes containing Mo, Fe, and $S^{=}$, most synthetic work to date has been directed toward the preparation of new Mo-Fe-S clusters as models for

Figure 4. Schematic of structural models proposed for the FeMo-cofactor.

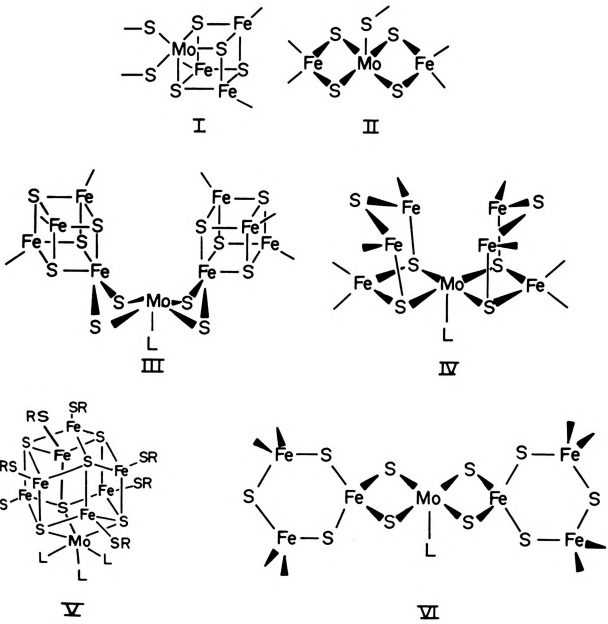

Figure 4

FeMo-co. Since 1978, two classes of Mo-Fe-S cluster have been prepared and characterized. The first consists of complexes containing the $MoFe_3S_4$ "cubane" core[40,49-70], including $[Mo_2Fe_6S_8(SEt)_9]^{3-}$, $[Mo_2Fe_7S_8(SEt)_{12}]^{4-}$ and $[MoFe_3S_4(R_{3,6}\text{-cat})]^{3-}$; see Figure 5. These complexes are prepared from simple starting materials in "self assembly" reactions similar to the approach used for synthesis of the ferredoxin analogues. Although the stoichiometry, spectroscopic properties and EXAFS results confirm that these complexes are not synthetic FeMo-co analogues, they represent, at present, the closest approach to such an entity.

The second class of Mo-Fe-S clusters consists of a series of compounds based on the MoS_2Fe unit. These clusters have an extended "linear" array of metal atoms compared to the cubane class. Examples of "linear" clusters[71-83] include: $[MoFeS_4X_2]^{2-}$ (X = SAr, OAr, Cl), $[MoFe_2S_6X_2]^{3-}$ (X = SAr; $X_2 = S_5$), $[Fe(MoS_4)_2]^{3-}$ and $[MoFe_2S_4Cl_4]^{2-}$ (shown in Figure 6). These clusters also do not represent synthetic FeMo-co analogues due to inappropriate stoichiometry and Mo oxidation state and to discrepancies in Mo-S distances obtained from EXAFS analysis.

A variety of factors, then, have stimulated interest in oxygen ligation of metal sulfur clusters. These include the incorporation of oxygen ligands into the proposed structure of the P-clusters as shown in Figure 3 and recent reports[44,84-86], including Fe edge EXAFS data, which suggest

Figure 5. Schematic of the structurally characterized clusters possessing the $MoFe_3S_4$ cubane core including the "double cubane" and the "single-cubane" complexes.

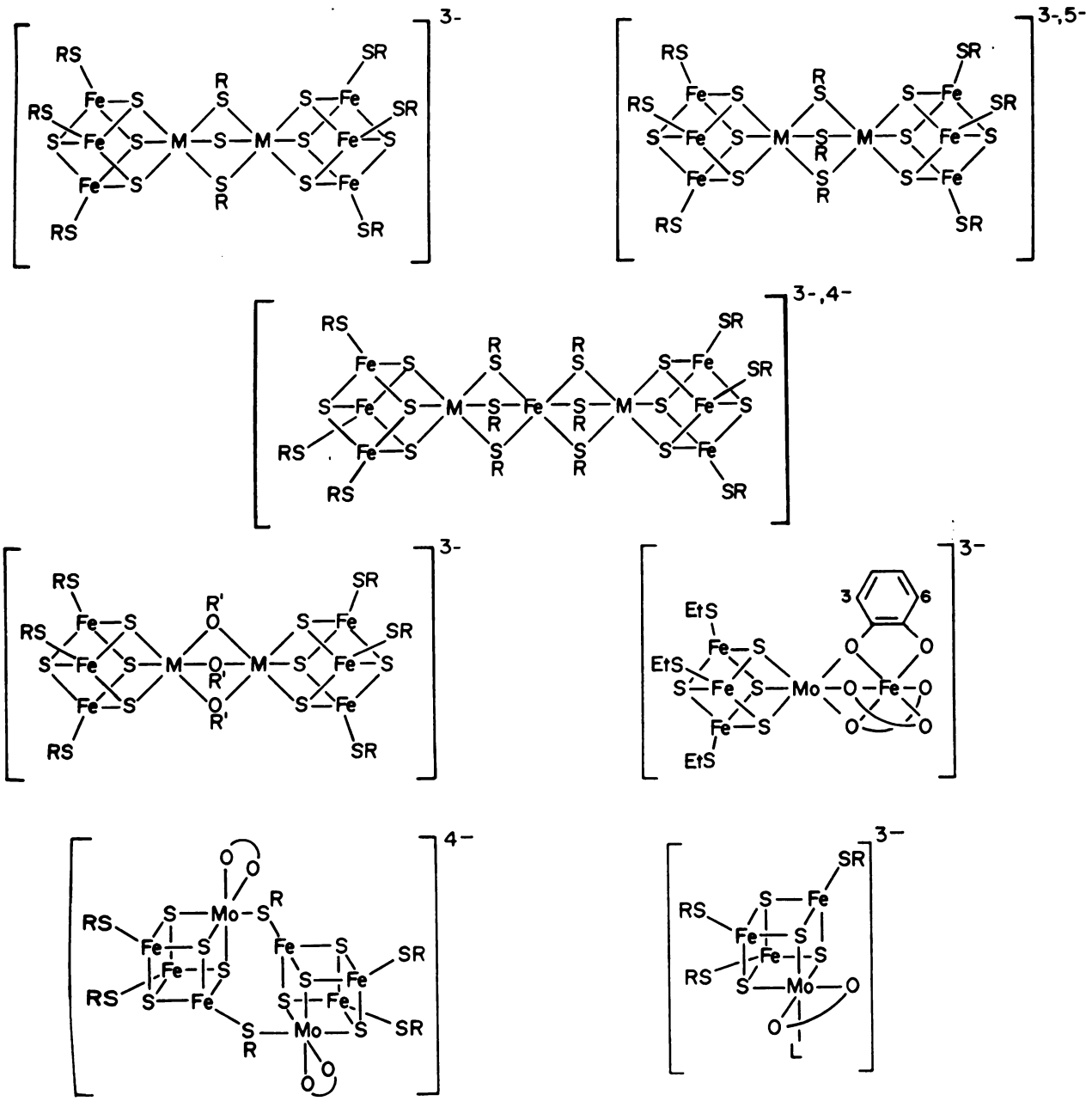

Figure 5

Figure 6. Schematic of the structurally characterized "linear" MoS_2Fe clusters.

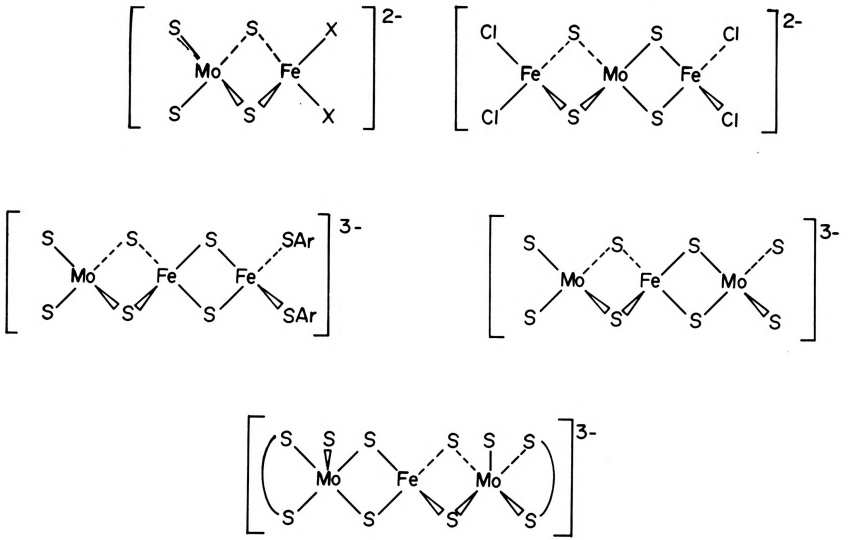
S
S
X
Mo
Fe
S
S
X
2-
Cl
S
S
Cl
Fe
Mo
Fe
Cl
S
S
Cl
2-
S
S
S
SAr
Mo
Fe
Fe
S
S
S
SAr
3-
S
S
S
S
Mo
Fe
Mo
S
S
S
S
3-
S
S
S
S
S
S
Mo
Fe
Mo
S
S
S
S
3-

Figure 6

that oxygen ligands are bound to the iron atoms within the FeMo-cofactor. In addition, preliminary X-ray diffraction studies of the recently discovered 3 Fe ferredoxins[87,88] indicate that one of the ligands is an oxygen donor ligand (ligand L in Figure 1). It should be noted that with two exceptions, none of the synthetic analogues of the iron sulfur sites nor any member of either class of Mo-Fe-S clusters has been isolated with oxygen ligands to iron. Those exceptions are brief reports on the isolation of the $[Fe(OAr)_4]^-$ ion[89] and the $[MoFeS_4(OAr)_2]^{2-}$ ion[81], which appeared subsequent to the beginning of the research described herein. Thus, an investigation of oxygen ligation of metal sulfur clusters was in order. Phenolate was the oxygen ligand of choice as it is a ligand available to nature in the tyrosine moiety. Further, since the thiophenolate analogs of many of the metal sulfur clusters are known, the use of phenolate would facilitate a more direct comparison of the change in physical properties upon exchange of an oxygen atom for a sulfur atom.

This dissertation describes the synthesis, characterization and reactivity of several oxygen ligated Fe-S and Mo-Fe-S clusters, including the first such cluster to be isolated[90], $[Fe_4S_4(OAr)_4]^{2-}$ (Ar = Ph, p-Tol). Also included are $[Fe_2S_2(OAr)_4]^{2-}$ (Ar = Ph, p-Tol, p-C_6H_4Cl), $[Mo_2Fe_6S_8(SEt)_3(OPh)_6]^{3-}$ and a compound of as yet unknown structure containing iron, sulfide and phenolate.

II. EXPERIMENTAL

A. Materials and Methods

All operations were carried out under an atmosphere of pure, dry dinitrogen unless otherwise specified. Dinitrogen was purified by passage over hot BASF R-3-11 catalyst and supported phosphorous pentoxide (Aquasorb). Solvents and reagents were either distilled under an inert atmosphere or thoroughly degassed by repeated evacuation and flushing with pure dinitrogen prior to use.

Acetonitrile was purified by the following three step procedure. Reagent grade acetonitrile was refluxed for several hours and distilled from calcium hydride. The distillate was stirred for 12 h with 5 g/L each of anhydrous sodium carbonate and potassium permanganate, followed by distillation at room temperature using a dry ice/icopropanol cold trap. Final distillation from phosphorous pentoxide produced acetonitrile of acceptable purity for synthesis as well as for electrochemistry and other physical measurements. Propionitrile was purified by a similar procedure using 2 g/L potassium permanganate rather than 5 g/L. Tetrahydrofuran and diethylether were purified by distillation from sodium/benzophenone ketyl or lithium

aluminum hydride. Methanol and isopropanol were distilled from magnesium methoxide and aluminum isopropoxide, respectively. N-methylpyrrolidinone was distilled from calcium hydride and then from barium oxide. Spectroscopic grade DMA and DMF were stored over 4 Å molecular sieves. Benzoyl chloride was distilled from barium oxide at room temperature using a liquid nitrogen trap. PhOH, p-TolOH, and p-ClC_6H_4OH were either sublimed twice or sublimed followed by vacuum distillation. Anhydrous sodium phenolates were prepared in one of two ways: by reaction of the approrpiate phenol with sodium methoxide in anhydrous MeOH, followed by removal of the solvent in vacuo, addition of MeCN and repeated evaporation to dryness; or by reaction with metallic sodium in THF, followed by filtration and evaporation to dryness. Thiols, lithium sulfide and all other reagents were of commercial reagent grade and used without further purification.

Tetra-n-butylammonium chloride was prepared from a 10% aqueous solution of the hydroxide by neutralization with 6N hydrochloric acid followed by removal of water in vacuo. Addition of MeCN to the oily mass and repeated evaporation to dryness resulted in a waxy material which was stored under an inert atmosphere. Tetraethylammonium phenoxide was prepared by the metathesis of sodium phenolate with tetraethylammonium chloride in MeCN. Filtration of the reaction mixture to remove NaCl followed by volume reduction

and cooling to -20°C caused separation of white crystals, which were collected by filtration, washed with diethyl ether and dried in vacuo. Tetra-n-butylammonium perchlorate and tetraethylammonium perchlorate were prepared by addition of a slight excess of perchloric acid to an aqueous solution of the corresponding tetraalkylammonium halide. The crude product was collected by filtration, washed with water, recrystallized twice from hot i-PrOH and dried in vacuo.

$(Et_4N)_2[Fe_4S_4(SPh)_4]$ and $(Me_4N)_2[Fe_4S_4(S\text{-}t\text{-}Bu)_4]$ were prepared by published procedures[91,92]. $(Et_4N)_2[Fe_4S_4Cl_4]$ and $(Me_4N)_2[Fe_4S_4Cl_4]$ were prepared from $(Et_4N)_2[Fe_4S_4(SPh)_4]$ and $(Me_4N)_2[Fe_4S_4(S\text{-}t\text{-}Bu)_4]$, respectively, by reaction with PhCOCl as described[93]. Several new salts of previously reported iron-sulfur tetramer dianions were prepared.

$(Et_4N)_2[Fe_4S_4(SEt)_4]$ - This compound was prepared by a modification in the stoichiometry of the procedure reported by Christou and Garner for the preparation of $[Fe_4S_4(SR)_4]^{2-}$ clusters[92]. Five, rather than four, equivalents of sodium alkyl thiolate were used in the preparation of the reaction mixture, which was stirred for 18 h. After filtration, the reaction mixture was treated with three equivalents of Et_4NCl dissolved in a minimum of MeOH. The crude product was precipitated by removal of ~70% of the solvent in vacuo, followed by addition of three volumes

of water. The crude crystalline product was collected by filtration and dried in a stream of dinitrogen, washed with THF and vacuum dried. Recrystallization was accomplished by dissolution of the crude product in a minimum of a 9:1 (v:v) mixture of THF/MeCN, filtration and slow cooling to -20°C. Typical yields of recrystallized product were 40-50%. UV-Vis and ^{1}H NMR spectroscopic properties due to the dianion were essentially the same as those reported for other salts of this dianion[94,95]. This compound is extremely soluble in a variety of polar organic solvents, making it an attractive candidate for experiments requiring high tetramer concentrations.

$(Bu_4N)_2[Fe_4S_4(SEt)_4]$ - This compound was prepared using the same stoichiometric modification described above. The filtered reaction mixture was treated with three equivalents of Bu_4NBr in MeOH, which caused immediate separation of the crude microcrystalline product. The material was collected by filtration, washed with MeOH and vacuum dried. The crude product was then dissolved in hot (∿60°C) DMF, filtered and cooled slowly to -20°C, which caused separation of well formed crystals. The yield was 43%. UV-Vis and ^{1}H NMR spectroscopic properties were consistent with its formulation[94,95].

$(Bu_4N)_2[Fe_4S_4(S\text{-}\underline{i}\text{-}Pr)_4]$ - This compound was prepared by the same modification of a literature procedure described above. Three equivalents of Bu_4NBr in MeOH was

added to the filtered reaction mixture followed by addition of one volume of water which caused separation of the product as microcrystals. The crystals were collected by filtration, washed with i-PrOH and dried in vacuo. The crude product was recrystallized by dissolution in hot (∿60°C) DMA, filtration, and slow cooling to -20°C. The yield was 40%. UV-Vis and ^{1}H NMR spectroscpic properties were the same as those previously reported for salts of this dianion[94,95].

$(Et_4N)_2[Fe_4S_4(S\text{-}t\text{-}Bu)_4]$ - This compound was prepared by the same stoichiometric modification of a literature procedure described above. Addition of three equivalents of Et_4NCl dissolved in water to the filtered reaction mixture caused separation of the product as an amorphous solid which was collected by filtration, washed with i-PrOH and dried in vacuo. The crude product was crystallized by dissolution in a hot (∿60°C) mixture of 3:1 (v:v), MeCN:DMA, filtration and slow cooling to -20°C. The yield was 70%. UV-Vis and ^{1}H NMR spectroscopic properties were the same as those previously reported for this tetrameric dianion[94,95].

$(Et_4N)_2[Fe_2S_2(SPh)_4]$[96,97] and $(Et_4N)_2[Fe_2S_2Cl_4]$[92] were prepared as described. $(Et_4N)FeCl_4$[98] was prepared as described and recrystallized from MeCN/i-PrOH. Ammonium[99] and benzyltriethylammonium[49] salts of tetrathiomolybdate and $(Et_3NCH_2Ph)_3[Mo_2Fe_6S_8(SEt)_9]$[49] were prepared by published procedures.

B. Preparation of $(R_4N)_2[Fe_4S_4(OAr)_4]$ (Ar = Ph, p-Tol) Salts.

These complexes were prepared by either of two methods. Typical examples of each are described in detail below.

Method 1, from $(R_4N)_2[Fe_4S_4(SR')_4]$ (R' = Et, t-Bu). To 5.5 g (6.5 mmol) of $(Et_4N)_2[Fe_4S_4(SEt)_4]$ dissolved in 100 mL of MeCN was added a solution of 26 g (260 mmol) of PhOH in 75 mL of MeCN. The reaction mixture was evaporated in vacuo at 30°C to $\leq$ 50 mL volume, diluted with 100 mL MeCN, and again evaporated to a final volume of $\leq$ 50 mL. The color of the solution at this point was an orange-brown, rather than the green-brown of the starting material. Addition of 300 mL of i-PrOH to the filtered solution resulted in separation of the product as dark orange-brown microcrystals, which were collected by filtration, washed twice with i-PrOH, and vacuum dried. Recrystallization was accomplished by dissolution of the crude product in a minimum volume of MeCN at room temperature, filtration, addition of $\sim$3 volumes of i-PrOH, and slow cooling to -20°C. Typical yields are $\sim$80% of analytically pure product after one recrystallization. Concentration of the mother liquors and slow cooling to -20°C affords a second crop ($\sim$10%).

Method 2, from $(R_4N)_2[Fe_4S_4Cl_4]$. A mixture of 1.46 g (2.52 mmol) of $(Et_4N)_2[Fe_4S_4Cl_4]$ and 1.23 g (10.6 mmol) of

anhydrous NaOPh was taken up in 80 mL MeCN. An immediate color change from brown to orange-brown was observed, accompanied by formation of a white precipitate. The reaction mixture was stirred for 2 h, and the precipitate was removed by filtration and washed with a small portion of MeCN. The combined filtrate and wash were concentrated in vacuo until a dark crystalline precipitate began to form. Addition of several volumes of THF and cooling to -20°C caused complete precipitation of the microcrystalline product, which was collected by filtration, washed with THF or i-PrOH, and recrystallized as in Method 1 to give analytically pure product in 85% yield. The product was found to be identical in all respects with that obtained by Method 1.

1. $(Et_4N)_2[Fe_4S_4(OPh)_4]$.

This compound was prepared as described above by Method 1 or 2. Analytical data were obtained on a sample prepared by Method 1. Anal. Calc'd for $C_{40}H_{60}N_2O_4S_4Fe_4$: C, 48.80; H, 6.14; Fe, 22.69; N, 2.84; O, 6.50; S, 13.03. Found: C, 48.49; H, 6.26; Fe, 22.08; O, 6.93; S, 13.14; m.p. 177°C (d).

2. $(Bu_4N)_2[Fe_4S_4(O\text{-}p\text{-}Tol)_4]$.

This compound was prepared by Method 1. Anal. Calc'd for $C_{60}H_{90}N_2O_4S_4Fe_4$: C, 56.96; H, 7.97; Fe, 17.66; N, 2.21;

S, 10.14. Found: C, 56.28; H, 7.79, Fe, 16.97; N, 1.92; S, 10.04; m.p. 132°C (d).

C. Preparation of $(R_4N)_2[Fe_2S_2(OAr)_4]$ (Ar = Ph, p-Tol, $p\text{-}C_6H_4Cl$) Salts.

These complexes were prepared by either of two methods. Typical examples of each are described in detail below.

Method 1. Direct Synthesis. To 1.3 g (8.1 mmol) $FeCl_3$ dissolved in 50 mL MeCN was added a solution of 2.2 g (8.1 mmol) of Bu_4NCl dissolved in 25 mL MeCN. The solution changed color at this point from orange-brown to light yellow. This solution was then added to a slurry of 3.75 g (32.3 mmol) of NaOPh in 50 mL of MeCN. The color of the supernatant solution changed immediately from light yellow to bright red. The reaction mixture was stirred for 30 min and the precipitate was removed by filtration. The filtrate was treated with 0.37 g (8.1 mmol) of Li_2S, and the mixture was stirred for 18 h, during which time a slow color change to a much more intense red occurred. The reaction mixture was then filtered and evaporated in vacuo to a volume of <20 mL. Addition of 80 mL Et_2O and cooling to -20°C for 8 h caused separation of the product as dark red microcrystals, which were collected by filtration, washed with Et_2O and vacuum dried. Recrystallization was accomplished by addition of 50 mL Et_2O to the crude product followed by addition with stirring of several

1 mL aliquots of MeCN until all of the material was dissolved. Filtration and slow cooling to -20°C caused separation of large dark red prisms. Volume reduction of the mother liquors, addition of ∿1 volume of Et_2O, and slow cooling to -20°C afforded a second crop (∿10%). Typical yields are 40-50% of analytically pure product after one recrystallization.

Method 2. From $(R_4N)_2[Fe_2S_2Cl_4]$. A solution containing 1 g (1.73 mmol) of $(Et_4N)_2[Fe_2S_2Cl_4]$ dissolved in 40 mL MeCN was added with stirring to a slurry of 0.84 g (7.26 mmol) of anhydrous NaOPh in 10 mL MeCN. An immediate color change from purple to deep red occurred. The reaction mixture was stirred for 0.5 h and filtered, and the filtrate was concentrated to half its volume. Slow addition of one volume of Et_2O to initiate crystallization, followed by cooling to -20°C for 18 h, caused complete separation of the microcrystalline product, which was collected by filtration, washed twice with Et_2O and vacuum dried. The crude product was recrystallized by dissolution in 25 mL MeCN, slow addition of 20 mL Et_2O, and slow cooling to -20°C. Concentration of the mother liquors and slow cooling to -20°C afforded a second crop. Total yield was 61%.

1. $(Bu_4N)_2[Fe_2S_2(OPh)_4]$.

This compound was prepared as described above by method 1. Anal. Calc'd for $C_{56}H_{92}N_2O_4S_2Fe_2$: C, 65.09; H, 8.98; N, 2.71; S, 6.22; Fe, 10.81. Found: C, 64.36; H, 8.71; N, 2.69; S, 6.30; Fe, 11.31. m.p. 182°C (d).

2. $(Et_4N)_2[Fe_2S_2(OPh)_4]$.

This compound was prepared as described above by method 2. Anal. Calc'd. for $C_{40}H_{60}N_2O_4S_2Fe_2$: C, 59.40; H, 7.48; N, 3.46. Found: C, 59.68; H, 7.57; N, 3.79.

3. $(Me_4N)_2[Fe_2S_2(O\text{-}\underline{p}\text{-}Tol)_4]$.

This compound was prepared by method 1. Anal. Calc'd for $C_{36}H_{52}N_2O_4S_2Fe_2$: C, 57.45; H, 6.97; N, 3.72; S, 8.52; Fe, 14.84. Found: C, 57.64; H, 6.67; N, 3.80; S, 8.12; Fe, 14.98. m.p. >225°C.

4. $(Et_4N)_2[Fe_2S_2(O\text{-}\underline{p}\text{-}C_6H_4Cl)_4]$.

This compound was prepared by method 1. Anal. Calc'd for $C_{40}H_{56}N_2O_4Cl_4S_2Fe_2$: C, 50.76; H, 5.96; N, 2.96; S, 6.78; Fe, 11.80. Found: C, 51.55; H, 6.09; N, 3.05; S, 7.99; Fe, 11.75. m.p. 138-140°C (d).

D. Preparation of $(Et_4N)_2[Fe_2S_2Cl_4]$.

This previously reported compound was prepared by a modification of method 1 above for the preparation of $(R_4N)_2[Fe_2S_2(OAr)_4]$ salts. This compound was also prepared using an alternative source of iron by a procedure analogous to method 1. A solution of 4 g (12.2 mmol) $(Et_4N)[FeCl_4]$ in 100 mL MeCN was treated with 0.56 g (12.2 mmol) Li_2S and stirred for 18 h. Subsequent workup of the reaction mixture proceeded as described in method 1. The yield was 51%. Anal. Calc'd for $C_{16}H_{40}N_2S_2Cl_4Fe_2$: C, 33.24; H, 6.97; N, 4.85. Found: C, 39.22; H, 8.10; N, 5.72.

E. Preparation of $(Et_3NCH_2Ph)_3[Mo_2Fe_6S_8(SEt)_3(OPh)_6]$.

To 3.16 g (1.65 mmol) $(Et_3NCH_2Ph)_3[Mo_2Fe_6S_8(SEt)_9]$ dissolved in 200 mL MeCN was added 14 g (148.8 mmol) PhOH dissolved in 75 mL MeCN. The reaction mixture was evaporated in vacuo at 30°C to <50 mL, diluted with 150 mL MeCN and again evaporated to a volume of <50 mL. This dilution and evaporation step was repeated once, followed by addition of 300 mL THF. Slow cooling to -20°C caused separation of the product as black plates, which were collected by filtration, washed twice with THF and vacuum dried. Recrystallization was accomplished by dissolution of the crude product in ~20 mL MeCN which was 25 mM in PhOH, filtration, addition

of ∿150 mL THF which was also 25 mM in PhOH, and slow cooling to -20°C. Typical yields were 50-60%. Anal. Calc'd for $C_{81}H_{111}N_3O_6S_{11}Fe_6Mo_2$: C, 46.30; H, 5.30; N, 2.00; S, 16.80; Fe, 15.90; Mo, 9.10. Found: C, 45.39; H, 5.55; N, 1.87; S, 16.72; Fe, 16.56; Mo, 8.10. m.p. 55°C (d).

F. Preparation of the Fe-S Long Wavelength Compounds.

1. Et_4N/O-p-C_6H_4Cl/LW.

To 5.15 g (5.3 mmol) $(Et_4N)_2[Fe_4S_4(S\text{-}t\text{-}Bu)_4]$ dissolved in 250 mL MeCN was added 27.33 g (213 mmol) p-ClC_6H_4OH dissolved in 100 mL MeCN. The resulting solution was evaporated in vacuo to a volume of <75 mL, diluted with 200 mL MeCN, and again evaporated to a final volume of <75 mL. A color change from green-brown to orange-brown occurred during this step. Addition of 300 mL i-PrOH and cooling to -20°C for 18 h caused separation of the product as microcrystals which were collected by filtration, washed with i-PrOH and vacuum dried. Recrystallization was accomplished by dissolution of the crude product in 100 mL MeCN, filtration, slow addition of 250 mL i-PrOH and slow cooling to -20°C. The yield was 0.91 g of dark brown crystals. Anal. Calc'd for $(Et_4N)_2[Fe_4S_4(O\text{-}p\text{-}C_6H_4Cl)_4]$, $C_{40}H_{56}N_2O_4S_4Cl_4Fe_4$: C, 42.80; H, 5.03; N, 2.50; S, 11.43; Cl, 12.64; Fe, 19.90. Found: C, 42.53, H, 5.02; N, 2.44; S, 12.30; Cl, 13.49; Fe, 20.80.

2. Me_4N/O-p-Tol/LW

A solution containing 1 g (1.55 mmol) $(Me_4N)_2[Fe_4S_4Cl_4]$ dissolved in 100 mL MeCN was treated with 0.85 g (6.54 mmol) NaO-p-Tol. An immediate color change from dull brown to orange-brown occurred. The mixture was stirred for 2 h, filtered, and the filtrate evaporated in vacuo until precipitation of a crystalline solid began. Addition of ~150 mL i-PrOH and cooling to -20°C for 12 h resulted in separation of the microcrystalline product, which was collected by filtration, washed with i-PrOH and vacuum dried. Recrystallization was affected by slowly cooling a saturated solution of the product in warm (~35°C) EtCN to -20°C for 18 h. The yield was 0.2 g Anal. Calc'd for $(Me_4N)_2$-$[Fe_4S_4(O\text{-}p\text{-}Tol)_4]$, $C_{36}H_{52}N_2O_4S_4Fe_4$: C, 46.56; H, 5.64; N, 3.02; S, 13.81; Fe, 24.06. Found: C, 45.32; H, 5.27; N, 3.14; S, 13.33; Fe, 23.30.

3. Et_4N/O-p-Tol/LW.

To 3.8 g (3.9 mmol) $(Et_4N)_2[Fe_4S_4(S\text{-}t\text{-}Bu)_4]$ dissolved in 300 mL MeCN was added 16.96 g (157 mmol) p-TolOH in 50 mL MeCN. The volume was reduced in vacuo to <75 mL, diluted with 250 mL MeCN and again reduced to a final volume of <75 mL. Slow addition of toluene until a few droplets of dark oil formed, filtration, and slow cooling to -20°C caused precipitation of a well formed crystalline solid,

which was collected by filtration, washed with THF and vacuum dried. UV-Vis and ^{1}H NMR spectroscopic properties of this product were essentially identical, except for cation resonances in the NMR, with those of Me_4N/O-*p*-Tol/LW.

G. Ligand Substitution Reactions.

1. Reaction of $[Fe_4S_4(OPh)_4]^{2-}$ with PhSH.

This reaction was monitored in separate experiments by ^{1}H NMR and electronic spectral measurements described below.

Two stock solutions, one 2.74 mM $(Et_4N)_2[Fe_4S_4(OPh)_4]$ in MeCN, the other 1 M PhSH in MeCN, were prepared. An aliquot of tetramer solution was introduced into a quartz optical cell with 0.2 mm path length, and a spectrum was recorded after each addition of each aliquot of thiol solution. Spectra were recorded within 5-10 min after each successive addition of thiol solution. Solution volume changes were negligible due to the high concentration of the thiol solution. A limiting spectrum was obtained on addition of >4 equivalents of thiol.

Two stock solutions were made up in d_3-MeCN: one 10 mM $(Et_4N)_2[Fe_4S_4(OPh)_4]$ and the other 0.1 M PhSH. A 0.4 mL aliquot of tetramer solution was transferred to a 5 mm NMR tube fitted with a rubber septum. Spectra were taken 15-20 min after each addition of thiol solution. A

limiting spectrum was obtained on addition of >4 equivalents of thiol as shown by the appearance of resonances due to free PhSH.

2. Reaction of $[Fe_4S_4(OPh)_4]^{2-}$ with PhCOCl.

To 5.0 mL of a 7.42 m$\underline{M}$ solution of $(Et_4N)_2[Fe_4S_4(OPh)_4]$ in MeCN was added 165 μL of 0.89 $\underline{M}$ PhCOCl in MeCN. The resulting solution was stirred for 0.5 h during which time a color change from orange-brown to a dull brown occurred. An optical spectrum of the solution showed 97% formation of $[Fe_4S_4Cl_4]^{2-}$.

3. Reaction of $[Fe_2S_2(OPh)_4]^{2-}$ with PhSH.

To 5.0 mL of a 7.88 m$\underline{M}$ solution of $(Bu_4N)_2[Fe_2S_2$-$(OPh)_4]$ in MeCN was added 166 μL of 0.95 $\underline{M}$ PhSH in MeCN. The resulting solution changed color from red to maroon rapidly and was stirred for ∿15 min. An optical spectrum of the solution was consistent with 98% formation of $[Fe_2S_2(SPh)_4]^{2-}$.

4. Reaction of $[Fe_2S_2(OPh)_4]^{2-}$ with PhCOCl.

To 5.0 mL of 7.88 m$\underline{M}$ $(Bu_4N)_2[Fe_2S_2(OPh)_4]$ in MeCN was added 0.7 mL of 0.89 $\underline{M}$ PhCOCl in MeCN. The mixture was stirred for 12 h. A gradual color change from red to purple took

place. An optical spectrum of the solution indicated 95% formation of $[Fe_2S_2Cl_4]^{2-}$.

5. Reaction of $[Mo_2Fe_6S_8(SEt)_3(OPh)_6]^{3-}$ with PhSH.

To 5.0 mL of 2.8 m$\underline{M}$ $(Et_3NCH_2Ph)_3[Mo_2Fe_6S_8(SEt)_3(OPh)_6]$ in MeCN was added 94 μL of 0.95 $\underline{M}$ PhSH in MeCN. The solution color changed rapidly from deep orange-brown to red-brown. An optical spectrum of the solution showed that $[Mo_2Fe_6S_8(SEt)_3(SPh)_6]^{2-}$ had been formed in 98% yield.

6. Reaction of $[Mo_2Fe_6S_8(SEt)_3(OPh)_6]^{3-}$ with PhCOCl.

To 5.0 mL of 2.8 m$\underline{M}$ $(Et_3NCH_2Ph)_3[Mo_2Fe_6S_8(SEt)_3(OPh)_6]$ in MeCN was added 94 μL of 0.89 $\underline{M}$ PhCOCl in MeCN. The solution changed color from deep orange-brown to dark brown with a purple cast over the course of 0.5 h. An optical spectrum of the solution was consistent with 95% formation of $[Mo_2Fe_6S_8(SEt)_3Cl_6]^{3-}$.

7. Reaction of Et_4N/O-$\underline{p}$-C_6H_4Cl/LW with PhSH.

This reaction was monitored by ^1H NMR spectroscopy. Two stock solutions were prepared in d_3-MeCN: one was 5.0 m$\underline{M}$ Et_4N/O-$\underline{p}$-C_6H_4Cl/LW assuming a formula weight of 1122.25, corresponding to $(Et_4N)_2[Fe_4S_4(O\text{-}\underline{p}\text{-}C_6H_4Cl)_4]$, and the other 0.1 $\underline{M}$ PhSH. A 0.4 mL aliquot of Et_4/O-$\underline{p}$-C_6H_4Cl/LW solution was introduced into a degassed 5 mm

NMR tube fitted with a rubber septum. Aliquots of PhSH solution were added and spectra recorded at 15 min intervals. Complete reaction, as shown by the appearance of free PhSH signals, was reached at 6-8 equivalents of added PhSH. At >8 equivalents of added PhSH the spectra showed further reaction to form substantial amounts of $[Fe_4S_4(SPh)_4]^{2-}$.

H. Physical Measurements.

All samples were handled under anaerobic conditions. Optical spectra were obtained on either a Cary 219 or a Cary 17 spectrophotometer. Proton NMR spectra were obtained on a Bruker WM-250 Fourier transform spectrometer equipped with a variable temperature unit. Room temperature magnetic susceptibility measurements were performed on an Alpha Faraday balance using $Hg[Co(SCN)_4]$ as calibrant. Variable temperature data were performed on an SHE Corporation SQUID susceptometer operating at 2 kG and on a modified PAR 155 vibrating sample magnetometer operating at 10 kG. Electrochemical measurements were performed on a PAR 174 Å polarographic analyzer equipped with an HP 4030 Å XY recorder. Either DC polarography at a dropping mercury electrode or cyclic voltammetry at Pt flag or glassy carbon electrodes were performed. All solutions contained either 50 m$\underline{M}$ $Et_4N(ClO_4)$ or 50 m$\underline{M}$ $Bu_4N(ClO_4)$ as supporting electrolyte. Potentials were measured versus the

saturated calomel electrode and a Pt wire was employed as the counter electrode. Mossbauer spectra were measured by Dr. T. Kent and Professor E. Munck at the Grey Freshwater Biology Institute, University of Minnesota, Mavarre, Minnesota. The Mossbauer spectrometer was of the constant acceleration type and has been described elsewhere[100]. Isomer shifts are reported versus metallic Fe foil at room temperature. Melting points were obtained in sealed capillaries in vacuo and are uncorrected. Elemental analyses were performed by Galbraith Laboratories, Inc., Knoxville, Tennessee.

III. RESULTS AND DISCUSSION

A. $[Fe_4S_4(OAr)_4]^{2-}$ (Ar = Ph, p-Tol)

1. Synthesis

Addition of excess phenol to an acetonitrile solution of the alkyl thiolate cluster $[Fe_4S_4(SR)_4]^{2-}$, R = alkyl, establishes an equilibrium whereby a small fraction of thiolates is displaced by phenolate (Reaction 1).

$$[Fe_4S_4(SR)_4]^{2-} + \text{xs ArOH} \rightleftarrows [Fe_4S_4(OAr)_4]^{2-} + 4\ RSH \quad (1)$$

The original observation of this equilibrium[101] suggested a route to the synthesis of phenolate substituted tetramers. By removal of solvent and volatile thiol (R = Et, t-Bu) in vacuo, the reaction can be driven to the right and complete substitution achieved. The resulting products, $[Fe_4S_4(OAr)_4]^{2-}$, are isolated as their tetraalkylammonium salts in 80% yield after recrystallization. These complexes are stable in the solid state and in solution in the absence of dioxygen and water. In some cases, it is difficult to purify the phenolate tetramers by recrystallization because of their high solubility in polar organic solvents, especially the parent

phenol. This constitutes a drawback of the preparative method utilizing a large excess of phenol, which can make precipitation of the compound difficult.

An alternative method of preparation employs a ligand exchange reaction between an appropriate salt of $[Fe_4S_4Cl_4]^{2-}$ and anhydrous sodium phenolate in acetonitrile (Reaction 2).

$$[Fe_4S_4Cl_4]^{2-} + 4\ NaOAr \rightarrow [Fe_4S_4(OAr)_4]^{2-} + 4\ NaCl \qquad (2)$$

This method makes use of the insolubility of NaCl in acetonitrile to drive the reaction to completion. Phenolate tetramers prepared by this method are of similar purity and obtained in yields comparable to those found for the first method of preparation.

2. X-Ray Structure

The crystal structure of $(Et_4N)_2[Fe_4S_4(OPh)_4]$ consists of discrete cations and anions in an 8:4 ratio, respectively, per unit cell. The structure of the core showing the numbering scheme and selected interatomic distances is presented in Figure 7. A stereoscopic view of the entire dianion is depicted in Figure 8, and stereoscopic view of the unit cell along the b axis is shown in Figure 9. Selected interatomic distances and angles for the anion are given in Table 1. The tetraethylammonium cations are crystallographically ordered, possess normal angles,

Figure 7. A portion of the $Fe_4S_4(OPh)_4$ core, showing 50% probability ellipsoids, the atom labelling scheme, and interatomic distances.

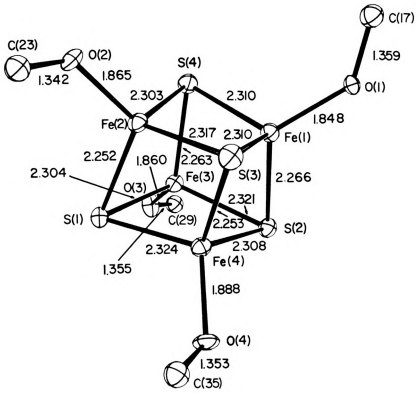
C(17)
1.359
O(1)
1.848
C(23)
O(2)
1.342
1.865
S(4)
2.303
2.310
Fe(2)
2.317
2.310
Fe(1)
2.252
1.860
2.263
2.304
O(3)
Fe(3)
S(3)
2.266
2.321
C(29)
S(1)
2.253
S(2)
2.324
2.308
1.355
Fe(4)
1.888
O(4)
1.353
C(35)

Figure 7

Figure 8. A stereoscopic view of the $[Fe_4S_4(OPh)_4]^{2-}$ ion. Probability ellipsoids are drawn at the 50% level. The hydrogen atoms are not included.

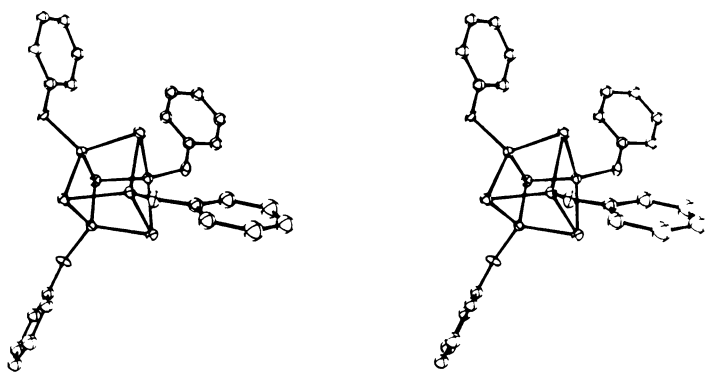

Figure 8

Figure 9. Stereodiagram of the unit cell of $(Et_4N)_2$-$[Fe_4S_4(OPh)_4]$ down the b axis. The 30% probability ellipsoids are shown. The hydrogen atoms are omitted for clarity.

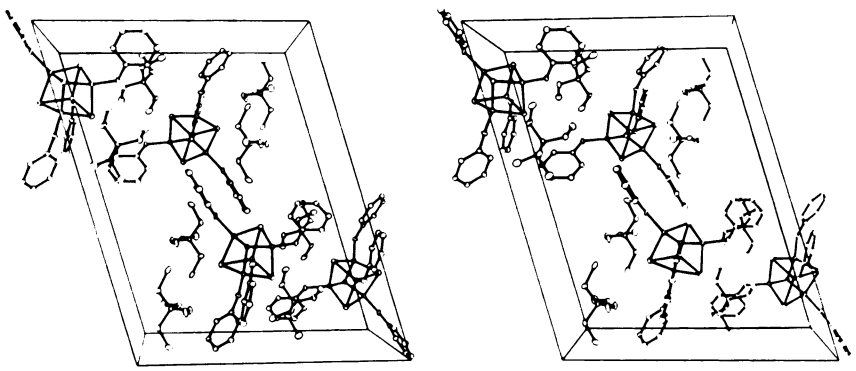

Figure 9

Table I. Bond Distances (A) and Angles (deg) for $[Et_4N]_2[Fe_4S_4(OC_6H_5)_4]$.

ANION

--------Fe....Fe--------	
Fe(1)-Fe(2)	2.747(2)
Fe(3)-Fe(4)	2.730(2)
Mean	2.739
Fe(1)-Fe(3)	2.762(2)
Fe(1)-Fe(4)	2.763(2)
Fe(2)-Fe(3)	2.756(2)
Fe(2)-Fe(4)	2.759(2)
Mean	2.760(3)
Mean (of 6)	2.753(13)

---------Fe-S---------	
Fe(1)-S(2)	2.266(3)
Fe(2)-S(1)	2.252(3)
Fe(3)-S(4)	2.263(3)
Fe(4)-S(3)	2.253(3)
Mean	2.259(7)
Fe(1)-S(3)	2.310(3)
Fe(1)-S(4)	2.310(3)
Fe(2)-S(3)	2.317(3)
Fe(2)-S(4)	2.303(3)
Fe(3)-S(1)	2.304(3)
Fe(3)-S(2)	2.321(3)
Fe(4)-S(1)	2.324(3)
Fe(4)-S(2)	2.308(3)
Mean	2.312(8)

--------S....S--------	
S(10)-S(2)	3.707(3)
S(3)-S(4)	3.684(3)
Mean	3.696(16)
S(1)-S(3)	3.586(3)
S(1)-S(4)	3.569(3)
S(2)-S(3)	3.573(3)
S(2)-S(4)	3.593(3)
Mean	3.580(11)

---------Fe-O---------	
Fe(1)-O(1)	1.848(6)
Fe(2)-O(2)	1.865(6)
Fe(3)-O(3)	1.860(6)
Fe(4)-O(4)	1.88(6)
Mean	1.865(17)

------O-C (ring)------	
O(1)-C(17)	1.359(9)
O(2)-C(23)	1.342(8)
O(3)-C(29)	1.355(8)
O(4)-C(35)	1.353(8)
Mean	1.352(7)

----------Fe-Fe-Fe----------	
Fe(4)-Fe(1)-Fe(3)	59.23(5)
Fe(4)-Fe(2)-Fe(3)	59.35(5)
Fe(1)-Fe(3)-Fe(2)	59.70(5)
Fe(1)-Fe(4)-Fe(2)	59.66(5)
Mean	59.49(23)
Fe(4)-Fe(1)-Fe(2)	60.09(5)
Fe(3)-Fe(1)-Fe(2)	60.05(5)
Fe(4)-Fe(2)-Fe(1)	60.25(5)
Fe(3)-Fe(2)-Fe(1)	60.26(5)
Fe(2)-Fe(3)-Fe(4)	60.37(5)
Fe(1)-Fe(3)-Fe(4)	60.40(5)
Fe(2)-Fe(4)-Fe(3)	60.28(5)
Fe(1)-Fe(4)-Fe(3)	60.37(5)
Mean	60.26(13)
Mean (of 12)	60.00(41)

----------S-Fe-S----------	
S(2)-Fe(1)-S(3)	102.7(1)
S(2)-Fe(1)-S(4)	103.5(1)
S(3)-Fe(1)-S(4)	105.8(1)
S(1)-Fe(2)-S(3)	103.4(1)
S(1)-Fe(2)-S(4)	103.2(1)
S(3)-Fe(2)-S(4)	105.7(1)
S(1)-Fe(3)-S(4)	102.8(1)
S(2)-Fe(3)-S(4)	103.2(1)
S(1)-Fe(3)-S(2)	106.5(1)
S(1)-Fe(4)-S(3)	103.2(1)
S(2)-Fe(4)-S(3)	103.1(1)
S(1)-Fe(4)-S(2)	106.31(9)
Mean	104.1(15)

Table I. Continued.

ANIONS - Continued

----------Fe-S----------	
Fe(1)-S(1)	3.909(3)
Fe(2)-S(2)	3.909(3)
Fe(3)-S(3)	3.893(3)
Fe(4)-S(4)	3.893(3)
Mean	3.901(9)

----------S-S-S---------	
S(4)-S(1)-S(3)	61.97(7)
S(4)-S(2)-S(3)	61.87(7)
S(1)-S(3)-S(2)	62.37(7)
S(1)-S(4)-S(2)	62.34(7)
Mean	62.14(25)
S(40S(1)-S(2)	59.15(7)
S(3)-S(1)-S(2)	58.63(6)
S(4)-S(2)-S(1)	58.51(7)
S(3)-S(2)-S(1)	59.00(7)
S(1)-S(3)-S(4)	58.78(6)
S(2)-S(3)-S(4)	59.33(6)
S(1)-S(4)-S(3)	59.25(6)
S(2)-S(4)-S(3)	58.79(6)
Mean	58.97(27)

----------Fe-S-Fe---------	
Fe(2)-S(1)-Fe(4)	74.13(8)
Fe(2)-S(1)-Fe(3)	74.44(9)
Fe(4)-S(1)-Fe(3)	72.30(8)
Fe(1)-S(2)-Fe(3)	74.04(9)
Fe(1)-S(2)-Fe(4)	74.32(9)
Fe(3)-S(2)-Fe(4)	72.29(8)
Fe(4)-S(3)-Fe(2)	74.25(8)
Fe(4)-S(3)-Fe(1)	74.52(9)
Fe(2)-S(3)-Fe(1)	72.82(8)
Fe(3)-S(4)-Fe(1)	74.32(9)
Fe(3)-S(4)-Fe(2)	74.25(9)
Fe(1)-S(4)-Fe(2)	73.08(8)
Mean	73.7(9)

----------O-Fe-S----------	
O(1)-Fe(1)-S(2)	116.2(2)
O(1)-Fe(1)-S(3)	113.9(2)
O(1)-Fe(1)-S(4)	113.5(2)
O(2)-Fe(2)-S(1)	116.6(2)
O(2)-Fe(2)-S(3)	112.8(2)
O(2)-Fe(2)-S(4)	113.8(2)
O(3)-Fe(3)-S(1)	106.9(2)
O(3)-Fe(3)-S(2)	113.7(2)
O(3)-Fe(3)-S(4)	122.4(2)
O(4)-Fe(4)-S(1)	112.8(2)
O(4)-Fe(4)-S(2)	111.3(2)
O(4)-Fe(4)-S(3)	119.0(2)
Mean	114.4(39)

--------Fe-O-C (ring)--------	
Fe(1)-O(1)-C(17)	132.5(5)
Fe(2)-O(2)-C(23)	128.7(5)
Fe(3)-O(3)-C(29)	132.2(6)
Fe(4)-O(4)-C(35)	122.6(5)

Table I Continues.

Table I. Continued.

CATIONS

----------N-C----------		----------C-C----------		----------C-N-C----------	
N(1)-C(1)	1.50(1)	C(1)-C(2)	1.49(2)	C(1)-N(1)-C(3)	109.4(8)
N(1)-C(3)	1.54(1)	C(3)-C(4)	1.51(2)	C(1)-N(1)-C(5)	112.2(8)
N(1)-C(5)	1.50(1)	C(5)-C(6)	1.50(2)	C(1)-N(1)-C(7)	107.7(7)
N(1)-C(7)	1.51(1)	C(7)-C(8)	1.52(2)	C(3)-N(1)-C(5)	106.3(7)
N(2)-C(9)	1.51(1)	C(9)-C(10)	1.51(1)	C(3)-N(1)-C(7)	110.4(8)
N(2)-C(11)	1.51(1)	C(11)-C(12)	1.50(2)	C(5)-N(1)-C(7)	110.9(8)
N(2)-C(13)	1.51(1)	C(13)-C(14)	1.51(2)	C(9)-N(2)-C(11)	111.6(8)
N(2)-C(15)	1.49(1)	C(15)-C(16)	1.50(2)	C(9)-N(2)-C(13)	107.2(7)
Mean	1.51(1)	Mean	1.51(1)	C(9)-N(2)-C(15)	110.6(8)
				C(11)-N(2)-C(13)	111.3(8)
---------N-C-C'--------				C(11)-N(2)-C(15)	106.0(8)
				C(13)-N(2)-C(15)	110.2(8)
N(1)-C(1)-C(2)	116.7(8)			Mean	109.5(21)
N(1)-C(3)-C(4)	114.3(8)				
N(1)-C(5)-C(6)	115.9(8)				
N(1)-C(7)-C(8)	114.8(8)				
N(2)-C(9)-C(10)	114.9(8)				
N(2)-C(11)-C(12)	114.3(9)				
N(2)-C(13)-C(14)	116.6(8)				
N(2)-C(15)-C(16)	116.3(9)				
Mean	115.5(10)				

distances and ethyl group conformations and will not be discussed further.

The basic cubane structure of the anion shown in Figures 7 and 8 is common to other iron-sulfur tetramer dianions, including $[Fe_4S_4(SPh)_4]^{2-}$ [101], $[Fe_4S_4Cl_4]^{2-}$, and $[Fe_4S_4(SCH_2Ph)_4]^{-}$ [91]. Comparative structural data for these related systems are given in Table 2. The highest possible symmetry for an Fe_4S_4 core is T_d; $[Fe_4S_4(OPh)_4]^{2-}$, however has a significant distortion from T_d toward D_{2d}, as do all other structurally characterized tetramers. This distortion arises from a compression of the Fe_4S_4 core along an approximate $\bar{4}$ symmetry axis that penetrates the top and bottom faces of the polyhedron in Figure 7. This results in dividing the bond distances and angles into sets: four short and eight longer Fe-S distances (short bonds parallel to $\bar{4}$, long bonds perpendicular to $\bar{4}$), two short and four longer Fe-Fe and S-S distances, and four smaller and eight larger Fe-Fe-Fe and S-S-S angles. A further consequence of this distortion apparent from Figure 7 is that each face of the Fe_4S_4 polyhedron is a non-planar rhomb with average Fe-S-Fe and S-Fe-S angles of 73.7 and 104.1, respectively. The anion core can also be regarded as consisting of two interpenetrating Fe_4 and S_4 tetrahedra, the iron tetrahedron being smaller and closer to ideal tetrahedral geometry than that of the sulfur counterpart. Examination of Table II reveals that the observations

Table II. Comparison of Structural Parameters for Compounds with the $[Fe_4S_4]^{2+}$ Core.

Distance/ Angle	$[Et_4N]_2[Fe_4S_4(SCH_2Ph)_4]$[a]	$[Me_4N]_2[Fe_4S_4(SPh)_4]$[b]	$[Et_4N]_2[Fe_4S_4Cl_4]$[c]	$[Et_4N]_2[Fe_4S_4(OPh)_4]$[d]
Fe-Fe	2.776(2)[e]; 2.732(4)	2.730(2); 2.739(4)	2.755(2); 2.766(4)	3.729(2); 2.760(4)
Fe-S*	2.239(4); 2.310(8)	2.267(4); 2.296(8)	2.260(4); 2.295(8)	2.259(4); 2.312(8)
Fe-X	2.251	2.263	2.216	1.865
S*-S*	3.645(2); 3.586(4)	3.650(2); 3.592(4)	3.637(2); 3.562(4)	3.696(2); 3.580(4)
Fe-Fe-Fe	61.11(4); 59.46(8)	59.79(4); 60.11(8)	59.63(4); 60.19(8)	59.49(4); 60.26(8)
Fe-S*-Fe	73.8	73.5	74.6	73.7
S*-Fe-S*	104.1	104.3	103.5	104.1
S*-Fe-X	114.4	115.1	114.9	114.4
S*-S*-S*	61.11(4); 59.45(8)	61.08(4); 59.47(8)	61.41(4); 59.30(8)	62.14(4); 58.97(8)

[a]Reference 91.

[b]Reference 101.

[c]Reference 102.

[d]This work.

[e]Figures in parentheses are the numbers of values averaged where two distances or angles are given.

described above with regard to the structure of the $[Fe_4S_4]^{2+}$ core of $[Fe_4S_4(OPh)_4]^{2-}$ are also applicable to the other members of this family of complexes possessing the same core but different terminal ligands. Thus, the phenoxide tetramer provides additional evidence for the invariance of the structure of the $[Fe_4S_4]^{2+}$ core with various terminal ligands.

The key structural feature of the $[Fe_4S_4(OPh)_4]^{2-}$ ion is the presence of the Fe-O bond. The mean Fe-O bond distance is 1.865 (17) Å. It is difficult, however, to analyze the chemical significance of this bond length due to the lack of structurally characterized complexes with tetrahedral iron oxygen bonds. This distance is intermediate between that found in $[MoFeS_4(OPh)_2]^{2-}$ [81] (1.897) (13) Å) and that in $[Fe(OAr)]^{1-}$ [89] (1.847 (13) Å for Ar = 2,3,5,6-Me_4C_6H, 1.866 (6) Å for Ar = 2,4,6-$Cl_3C_6H_2$). This trend is consistent with an increasing average Fe oxidation state in these complexes: 2+ for the MoFe dimer, 2.5+ for the phenoxide tetramer, and 3+ for the iron phenolate monomers. The range of these Fe-O distances is somewhat small, and less than expected based on trends in ionic radius. This suggests the presence of substantial covalent character in these bonds.

Typical five and six coordinate complexes with oxygen ligands show longer Fe-O distances than those observed for the monodentate phenoxide ligands in $[Fe_4S_4(OPh)_4]^{2-}$.

Examples include [Fe(salen)Cl][103] and $[Fe(salen)]_2O$ [104] which have Fe-O distances of 1.88-1.92 Å and [Fe(catecholate)$_3$] [105] which has Fe-O distances of 2.02 Å. Some of the difference between these Fe-O distances and that observed in $[Fe_4S_4(OPh)_4]^{2-}$ may be due to the expected decrease in bond distances between octahedral and tetrahedral geometry[106]. This effect, however, does not seem to fully explain the short Fe-O distances in $[Fe_4S_4(OPh)_4]^{2-}$ or $[MoFeS_4(OPh)_2]^{2-}$. Recently it has been shown that axial monodentate phenoxide coordination in certain five-coordinate Schiff base complexes, such as [Fe(saloph(CatH))] (CatH = catecholate) and [Fe(salen)HQ], (HQ = p-hydroquinone dianion), results in quite short Fe-O distances[107] (1.828 (4) Å and 1.861 (2) Å, respectively). One might view coordination of phenolate to the trigonal FeS_3 corner of a cubane as a situation somewhat analogous to the axial phenolate coordination in these five-coordinate Schiff base complexes.

3. Optical Spectra

The optical spectra of $[Fe_4S_4(OPh)_4]^{2-}$ and $[Fe_4S_4(SPh)_4]^{2-}$ are shown in Figure 10. Comparative spectral data are given in Table 3.

The first observation to be made is that the spectra are qualitatively quite similar. Both exhibit a strong absorption maximum in the 400-500 nm range, with less well

Figure 10. Electronic spectra of the $[Fe_4S_4(OPh)_4]^{2-}$ and $[Fe_4S_4(SPh)_4]^{2-}$ ions in acetonitrile solution at 22°C.

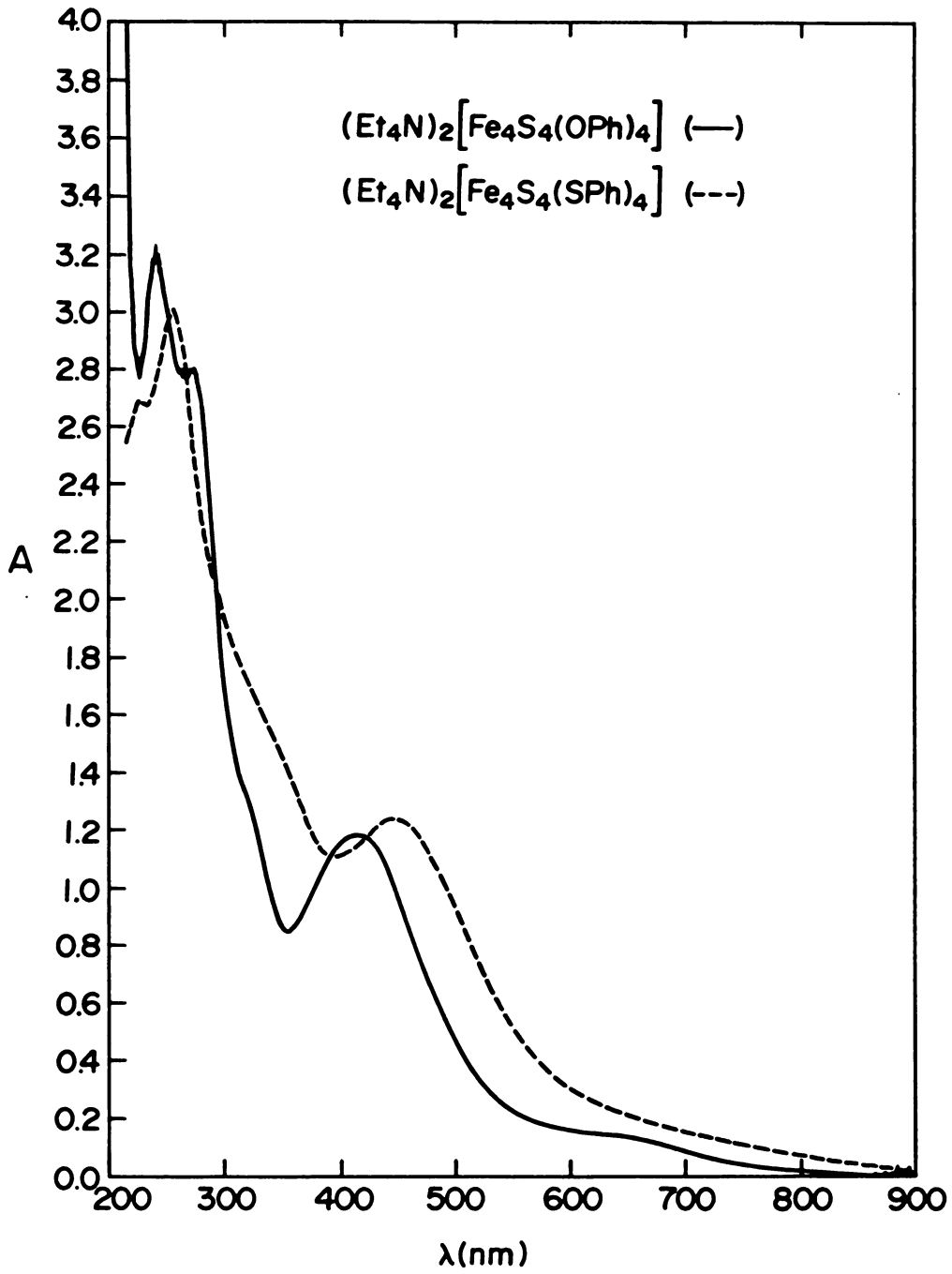
(Et4N)2[Fe4S4(OPh)4] (—)
(Et4N)2[Fe4S4(SPh)4] (---)
A
λ(nm)
4.0
3.8
3.6
3.4
3.2
3.0
2.8
2.6
2.4
2.2
2.0
1.8
1.6
1.4
1.2
1.0
0.8
0.6
0.4
0.2
0.0
200
300
400
500
600
700
800
900

Figure 10

Table III. Electronic Spectral Features, Magnetic Moments, and Isotropic Shifts of Phenoxide Protons of $[Fe_4S_4(OAr)_4]^{2-}$ Complexes.

	$[Fe_4S_4(OPh)_4]^{2-}$	$[Fe_4S_4(O\text{-}\underline{p}\text{-}Tol)_4]^{2-}$
Electronic Spectral Features[a]	650(sh), 410(15.7), 270(sh), 239(44.0)	50(sh), 424(14.2) 270(sh), 246(42.2)
Magnetic Moment, per iron, (μ_{Fe})[b], μ_B	1.32	1.25
Isotropic Shifts of Phenoxide protons[c], ppm	+2.31(<u>o</u>-H), -2.23(<u>m</u>-H), +2.86(<u>p</u>-H)	+2.33(<u>o</u>-H), -2.23(<u>m</u>-H) -2.77(<u>p</u>-CH_3)

[a] In acetonitrile solution at 22°C. λ_{max} (E) in nm (M^{-1} cm^{-1} x 10^{-3}).

[b] In the solid state at 23°C.

[c] In CD_3CN solutions at 22°C, shifts vs. diamagnetic phenols, PhOH: -7.02; <u>p</u>-TolOH: -6.85, -2.21 (<u>p</u>-CH_3). Chemical shifts downfield of TMS are taken as negative.

resolved features at lower (600-700 nm) and higher (240-300 nm) energy. Corresponding bands at 410 nm (OPh) and 457 nm (SPh) are tentatively assigned to terminal ligand-to-metal core charge transfer transitions. The relatively large blue shift seen upon oxygen substitution is consistent with increased electronegativity of the coordinating atom, and thus increased energy differences between the ligand and metal orbitals. Recent Xα molecular orbital calculations on $[Fe_4S_4(SH)_4]^{2-}$,[108,109] and $[Fe_4S_4(SMe)_4]^{2-}$,[109-111] indicate that this assignment is a reasonable but somewhat oversimplified one. Substitution of the p-H for a CH_3 group in the phenoxide tetramers results in a significant red shift (∿14 nm) in the energy of the absorption maximum, as expected for replacement with an electron releasing group; this is in contrast with the arylthiolate complexes which show only a small perturbation. Due to difficulty in crystallization of the phenoxide tetramers, a more extensive series of complexes with various substituents has not yet been prepared and characterized. However, this inductive methyl group effect seems to indicate that the phenoxide complexes are more sensitive to substituent effects than their thiophenoxide counterparts.

The feature at 600-700 nm, which is more clearly resolved in the phenolate than in the thiolate tetramers is similar to features of the halide tetramers in that region. They are presumably due to $[Fe_4S_4]^{2+}$ core transitions

with at least partial d-d character.

The spectra of the phenoxide complexes are in contrast to the spectrum of the acetate ligated tetramer, $[Fe_4S_4(OAc)_4]^{2-}$, which shows only weak rising featureless absorption in the 400-700 nm region[28]. This may be viewed as being a consequence of the less conjugated π system in the carboxylate vs the phenolate ligands.

4. Magnetic Susceptibility

The room temperature magnetic susceptibilities of solid samples of the compounds $(Et_4N)_2[Fe_4S_4(OPh)_4]$ and $(Bu_4N)_2[Fe_4S_4(O\text{-}\underline{p}\text{-}Tol)_4]$ have been measured by the Faraday method. The data correspond to effective magnetic moments per iron (μ/Fe) of approximately 1.3 BM, suggestive of intramolecular antiferromagnetic coupling. These values have been corrected for the diamagnetic contributions to the susceptibility due to the ligands and cations by use of Pascal's constants[112]. These effective magnetic moments are virtually identical with those reported for the thiolate[113,114] and halide[93] tetramers under similar conditions.

The susceptibility of a freshly recrystallized sample of $(Et_4N)_2[Fe_4S_4(OPh)_4]$ was measured from 4.2 - 300 K. As with the corresponding thiolate and halide analogs, this tetramer showed paramagnetic impurities at low

temperatures, as evidenced by a minimum near 50 K in the susceptibility curve. Impurity corrections[113] were made by fitting the data between 20 and 60 K to the equation $\chi_{impurity} = C/T + A$ where C/T was used as an impurity correction and the intercept A was used to estimate the apparent temperature independent paramagnetism (TIP). The magnitude of the correction corresponds to approximately 0.4% high spin Fe(III) impurity. The data were also corrected for the diamagnetism of the ligands and cations as usual. The final results are plotted in Figure 11.

The observed increase in susceptibility with increasing temperature above 50 K provides clear evidence for intramolecular antiferromagnetic spin coupling. The residual low temperature peak in the curve is presumably due to inadequate impurity corrections using the normal Curie law approximation. The apparent value of 780×10^{-6} cgsu for TIP is somewhat higher than those formed for the isoelectronic thiolate clusters[112] (ca. 440×10^{-6} cgsu). It should be noted, however, that the apparent value for TIP is quite sensitive to the exact method used to correct for impurities. Throughout the entire temperature range, the value of μ_{eff}/Fe at a given temperature is very similar to that observed for the thiolate[113] and halide[93] tetramers.

Theoretical χ vs. T curves simulated using a simple,

Figure 11. Magnetic susceptibility of solid $(Et_4N)_2[Fe_4S_4(OPh)_4]$ (O) as a function of temperature, compared to curves calculated for single J values of -160 (---), -175 (——), and -190 (...) cm^{-1}.

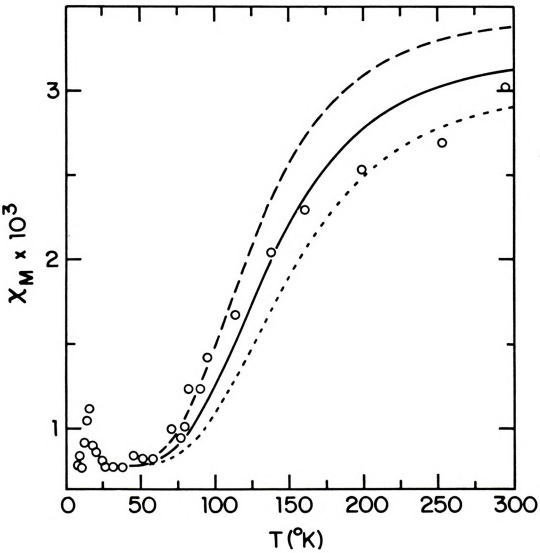

Figure 11

single J antiferromagnetic spin-coupled model[115] extended to the cluster system $2Fe^{2+} + 2Fe^{3+}$ [113] are plotted in Figure 11. It is apparent that the data does not fit any single curve, and therefore no single J value adequately describes the observed data. This discrepancy is also found for the thiolate and halide tetramers using a similar analysis[113,93]. The magnitude of $-J = 160\text{-}190\ cm^{-1}$ is somewhat less than that estimated for the thiophenolate, $-J = 226\ cm^{-1}$,[113] and halide, $-J = 220\ cm^{-1}$,[93] tetramers. Antanaitis and Moss, however, have estimated $-J < 200\ cm^{-1}$ for HP_{red}[116]. In a more detailed analysis, Holm[117] and coworkers have very recently shown that the magnetic properties of the thiophenolate tetramer are more accurately simulated using a model incorporating three exchange coupling constants.

5. Proton Magnetic Resonance

The proton magnetic resonance spectra of the complexes $(R_4N)_2[Fe_4S_4(OAr)_4]$ Ar = Ph, p-Tol have been measured as a function of temperature in deuterated acetonitrile. Chemical shifts were determined relative to TMS internal standard. In the usual convention for reporting chemical shifts for paramagnetic species and their diamagnetic references, $(\Delta H/H)^{obsd}$ and $(\Delta H/H)^{dia}$ are assigned negative values for chemical shifts downfield of TMS. This convention will be used here and in the subsequent discussion.

Isotropic shifts are calculated using the relation $(\Delta H/H)^{iso} = (\Delta H/H)^{obsd} - (\Delta H/H)^{dia}$, where $(\Delta H/H)^{dia}$ is obtained from the free phenol in acetonitrile at room temperature. In addition to the resonances due to the cations, residual undeuterated solvent and a minute amount of water, signals arising from the aryl protons, isotropically shifted from the diamagnetic phenol, are observed. Representative 250 MHz spectra of $(Et_4N)_2[Fe_4S_4(OPh)_4]$ and $(Bu_4N)_2[Fe_4S_4(O\text{-}\underline{p}\text{-}Tol)_4]$ at various temperatures are shown in Figures 12 and 13, respectively. Room temperature isotropic shifts are listed in Table III. Plots of the isotropic shifts versus temperature are displayed in Figure 14. Resonances due to the quaternary ammonium cations are broadened and slightly shifted, but remain essentially temperature independent and will not be discussed further.

Before discussion of the data obtained for the phenoxide tetramers, a summary of the factors contributing to the isotropic shifts and of the results for the mercaptide analogs $[Fe_4S_4(SR)_4]^{2-}$ R = aryl is in order. Total isotropic shifts are the sum of two components according to the relation[118] $(\Delta H/H)^{iso} = (\Delta H/H)^{contact} + (\Delta H/H)^{dipolar}$. It can be shown that the contact term results from delocalization of the unpaired spin onto the nucleus being observed. The contact term can be expressed by the equation[118]

Figure 12. Proton magnetic resonance spectra (250 MHz) of $(Et_4N)_2[Fe_4S_4(OPh)_4]$ in d_3-MeCN solution at various temperatures. Peaks from protons of the cation are indicated by Q, solvent by S, and unidentified impurities by X. Chemical shifts are in ppm from internal Me_4Si (TMS).

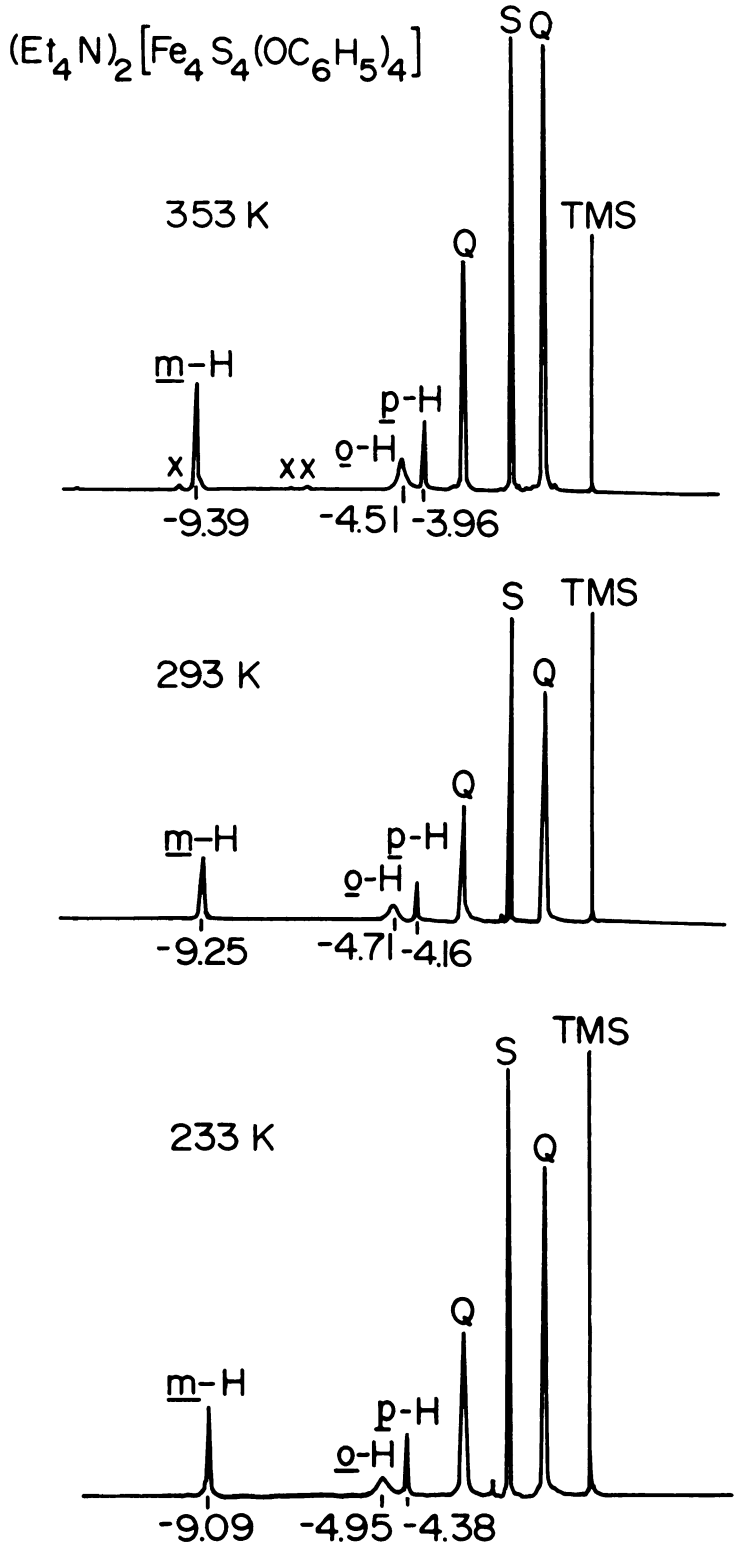
(Et4N)2[Fe4S4(OC6H5)4]
353 K
S
Q
Q
TMS
m-H
p-H
o-H
x
xx
-9.39
-4.51
-3.96
293 K
S
TMS
Q
Q
m-H
p-H
o-H
-9.25
-4.71
-4.16
233 K
TMS
S
Q
Q
m-H
p-H
o-H
-9.09
-4.95
-4.38

Figure 12

Figure 13. Proton magnetic resonance spectra (250 MHz) of $(Bu_4N)_2[Fe_4S_4(O\text{-}\underline{p}\text{-}Tol)_4]$ in d_3-MeCN solution at various temperatures. Peaks from protons of the cation are indicated by Q, solvent by S, residual water by W, and unidentified impurities by X. Chemical shifts are in ppm from internal Me_4Si (TMS).

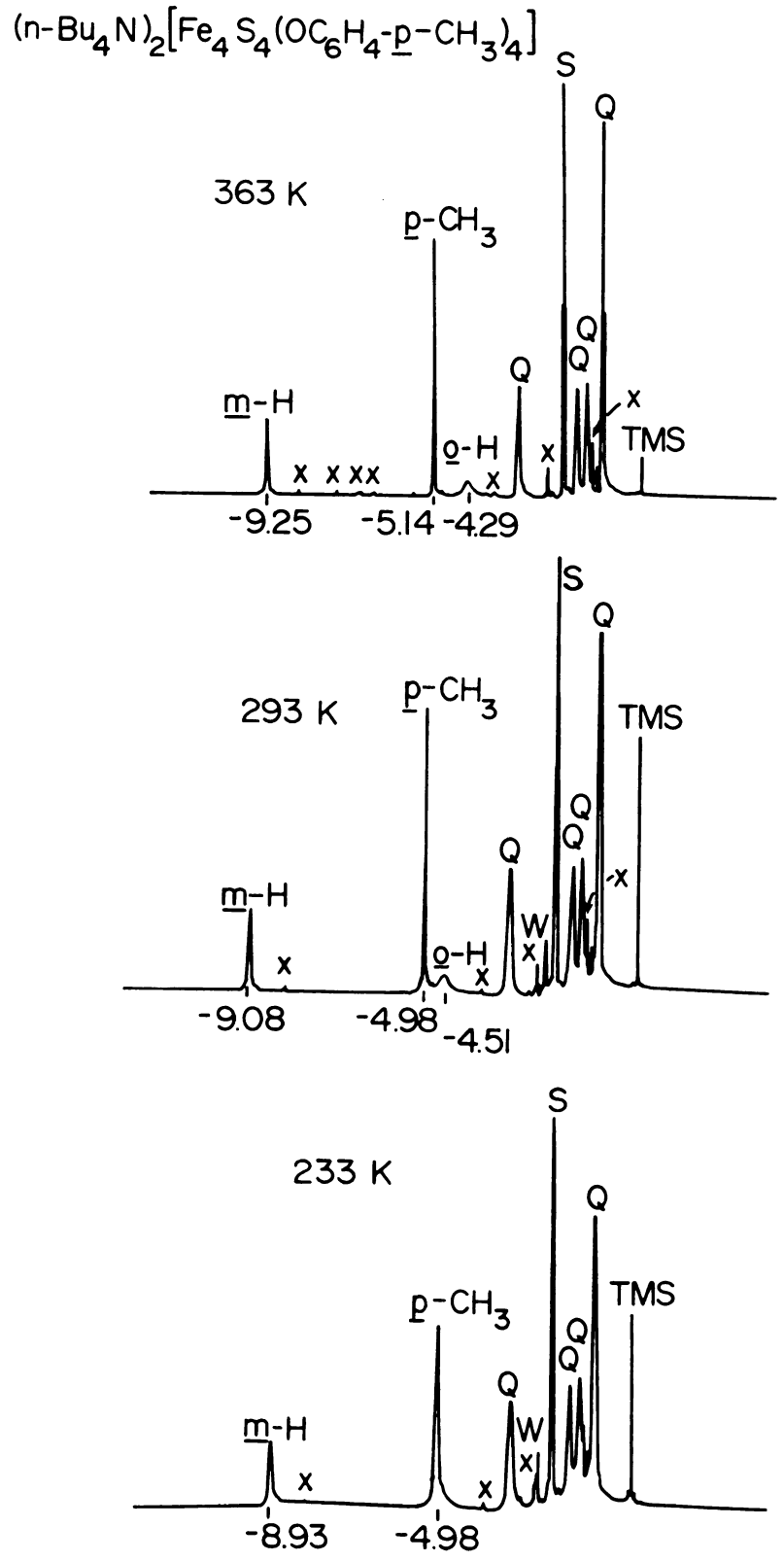
(n-Bu4N)2[Fe4S4(OC6H4-p-CH3)4]
363 K
S
Q
p-CH3
Q
Q
Q
m-H
x
o-H
x
x
x x xx
x
TMS
-9.25
-5.14
-4.29
293 K
S
Q
p-CH3
TMS
Q
Q
Q
m-H
x
W
x
o-H
x
x
-9.08
-4.98
-4.51
233 K
S
Q
p-CH3
TMS
Q
Q
Q
m-H
x
W
x
x
-8.93
-4.98

Figure 13

Figure 14. Temperature dependence of isotropically shifted ligand proton resonances of $(Et_4N)_2[Fe_4S_4(OPh)_4]$ (o) and $(Bu_4N)_2[Fe_4S_4(O\text{-}\underline{p}\text{-}Tol)_4]$ (●) in d_3-MeCN.

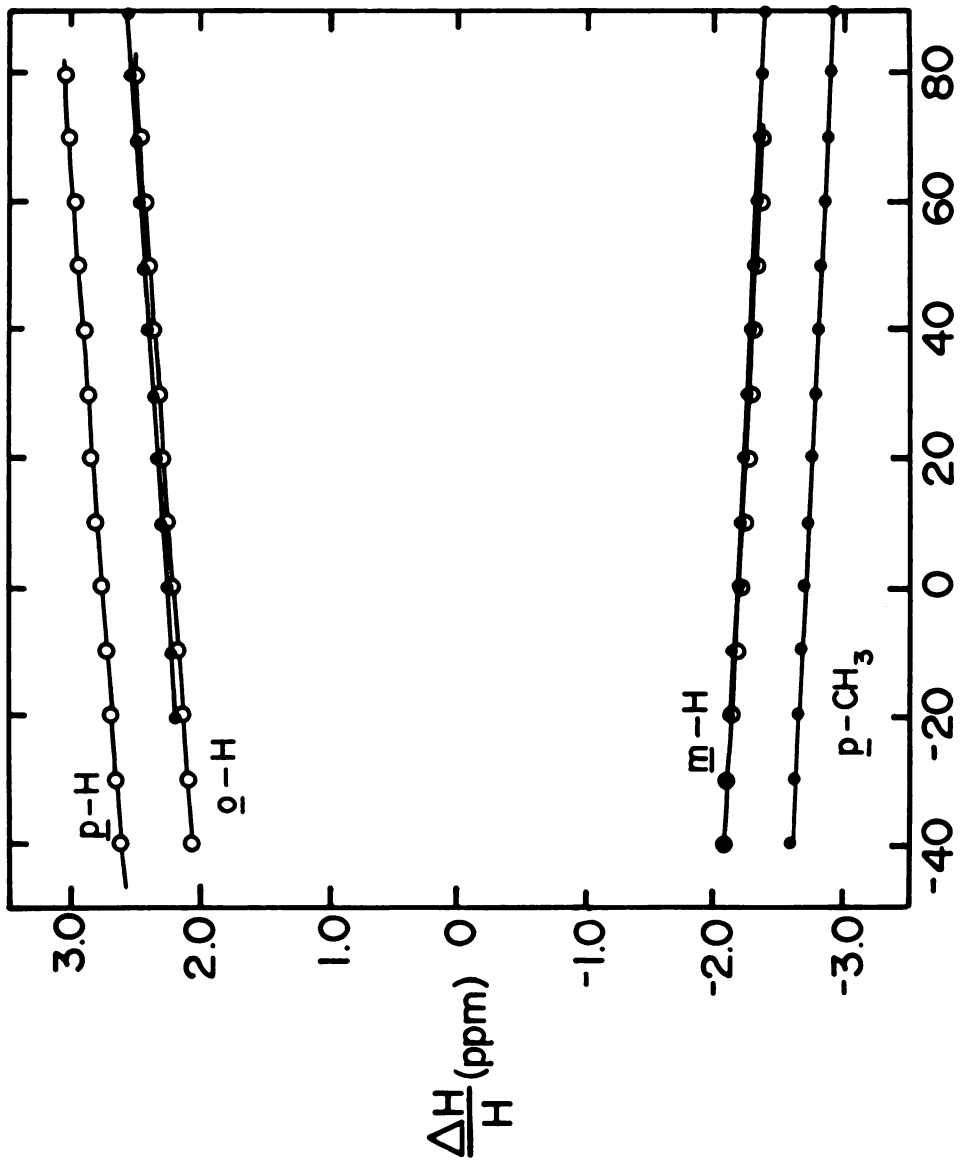

Figure 14

$$\left(\frac{\Delta H}{H}\right)^{\text{contact}} = -\frac{A\gamma_e}{\gamma_H}\frac{gBS(S+1)}{3KT} ,$$

where A is the proton-electron coupling constant, γ_e and γ_H are the gyromagnetic ratios of the electron and proton, respectively; B is the Bohr magneton and g is the nuclear g factor. Thus, the contact shift is proportional to the magnetic susceptibility. The dipolar term[118] is given by:

$$\left(\frac{\Delta H}{H}\right)^{\text{dipolar}} = -(\chi_{||} - \chi_{\perp})\left[\frac{3\cos^2\theta-1}{r^3}\right] ,$$

where $\chi_{||}$ and $\chi_{\perp}$ are the axial and equatorial components of the magnetic susceptibility; θ is the angle between the magnetic axis and the nucleus being observed; and r is the distance between the nucleus and the paramagnetic center. Single crystal magnetic anisotropy measurements are required to evaluate the magnitude of the dipolar term. In practice, however, the r^{-3} dependence[118] can be observed in the NMR spectra. There are two pathways for delocalization of spin onto a ligand, σ and π delocalization[118]. Characteristic features of contact shifted resonance arising from σ delocalization are rapid attenuation of the shifts as the protons become further from the paramagnetic center and non-alternation of the signs of the shifts. Also, replacement of a proton by a methyl

group usually results in a methyl resonance shifted in the same direction but smaller in magnitude than the proton shift. Features of contact shifts resulting from π spin delocalization include: both upfield and downfield shifts which alternate in direction between protons attached to adjacent carbon atoms; insignificant attenuation of the magnitudes of the shifts as the number of bonds between the metal center and the proton is increased; and substitution of a methyl group for a proton affords a shift in the opposite direction and comparable in magnitude to that of the replaced proton. Thus, contact shifts in aliphatic ligands usually arise from σ delocalization while in aromatic ligands contact shifts usually arise mainly from π delocalization.

Dominant contact interactions have been established for the series of complexes[94] $[Fe_4S_4(SR)_4]^{2-}$ where R = alkyl, aryl. All alkyl tetramers show rapid attenuation of the shifts as the number of carbon atoms in the chain are increased. In addition, all shifts are downfield, a situation consistent with antiparallel ligand to metal spin transfer as σ delocalization of the parallel (positive) spin on sulfur would result in negative contact shifts. It should be noted that ligand to metal spin transfer in this system must necessarily be antiparallel, regardless of whether one considers the tetrahedral metal sites as Fe(II) ($e^3t_2^3$) or Fe(III) ($e^2t_2^3$). When R = Ph, high

field shifts are observed for the ortho and para protons while the meta protons are displaced to low field. When R = p-Tol, the ortho and meta protons remain unchanged in sign and magnitude, while the methyl shift at the para position is reversed in sign and comparable in magnitude to that of the replaced proton. Antiparallel ligand to metal spin transfer would leave positive spin on sulfur, which could be delocalized through the π system of the phenyl ring as shown below:

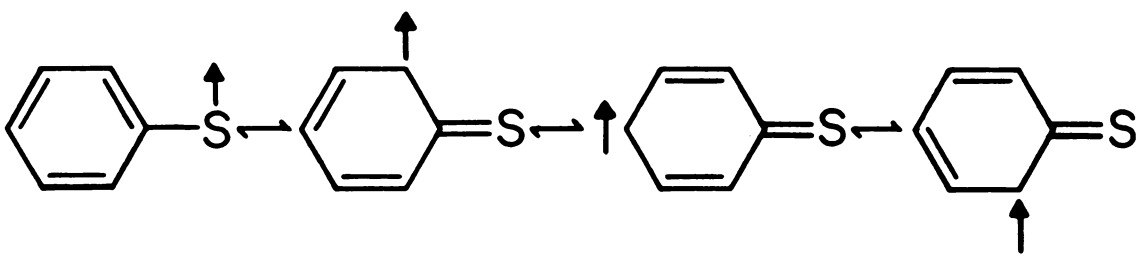

Thus, positive spin would be placed on the ortho and para positions and negative spin at the meta positions would result from spin correlation effects. The results[94] for the mercaptide tetramers, therefore, are consistent with a σ delocalization mechanism when R = alkyl and a π delocalization mechanism when R = aryl.

In the phenoxide tetramer $[Fe_4S_4(OAr)_4]^{2-}$ Ar = Ph the room temperature spectrum shows resonances due to the phenyl protons at -4.16, -4.71 and -9.25 ppm. Assignments are based on relative linewidths and the results of substitution of the p-H by CH_3. The ortho proton resonance at approximately -4.3 to -4.9 ppm is clearly identifiable

by its relatively large linewidth, as dipolar broadening is expected to have an r^{-6} dependence[118]. Upon substitution of the p-H for CH_3, the resonance at -4.16 ppm disappears and is replaced by a signal at -4.9 ppm, with integrated intensity corresponding to three protons. Thus, the resonance at -4.16 ppm is assigned to the p-H, and the resonance at -9.25 ppm must therefore be due to the m-H. The alternation of the signs of the shifts as one proceeds from o-H to m-H to p-H, the lack of attenuation of the shifts with increasing distance from the metal center, and the sign reversal of the CH_3 shift upon replacement of the p-H all suggest that dominant contact interactions with a π delocalization mechanism as described above are responsible for the observed isotropic shifts. These results are qualitatively similar to those observed for the arenethiolate analogs[94] described above. The magnitudes of the shifts relative to those of the meta protons are listed in Table IV. The relative shifts for the para protons are slightly less than the corresponding values for $[Fe_4S_4(SPh)_4]^{2-}$ due to a somewhat larger increase in the meta vs the para shifts, but the general trend para > ortho > meta is obeyed. Since the relative shifts should reflect relative spin densities[94] provided the shifts are contact in origin, the data support the conclusion that dipolar interactions are negligible in these systems.

The only significant difference between the proton NMR

Table IV. Comparison of Relative Isotropic Shifts[a] for Various Metal-Sulfur Centers in CD_3CN Solutions.

Complex	ortho	meta	para
$[Fe_4S_4(SPh)_4]^{2-}$ [b]	1.34	1.00	1.96
$[Fe_4S_4(OPh)_4]^{2-}$	1.04	1.00	1.29
$[Fe_4S_4(SPh)_4]^{3-}$ [c]	h	1.00	1.68
$[Fe_2S_2(SPh)_4]^{2-}$ [d]	1.09	1.00	1.81
$[Fe_2S_2(OPh)_4]^{2-}$	h	1.00	1.27
$[MoFeS_4(SPh)_2]^{2-}$ [e]	1.25	1.00	1.49
$[MoFeS_4(OPh)_2]^{2-}$ [f]	1.03	1.00	1.09
$[Mo_2Fe_6S_8(SEt)_3(SPh)_6]^{3-}$ [g,h]	h	1.00	1.65
$[Mo_2Fe_6S_8(SEt)_3(OPh)_6]^{3-}$	h	1.00	1.30

[a]Relative to meta shift; 22-25°C.

[b]Reference 94.

[c]Reference 137.

[d]Reference 96.

[e]Reference 72.

[f]Reference 81.

[g]Reference 136.

[h]Obscured.

spectra of the phenolate and arenethiolate tetramers is the magnitude of the observed shifts, which at any temperature are approximately twice as large for the phenolate derivative as for the corresponding arenethiolate complex. Since the magnetic properties of the two clusters are virtually identical, the difference must be due to a larger hyperfine interaction in the phenolate complexes. This is consistent with the structural data, which suggest a relatively covalent Fe-O interaction.

The isotropic shifts of the phenyl protons of the phenoxide tetramers are temperature dependent. The data plotted in Figure 14 show that the magnitude of the shifts increases with increasing temperature throughout the temperature range. This behavior parallels the magnetic properties of the clusters, as expected, and is similar to the temperature dependence of the shifts of the corresponding arenethiolate tetramers[94]. These results are again consistent with intramolecular antiferromagnetic coupling.

6. Mossbauer Spectra

The ^{57}Fe Mossbauer spectrum of a solid sample of $(Et_4N)_2[Fe_4S_4(OPh)_4]$ diluted with boron nitride was obtained at 4.2 K. It consists of a single quadrupole doublet with δ = 0.50 mm/s, ΔE_Q = 1.21 mm/s and Γ = 0.32 mm/s. The isomer shift is measured relative to Fe metal at room temperature. The spectrum is shown in Figure 15. Upon

Figure 15. ^{57}Fe Mossbauer spectrum of polycrystalline $(Et_4N)_2[Fe_4S_4(OPh)_4]$ at 4.2 K in zero applied field.

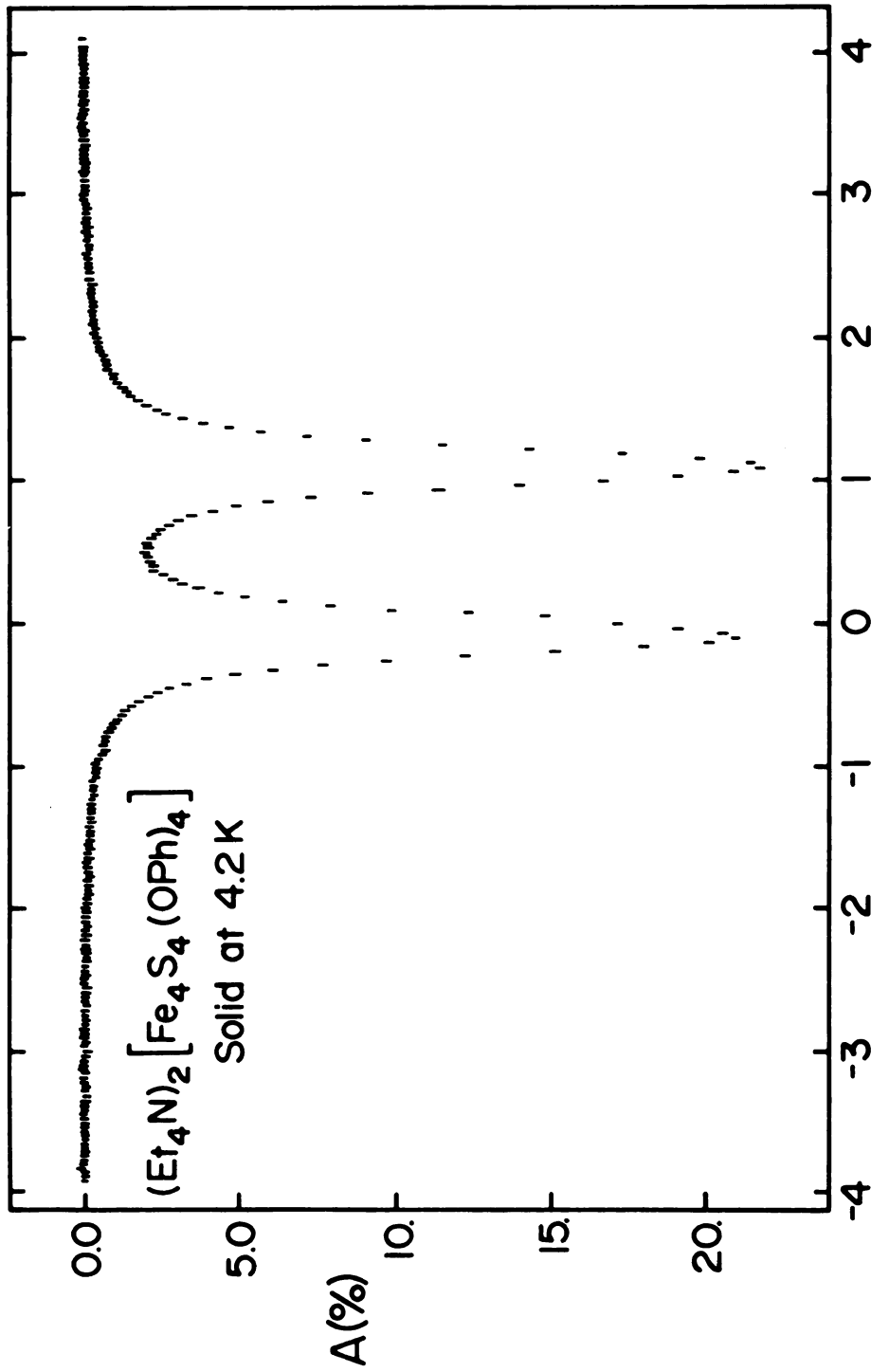

Figure 15

application of a small (~600 G) magnetic field, the spectrum remains essentially unchanged. This result is indicative of a diamagnetic ground state (S = 0) and is consistent with the magnetic susceptibility data. Similar spectra are obtained for both solid and frozen solution samples.

These results are comparable to the arenethiolate clusters[119] under similar conditions, except for the magnitude of the isomer shift, δ. Because the isomer shift of the arenethiolate tetramers have previously been reported relative to that of Fe metal at the same temperature as the sample, the spectrum of $(Et_4N)_2[Fe_4S_4(SPh)_4]$ was remeasured versus Fe metal at room temperature. The following parameters were obtained: δ = 0.46 mm/s and ΔE_Q = 1.20 mm/s. The increased isomer shift for the phenolate tetramer is consistent with increased ferrous character of the iron. This suggests increased electron donation of phenoxide versus thiophenoxide to the Fe_4S_4 core and is consistent with increased covalency in the Fe-O bond relative to the Fe-S bond. This result is somewhat surprising since phenoxide is an inherently poorer electron donor than thiophenoxide, considering the relative oxidizing power of PhOOPh versus PhSSPh. This is consistent, however, with the structural results presented above and electrochemical data discussed below.

7. Electrochemistry

The electrochemical behavior of the phenoxide clusters $[Fe_4S_4(OAr)_4]^{2-}$ (Ar = Ph, p-Tol) were examined by three methods including direct current polarography (DCP), differential pulse polarography (DDP), and cyclic voltammetry (CV). Over the potential range +1.0 to -2.0 V, approximately 1 mM solutions of the complexes in acetonitrile and N-methylpyrrolidinone were used. Both compounds exhibit two well-defined quasireversible one-electron reductions corresponding to sequential generation of the tri- and tetraanions. No evidence for a discrete oxidation process, corresponding to formation of the monoanion, $[Fe_4S_4(OAr)_4]^{-}$, containing the as yet unisolated $[Fe_4S_4]^{3+}$ core, was found. Examples of a typical cyclic voltammogram and differential pulse polarogram are displayed in Figure 16. Data for both complexes as well as for the thiophenolate tetramer in NMP are tabulated in Table V.

Comparison of the data for the well-characterized complexes $[Fe_4S_4(SAr)_4]^{2-}$ (Ar = Ph, p-Tol) with that for the corresponding phenolate tetramers shows that both the 2-/3- and the 3-/4- reduction processes are approximately electrochemically reversible by any method used to examine them. Plots of $\log[i/(i_d-i)]$ vs. potential in all cases yielded slopes acceptably close to the theoretical value of 59 mV for a reversible one-electron process. In DPP, the widths at half-height, $W_{1/2}$, were somewhat less

Figure 16. Cyclic voltammetry and differential pulsed polarography scans for $(Et_4N)_2[Fe_4S_4(OPh)_4]$. Solvents and scan rates are indicated.

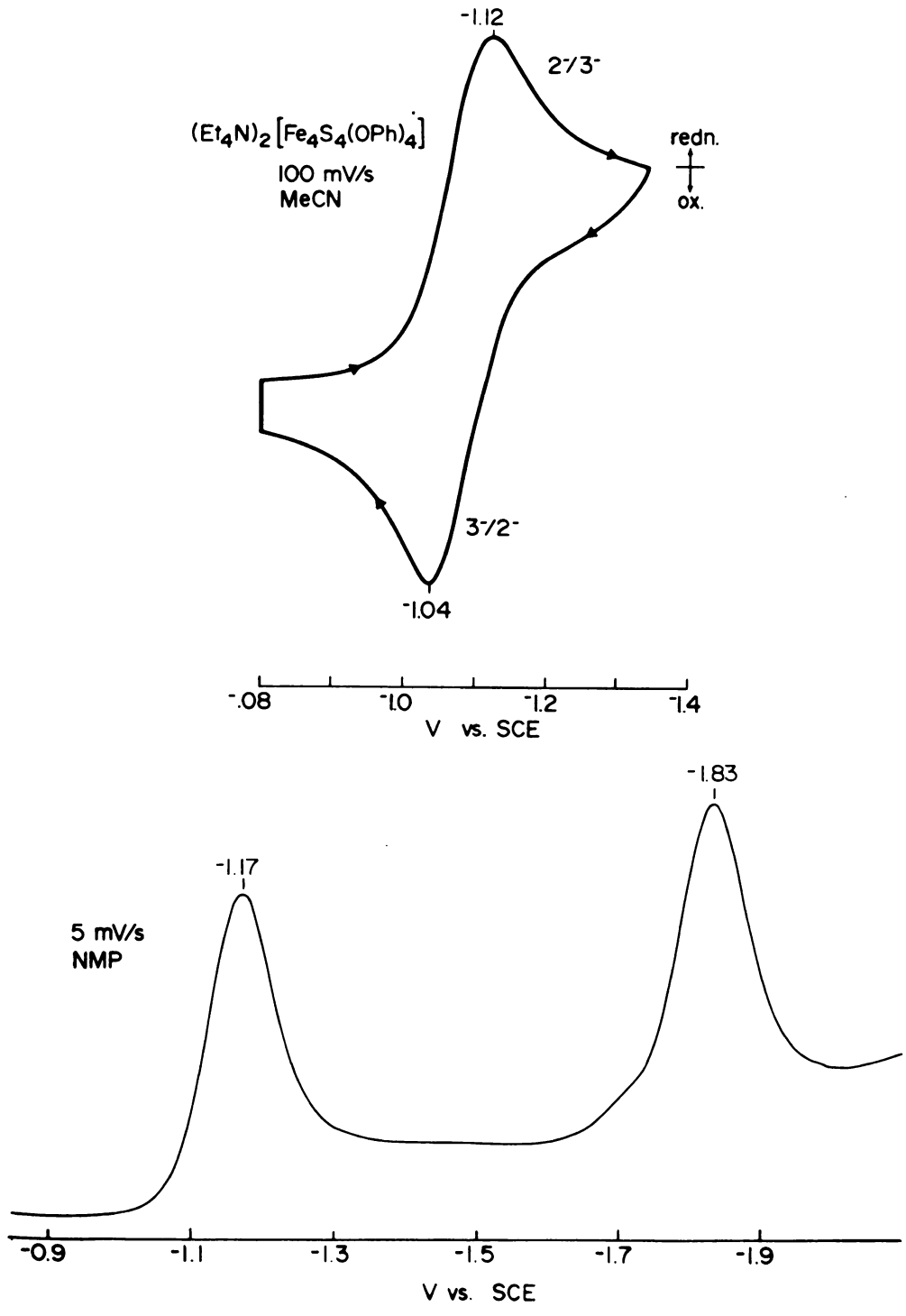
-1.12
2-/3-
(Et4N)2 [Fe4S4(OPh)4]
100 mV/s
MeCN
redn.
ox.
3-/2-
-1.04
-.08
-1.0
-1.2
-1.4
V vs. SCE
-1.83
-1.17
5 mV/s
NMP
-0.9
-1.1
-1.3
-1.5
-1.7
-1.9
V vs. SCE

Figure 16

Table V. Electrochemical Data for $[Fe_4S_4(OAr)_4]^{2-}$ Complexes.

Compound	Solv.	Process	DCP[a] $E_{1/2}$ (V)	DCP[a] Slope (mV)	DCP[a] i_d/C (μA/mM)	DPP[a] E_p(V)	DPP[a] $W_{1/2}$ (mV)	CV[b] E(V)	CV[b] $E_{pc}-E_{pa}$ (mV)	CV[b] i_{ap}/i_{cp}
$[Et_4N]_2[Fe_4S_4(OPh)_4]$	NMP	2-/3-	-1.15	-53	0.91	-1.17	111	-1.14	-132	1.07
	NMP	3-/4-	-1.80	-59	0.93	-1.83	125			
	MeCN	2-/3-	-1.08	-52	2.4			-1.08	- 99	0.97
$[Bu_4N]_2[Fe_4S_4(O\text{-}p\text{-}Tol)$	NMP	2-/3-	-1.19	-49	0.69	-1.20	134	-1.18	-116	0.95
	NMP	3-/4-	-1.83	-53	0.92	-1.85	140			
	MeCN	2-/3-	-1.13	-47	1.67			-1.12	- 93	0.99
	MeCN	3-/4-	-1.84	-52	1.83					
$[Et_4N]_2[Fe_4S_4(SPh)_4]$	NMP	2-/3-	-1.05	-52	1.05	-1.06	125	-0.99	-151	1.00
	NMP	3-/4-	-1.68	-52	0.95	-1.69	119			

[a] 23°C vs SCE; 5 mV/s.

[b] 23°C vs SCE; 100 mV/s.

satisfactory, as the theoretical value for a reversible one-electron reduction is 90 mV. They are acceptable, however, when compared to the arenethiolate analogs measured under identical conditions. In the CV experiments, i_{pa}/i_{pc} values were very close to the theoretical value of 1.0 in all cases. The $E_{pc}-E_{pa}$ values were in accord with those obtained for the corresponding arenethiolate complexes examined under similar conditions and approached the theoretical value of 59 mV at slower scan rates.

As with an extensive series of thiolate tetramers, several solvent and substituent effects are observed. NMP was chosen as it has been suggested that it is capable of stabilizing highly reduced species[120]. Indeed, data for the 3-/4- reduction of the phenolate and thiophenolate tetramers indicate more reversible processes than in MeCN. In addition, the phenolate tetramers are stable in NMP where as they are solvolyzed in DMF, a solvent commonly used for electrochemical studies. As with the thiolate tetramers, there are small (<0.07 V) negative shifts in the reduction potentials in NMP vs. MeCN for the phenolate tetramers. The polarographic diffusion currents are decreased by a factor of two in NMP vs. MeCN, which may be due to the higher viscosity of NMP relative to MeCN. This behavior is also observed in the thiolate tetramers[95] in NMP and in DMF. In fact, data obtained in DMF for the thiophenolate complex, when compared to corresponding

data in NMP, show that $E_{DMF} \simeq E_{NMP}$ as do the slopes and diffusion currents. Substitution of the p-H by CH_3 results in a small (30-50 mV) negative shift in the reduction potentials. This can be explained as a simple inductive effect of the electron releasing methyl group on the phenyl ring and is also observed in the corresponding arenethiolate tetramers[95].

Most importantly, the phenolate tetramers exhibit the same pattern of two one-electron reductions separated by approximately 600 mV that is typical of all $[Fe_4S_4L_4]^{2-}$ clusters[93,95]. The potentials of these reductions are, however, 100 to 150 mV more negative than those of the arenethiolate complexes. Simple electronegativity arguments would predict the phenolate tetramer to be more susceptible to reduction as the more electronegative oxygen atoms should decrease the electron density at the $[Fe_4S_4]^{n+}$ core relative to the thiophenoxide analog, as is observed for the $[Fe_4S_4Cl_4]^{2-}$ [93] and $[Fe_4S_4(OAc)_4]^{2-}$ [121] tetramers. Phenoxide must therefore be capable of transferring more electron density to the $[Fe_4S_4]^{2+}$ core than thiophenoxide. This is consistent with a more covalent Fe-O interaction as suggested by the structural results. Similar behavior has been observed for the $[S_2MoS_2FeL_2]^{2-}$ system where L = SAr[72], OAr[81].

8. Ligand Exchange Reactions

The phenoxide cluster complexes are extraordinarily sensitive to water or other acidic solvent impurities, necessitating rigorous purification procedures for solvents used in synthesis and for spectroscopic characterization. These compounds are not stable for long periods of time in solvent mixtures containing protic solvents such as methanol and ethanol, highly coordinating solvents such as N,N-dimethylacetamide, N,N-dimethylformamide, and dimethylsulfoxide, and to a lesser extent ether solvents such as tetrahydrofuran. They are relatively stable in NMP and MeCN. Whether the observed decomposition is due to direct solvolysis or to reaction with trace acidic impurities is not clear, but the reactivity is comparable to that of the halide ligated clusters $[Fe_4S_4X_4]^{2-}$,[93] where X = Cl, Br, I. Decomposition is accompanied by gradual loss of the longest wavelength feature in the optical absorbtion spectrum and eventual formation of insoluble black precipitates.

The phenolate tetramers also react with electrophiles such as acyl halides, as shown by quantitative formation of $[Fe_4S_4Cl_4]^{2-}$ (demonstrated by optical spectra) and presumably phenyl benzoate upon treatment with four equivalents of benzoyl chloride (reaction 3). This reactivity is completely analogous to the reaction of acyl halides with thiolate ligated tetramers[121], although somewhat surprising

when one considers the lack of known examples of nucleophilic behavior of coordinated oxygen ligands.

$$[Fe_4S_4(OPh)_4]^{2-} + 4PhCOCl \rightarrow [Fe_4S_4Cl_4]^{2-} + 4PhCOOPh \quad (3)$$

Reaction of the phenolate tetramers with thiols such as thiophenol results in immediate and quantitative formation of the thiolate derivative (Reaction 4), as expected from the evident lability of terminal phenolate ligands and the relative acidity of phenols and thiols[101]. Previous investigation of the thiolate tetramer series has demonstrated facile ligand exchange reactions in which coordinated thiolates are sequentially substituted. In this series, substitution tendencies roughly parallel aqueous acidities[101] and arylthiols effect full substitution of alkylthiolate ligated clusters. Further, kinetics data[122] suggest a simple mechanism in which the rate limiting step is protonation of the coordinated ligand followed by rapid separation of alkylthiol and coordination of arylthiolate. The phenolate tetramers fit into this reactivity pattern, as phenol is slightly more acidic than alkylthiols and substantially less acidic than arylthiols. Reaction of phenolate tetramers with arylthiols have been demonstrated by monitoring optical and ^1H NMR spectra of the reaction mixtures.

$$[Fe_4S_4(OAr)_4]^{2-} + 4Ar'SH \rightarrow [Fe_4S_4(SAr')_4]^{2-} + 4ArOH \quad (4)$$

Optical spectra of a solution of $(Et_4N)_2[Fe_4S_4(OPh)_4]$ titrated with 0-5 equivalents of PhSH are shown in Figure 17. The most notable effects of addition of PhSH are a progressive shift in the position of the lowest energy peak to longer wavelength, together with appearance of a peak at approximately 260 nm with the concomitant disappearance of the original peak at 240 nm. Apparant isosbestic points are observed at 408, 398, 297, 290, and 248 nm. The final spectrum obtained upon addition of > 4 equivalents of PhSH is identical to that of the $[Fe_4S_4(SPh)_4]^{2-}$ ion[95] measured separately.

Examination of solutions containing $(Et_4N)_2[Fe_4S_4(OPh)_4]$ are PhSH by ^1H NMR spectroscopy provides more detailed information on the nature of the species present. Selected spectra are displayed in Figure 18. Addition of n equivalents of PhSH ($n \leq 4$) results in the release of n equivalents of free PhOH as estimated by integration of the aromatic resonances of the free PhOH versus the cation peaks. This indicates that, as expected[101], the more acidic thiophenol quantitatively displaces coordinated phenolate. In addition, the isotropically shifted proton resonances of coordinated phenolate decrease in intensity and exhibit multiple peaks. At the same time, new sets of resonances appear at approximately -8.3 (m-H), -5.9 (o-H),

Figure 17. Optical spectra of a 3 m$\underline{M}$ solution of $(Et_4N)_2[Fe_4S_4(OPh)_4]$ in MeCN treated sequentially with 0-5 equivalents of PhSH at 22°C. Optical pathlength: 0.2 mm.

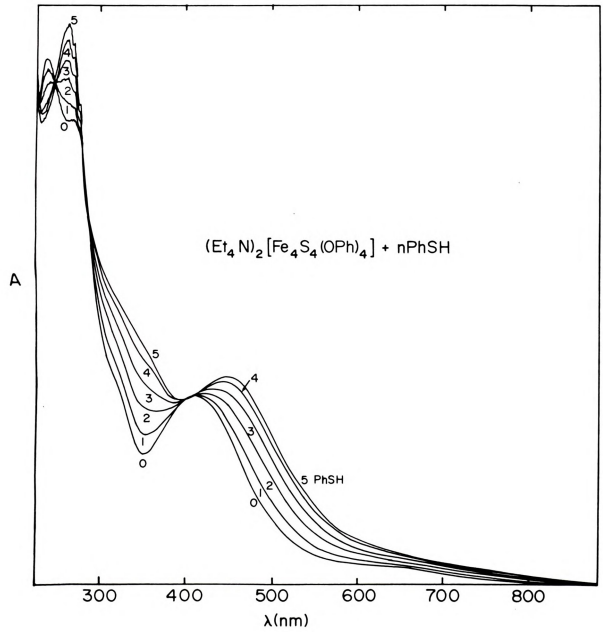
A
$(Et_4N)_2[Fe_4S_4(OPh)_4]$ + nPhSH
5
4
3
2
1
0
5 PhSH
300
400
500
600
700
800
λ(nm)

Figure 17

Figure 18. Proton magnetic resonance spectra (250 MHz) of a 10 m$\underline{M}$ solution of $(Et_4N)_2[Fe_4S_4(OPh)_4]$ treated sequentially with the indicated amounts of PhSH at 22°C. Peaks from protons of the cation are indicated by Q, solvent by S, residual water by W, and unidentified impurities by X. Chemical shifts are in ppm vs. Me_4Si internal standard (TMS).

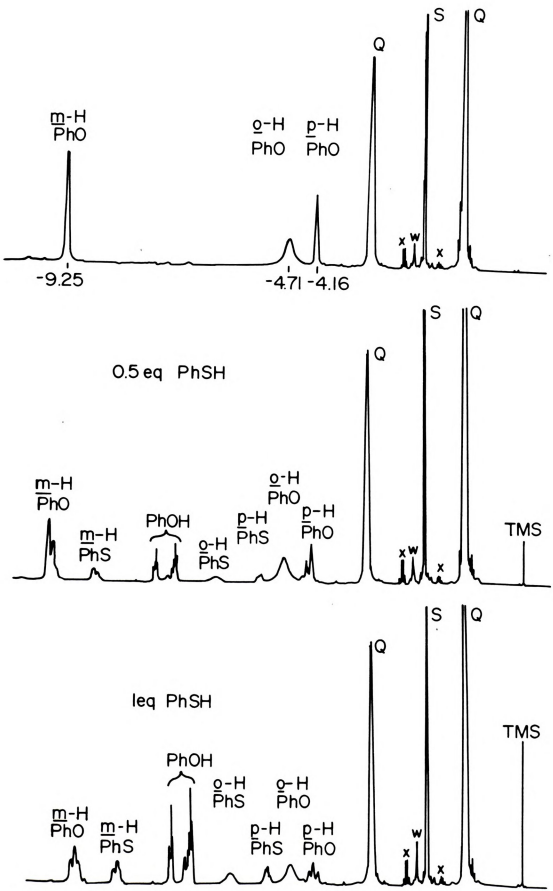
m-H PhO
o-H PhO
p-H PhO
Q
S
Q
x
w
x
-9.25
-4.71
-4.16
0.5 eq PhSH
m-H PhO
m-H PhS
PhOH
o-H PhS
p-H PhS
o-H PhO
p-H PhO
TMS
1eq PhSH

Figure 18

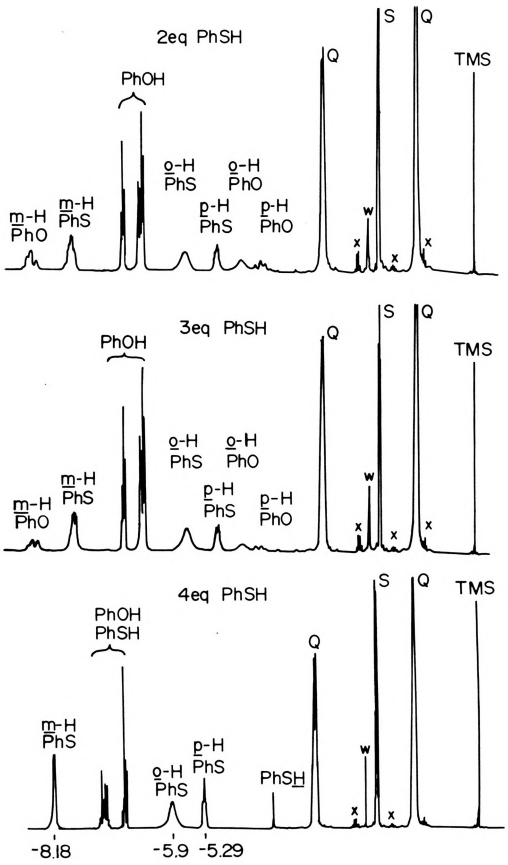
2eq PhSH
PhOH
o-H PhS
o-H PhO
m-H PhO
m-H PhS
p-H PhS
p-H PhO
Q
S
Q
TMS
w
x
x
x
3eq PhSH
PhOH
o-H PhS
o-H PhO
m-H PhO
m-H PhS
p-H PhS
p-H PhO
Q
S
Q
TMS
w
x
x
x
4eq PhSH
PhOH PhSH
m-H PhS
o-H PhS
p-H PhS
PhSH
Q
S
Q
TMS
w
x
x
-8.18
-5.9
-5.29

Figure 18

and -5.2 (p-H) ppm, which correspond to coordinated thiophenolate[94]. The intensity of these sets of multiple peaks vary as n is changed. This variation in intensity of the peaks with PhS/PhO ratio allows the individual peaks to be assigned to the meta and para protons of the ligands in the mixed-ligand species $[Fe_4S_4(OPh)_{4-n}(SPh)_n]^{2-}$ where n = 0-4. Chemical shifts of the mixed ligand tetramers are given in Table VI. The linewidth of the ortho proton signals is greater than their chemical shift differences in the mixed ligand species. No evidence for disruption of the Fe_4S_4 core was observed.

In view of the evidence for relatively covalent Fe-O interactions in $(Et_4N)_2[Fe_4S_4(OPh)_4]$ and the extreme difference in acidities of phenol and thiophenol, one might anticipate the equilibria to favor certain mixed-ligand species at the expense of others. That is, one might expect a non-statistical distribution of ligands among the various species present. The relatively well separated m-H and p-H signals of coordinated phenoxide and thiophenoxide provide a direct method of examining this. Concentrations of each mixed-ligand species were estimated from peak heights of the partially resolved m-H peaks of coordinated phenolate and thiophenolate, assuming that the linewidths for all mixed-ligand species are the same. Their relative areas were determined and compared with the total integrated intensity of each set of peaks

Table VI. Chemical Shifts[a] for Phenoxide and Thiophenoxide Ligands in $[Fe_4S_4(OPh)_{4-n}(SPh)_n]^{2-}$ Species (n= 0,1,2,3,4) in CD_3CN Solution at 22°C.

Proton	n = 0	1	2	3	4
m-H(PhO)	-9.25	-9.17	-9.10	-8.99	-----
p-H(PhO)	-4.15	-4.25	-4.34	-4.45	-----
m-H(PhS)	-----	-8.38	-8.31	-8.25	-8.18
p-H(PhS)	-----	-5.21	-5.24	-5.27	-5.29

[a] vs. TMS (ppm).

measured versus the cation proton resonances as internal standard. Seven individual equilibrium constants, three of which are independent[101], are required to describe the equilibria of this system. The sequential substitution reactions are described by the set of equilibrium constants K_n (n = 0-3).

$$K_n = \frac{[Fe_4S_4(OPh)_{4-(n+1)}(SPh)_{n+1}][PhOH]}{[Fe_4S_4(OPh)_{4-n}(SPh)_n][PhSH]}$$

Since the exact concentration of added thiophenol could not be measured, all of the individual equilibrium constants could not be obtained. The ratios $K_4 = K_0/K_1$, $K_5 = K_1/K_2$ and $K_6 = K_2/K_3$ can be determined independently. These ratios are also the equilibrium constants that represent ligand exchange reactions between tetramers. Experimental values of K_4, K_5, and K_6 obtained at various PhSH/tetramer ratios are given in Table VII. The average values do not differ significantly from those calculated for a statistical distribution of ligands among the various species present. Similar statistical distributions of ligands have been observed for exchange of thiolate ligands with other thiolates[101], and approximately statistical distributions are reported for mixed thiolate-acetate clusters as well[121].

Table VII. Ratios of Equilibrium Constants for PhS-PhO Exchange in CD_3CN Solution at 22°C.

$\frac{[PhSH]}{[Fe_4S_4]}$	K_4	K_5	K_6
	m-H(PhO)		
0.57	2.0	1.5	---
0.89	2.5	2.6	---
1.30	2.5	3.2	---
1.67	2.6	2.8	---
2.17	2.3	2.5	---
2.77	---	2.7	---
	m-H(PhS)		
1.30	---	2.5	3.7
1.67	---	2.5	2.8
2.17	---	2.7	2.5
2.77	---	3.4	2.7
Average	2.4(2)	2.7(4)	2.9(5)
Statistical	2.66	2.25	2.66

9. Fe-S Long Wavelength Compounds

Preparation of an extensive series of substituted phenolate tetramers has been difficult because of a combination of high solubility of the clusters in polar organic solvents, their sensitivity to protic and strongly coordinating solvents, and a tendency to form oils. In an effort to obtain crystalline samples of certain phenolate tetramers, the size of the quaternary cation was varied. In certain of these preparations, a crystalline product with physical properties distinctly different from samples of authentic tetramer salts with the same phenolate were obtained. These materials were recrystallized from MeCN/i-PrOH or MeCN/THF and gave essentially identical spectroscopic properties before and after recrystallization. Specifically, two compounds were obtained both starting with $(R_4N)_2[Fe_4S_4(SR')_4]$ (R' = Et, t-Bu) and either p-$CH_3C_6H_4OH$ or p-ClC_6H_4OH according to Reaction 1 in Section III.A.1. As will be discussed in more detail below, the main absorption band in the optical spectrum of these new compounds is shifted to longer wavelength relative to the corresponding phenolate tetramer; they have therefore been termed 'long wavelength' compounds. The abbreviations Me_4N/O-p-Tol/LW, Et_4N/O-p-Tol/LW and Et_4N/O-p-ClC_6H_4/LW are used to indicate the cation and phenol. Two different salts, Me_4N and Et_4N, of O-p-Tol/LW were obtained in

separate preparations. Materials possessing identical spectroscopic properties have been obtained using the appropriate starting materials and following Reaction 2 (Section III.A.1). By either procedure the yields of these compounds vary between 20 and 50%. Analytical results show N/Fe/S mole ratios of 0.5/1/1 for Me_4N/O-p-Tol/LW and N/Fe/S/Cl ratios of 0.5/1/1/1 for Et_4N/O-p-C_6H_4Cl/LW. These data indicate one $S^=$ and one phenolate per iron atom, consistent with a cluster formulation. Despite extensive efforts, crystals of sufficient quality for X-ray structural analysis have not been obtained.

The optical spectra of $(Bu_4N)_2[Fe_4S_4(O\text{-}p\text{-}Tol)_4]$ and Et_4N/O-p-Tol/LW are shown in Figure 19. Optical data for the two compounds are given in Table VIII. As can be seen in Figure 19, the absorption spectra of Et_4N/O-p-Tol/LW and p-cresolate tetramer are very similar. The major differences are a shift to longer wavelength of the main absorption band by ∿20 nm, while the band at 650 nm in the tetramer spectrum is unresolved in the LW spectrum and the shoulder at ∿282 nm in the tetramer is more fully resolved in the LW complex. Corresponding bands at 424 nm (tetramer) and 435 nm (LW) are tentatively assigned to ligand-to-metal charge transfer.

The magnetic susceptibility of the Me_4N/O-p-Tol/LW compound has been measured at room temperature by the Faraday method. A value of $\chi_g = +8.79 \times 10^{-6}$ cgsu

Figure 19. Electronic absorption spectra of Et_4N/O-p-Tol/LW (——) and $(Bu_4)_2[Fe_4S_4(O\text{-}p\text{-}Tol)_4]$ (---) in acetonitrile solution at 23°C.

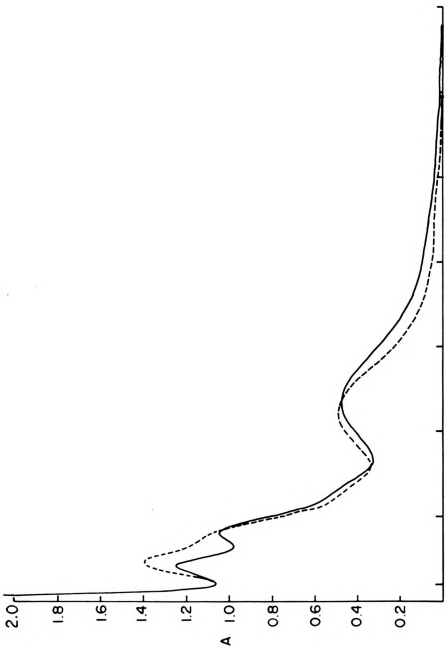

Figure 19

Table VIII. Electronic Spectral Features and Isotropic Shifts of Phenoxide Protons of $[Fe_2S_2(OAr)_4]^{2-}$, $[Mo_2Fe_6S_8(SEt)_3(OPh)_6]^{3-}$ and Fe-S Long Wavelength Complexes.

Complex	Electronic Spectral Features[a], nm	$(\Delta H/H)^{iso}$, ppm[b]
$[Fe_2S_2(OPh)_4]^{2-}$	240(38.7), 280(29.6), 405(12.9),∿500(sh,6.1)	c (o-H) -3.84 (m-H) 4.87 (p-H)
$[Fe_2S_2(O\text{-}p\text{-}Tol)_4]^{2-}$	245(38.5), 284(29.5) 418(13.7), ∿500(sh,8.0)	4.34 (o-H) -3.94 (m-H) -4.60 ($p\text{-}CH_3$)
$[Fe_2S_2(O\text{-}p\text{-}C_6H_4Cl)_4]^{2-}$	248(36.6), 282(23.1) 410(11.0), ∿500(sh,5.0)	c (o-H) -3.63 (m-H)
$[Mo_2Fe_6S_8(SEt)_3(OPh)_6]^{3-}$	233(87.5), 270(74.2), 400(31.3)	c (o-H) -9.66 (m-H) 12.55 (p-H) -16.36 (CH_2)[d]
O-p-Tol/LW	242,282,436	5.56 (o-H) -5.15 (m-H) -6.10 ($p\text{-}CH_3$)
$O\text{-}p\text{-}C_6H_4Cl$/LW	247,280,428	5.32 (o-H) -5.00 (m-H)

[a]Measured in MeCN at 22°C; λ_{max} (ε), nm ($M^{-1}cm^{-1}$ x 10^{-3}). [b]Measured in d_3-MeCN solution at 22°C; shifts vs diamagnetic references, PhOH: -7.02; p-TolOH: -.685, -2.21 ($p\text{-}CH_3$); $p\text{-}ClC_6H_4OH$; -6.87; EtSH: -2.51 (CH_2), -1.27 (CH_3). [c]Obscured. [d]Resonance due to bridging ethanethiolate.

(uncorrected) was obtained. Assuming a formulation as $(Me_4N)_2[Fe_4S_4(O\text{-}\underline{p}\text{-}Tol)_4]$ (molecular weight 928.46) and a ligand correction of -555.7×10^{-6}, a μ_{eff}/Fe of 1.15 BM was calculated. This result is approximately the same as that obtained for authentic p-cresolate tetramer (1.32 BM), suggesting antiferromagnetic coupling and the possibility that the Fe_4S_4 core may be intact.

Proton NMR spectra have been recorded at room temperature for $O\text{-}\underline{p}\text{-}C_6H_4Cl$/LW and as a function of temperature for O-p-Tol/LW complexes in d_3-MeCN solution. In addition to resonances of the cation and residual undeuterated solvent, isotropically shifted resonances due to the phenolate ligands were observed. Room temperature isotropic shift data for the complexes are given in Table VIII. Representative 250 MHz spectra of Et_4N/O-p-Tol/LW at various temperatures are displayed in Figure 20; a plot of isotropic shift vs. temperature for this complex is shown in Figure 21.

The room temperature spectrum for Et_4N/O-p-Tol/LW shows resonances at -12.00, -8.31, and -1.29 ppm. Qualitatively, this spectrum is very similar to the room temperature spectrum of $[Fe_4S_4(O\text{-}\underline{p}\text{-}Tol)_4]^{2-}$ (Figure 13). Assignments are based on this similarity in addition to relative line widths and results of substitution of $\underline{p}\text{-}CH_3$ by p-Cl. The *ortho* proton resonance at approximately -1.29 ppm is clearly identifiable by its relatively large linewidth, as discussed

Figure 20. Proton magnetic resonance spectra (250 MHz) of Et_4N/O-p-Tol/LW in d_3-MeCN solution at various temperatures. Peaks from protons of the cation are indicated by Q, solvent by S, and unidentified impurities by X. Chemical shifts are in ppm from internal Me_4Si (TMS).

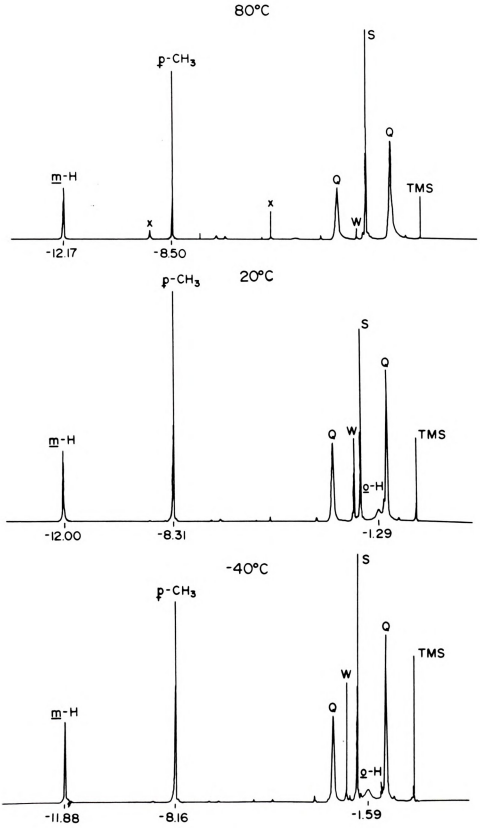
80°C
S
p-CH3
Q
m-H
Q
TMS
x
x
W
-12.17
-8.50
p-CH3
20°C
S
Q
m-H
Q
W
TMS
o-H
-12.00
-8.31
-1.29
-40°C
S
p-CH3
Q
TMS
W
m-H
Q
o-H
-11.88
-8.16
-1.59

Figure 20

Figure 21. Temperature dependence of isotropically shifted ligand proton resonances of Et_4N/O-p-Tol/LW in d_3-MeCN solution.

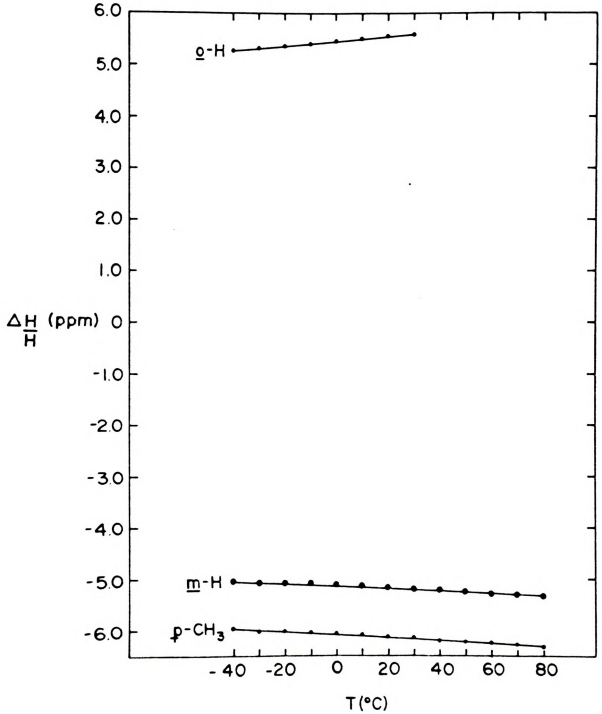
6.0
5.0
4.0
3.0
2.0
1.0
0
-1.0
-2.0
-3.0
-4.0
-5.0
-6.0
ΔH/H (ppm)
o-H
m-H
p-CH3
-40
-20
0
20
40
60
80
T(°C)

Figure 21

in Section III.A.5. Upon substitution of the p-CH_3 group by p-Cl, the resonance at -8.31 ppm disappears and no new resonances are observed. The remaining resonance at -12.00 ppm must therefore be due to the meta protons. This pattern is also observed for the p-cresolate tetramer, which, together with the alternation of the sign of the shift as one proceeds from o-H to m-H and reversal of sign at the p-CH_3 and the lack of attenuation of the shifts with increasing distance from the metal, suggests that dominant contact interactions are responsible for the isotropic shifts of the LW complexes as with the phenolate tetramers.

The only significant difference between O-p-Tol/LW and O-p-Tol tetramer is in the magnitude of the isotropic shifts, which at any temperature are approximately twice (2x) as large for the LW complexes as for the corresponding phenolate tetramer. The isotropic shifts of the O-p-Tol/LW complexes vary with temperature. The data plotted in Figure 21 show that the magnitude of the shifts increases with increasing temperature throughout the temperature range. This behavior should parallel the magnetic behavior of the complex, assuming dominant contact interactions are responsible for the isotropic shifts. These results are similar to those described above for the phenolate tetramers and suggest that the phenolate ligands in the LW complexes are bound to Fe atoms that are antiferromagnetically coupled.

Since the molecular structure of the LW complex is not yet known, these NMR results cannot fully be interpreted. They are, however, qualitatively similar to those obtained for the phenolate and arenethiolate tetramers and suggest that the above interpretation is consistent with the data obtained.

The ^{57}Fe Mossbauer spectrum of polycrystalline Et_4N/O-p-Tol/LW has been measured at 4.2 K in a boron nitride matrix. It consists of a single quadrupole doublet with δ = 0.54 mm/s and ΔEq = 1.12 mm/s. The spectrum is shown in Figure 22. Application of a small ($\sim$600 G) magnetic field results in essentially no change in the spectrum suggesting a diamagnetic ground state. In addition, the isomer shift and quadrupole splitting are not significantly different from those obtained for $(Et_4N)_2[Fe_4S_4(OPh)_4]$ under the same conditions. These data indicate that the LW compound possesses an intact $(Fe_4S_4)^{2+}$ core or at the least a single iron environment with very similar ligand set and oxidation level. These results are consistent with the proton NMR data described above.

The electrochemical properties of the LW compounds have been measured by DC polarography (DCP) and differential pulse polarography (DPP) and also by cyclic voltammetry (CV) at glassy carbon and Pt flag electrodes. Approximately 1-2 m<u>M</u> concentrations were used, based on their formulation as tetrameric species. Measurements were

Figure 22. ^{57}Fe Mossbauer spectrum of polycrystalline Et_4N/O-p-Tol/LW at 4.2 K in zero applied field.

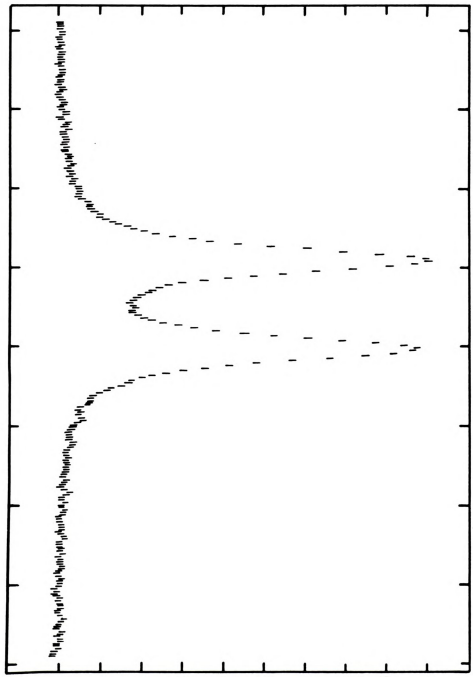

Figure 22

performed in NMP solution over the potential range +1.0 V to -2.5 V. Both O-p-Tol/LW and O-p-C_6H_4Cl/LW exhibit three reductions. No evidence for a discrete oxidation process was found. Electrochemical data are collected in Table XIX. Representative differential pulse polarograms and cyclic voltammograms of both complexes are displayed in Figure 23.

This electrochemical behavior of the LW compounds is in contrast to the corresponding phenolate tetramers that exhibit two reductions over the same potential range. Examination of the DCP and DPP results show that the first two reductions of the LW complexes have about the same potential separation (~600 mV) and approximately the same potentials as the corresponding processes for the phenolate tetramers. Specifically, the potential of the first reduction of O-p-Tol/LW is within 10 mV of the 2-/3- reduction of O-p-Tol tetramer and the potential of the second reduction of O-p-Tol/LW is approximately 120-130 mV more negative than the 3-/4- potential of O-p-Tol tetramer. In addition, the slope and $W_{1/2}$ values for both reductions are reasonably close to the values obtained for the O-p-Tol tetramer, indicating quasireversible one electron processes. It should also be noted that i_d/C values for the first reduction at least are in good agreement with corresponding values of the phenolate tetramers, suggesting that the formulation of LW compounds as Fe_4S_4 species is not unreasonable.

Table XIX. Electrochemical Data for $[Fe_2S_2(OAr)_4]^{2-}$, $[Mo_2Fe_6S_8(SEt)_3(OPh)_6]^{3-}$, and Fe-S Long Wavelength Complexes.

		DCP[a,b]			DPP[a,b]		CV[a,c]	
Complex	Process	$E_{1/2}$ (V)	Slope (mV)	i_d/C (uA/mM)	E(V)	$W_{1/2}$ (mV)	E_{pc} (V)	$E_{pc}-E_{pa}$ (mV)
$Fe_2S_2(OPh)_4]^{2-}$	2-/3-	-1.35	-75	0.94	-1.39	250	-1.38	
	3-/4-	-1.85	-93	1.14	-1.90	225	-1.95	
$[Fe_2S_2(O\text{-}\underline{p}\text{-}Tol)_4]^{2-}$	2-/3-	-1.38	-54	0.86	-1.42	180	-1.52	
	3-/4-	-1.73	-43	0.94	-1.76	135	-1.94	
$[Fe_2S_2(O\text{-}\underline{p}\text{-}C_6H_4Cl)_4]^{2-}$	2-/3-	-1.26	-52	1.54	-1.29	140	-1.41	
	3-/4-	-1.65	-51	1.84	-1.69	125	-1.85	
$[Mo_2Fe_6S_8(SEt)_3(OPh)_6]^{3-}$	3-/4-				-1.14	121	-1.13[g]	
	4-/5-				-1.33	120	-1.31[g]	108
O-$\underline{p}$-Tol/LW		-1.18	-50	1.06[d]	-1.19	132	-1.21[g]	130
		-1.70	-36	1.30[d]	-1.73	123	-1.76	
		e	e	e	-1.99	e	-2.15	
O-$\underline{p}$-C_6H_4Cl		-1.10	-55	0.91[d]	-1.12	e	-1.20[g]	250
		-1.72	-51	1.84[d]	-1.73	143	-1.93	
		-2.01	-78	2.15[d]	-2.04	144	-2.15[g]	200

[a]In NMP solution at 23°C vs SCE; all are average values of 3 scans. [b]5 mV/s; 2 drops/sec. [c]100 mV/s. [d]1-2 mM solutions based on formulation of the complex as an Fe_4S_4 tetramer. [e]Maxima distorted. [f]In MeCN solution. [g]E_o (V).

Figure 23. Cyclic voltammograms (above) and differential pulse polarograms (below) of Et_4N/O-p-C_6H_4Cl/LW and Me_4N/O-p-Tol/LW in NMP. Cyclic voltammetry was performed at glassy carbon electrode at 100 mV/s. DPP was performed at DME at 5 mV/s.

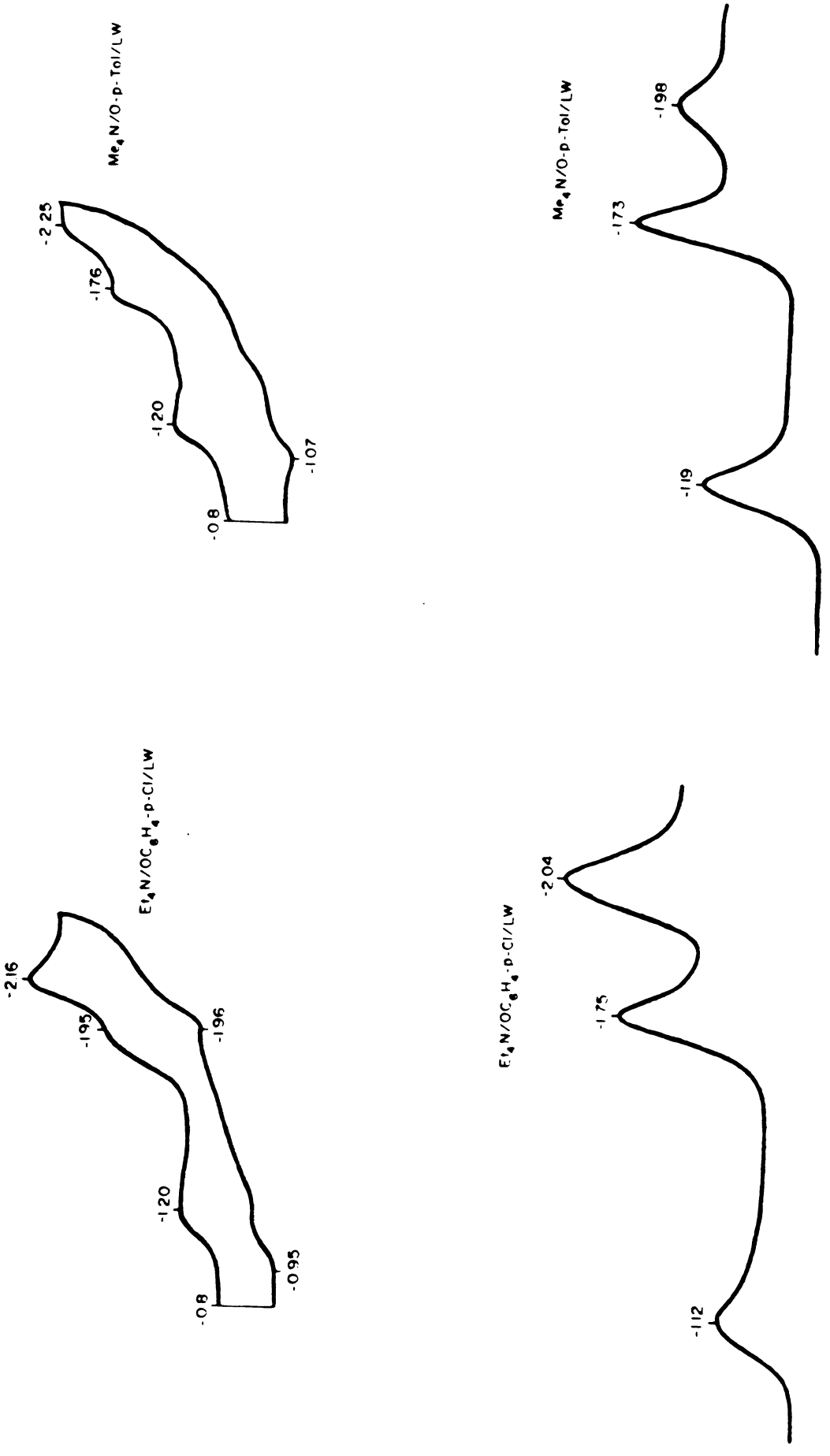
Me4N/O-p-Tol/LW
-225
-176
-120
-107
-08
Me4N/O-p-Tol/LW
-173
-198
-119
Et4N/OC6H4-p-Cl/LW
-216
-195
-196
-120
-095
-08
Et4N/OC6H4-p-Cl/LW
-204
-175
-112

Figure 23

Cyclic voltammetry of the LW compounds are somewhat less satisfactory. The anodic peaks are relatively ill defined, suggesting irreversible processes. The reverse waves for the first reductions, however, are fairly well developed and $E_{p_c} - E_{p_a}$ for O-p-Tol/LW is within 5 mV of the corresponding value of the first reduction for O-p-Tol tetramer.

These data suggest that the LW complexes may have an intact $[Fe_4S_4]^{2+}$ core with the first two reductions corresponding to the 2+/1+ and 1+/0 core oxidation level processes respectively. The third reduction is of unknown origin but may be due to a multiple electron ligand reduction.

In an effort to obtain more detailed information on the nature of the LW complexes, a ligand exchange reaction was performed and monitored by proton NMR. Solutions containing Et_4N/O-p-C_6H_4Cl/LW and PhSH in various ratios were examined. Selected spectra are presented in Figure 24.

As with the phenolate tetramers, addition of PhSH results in release of free p-ClC_6H_4OH, shown by the appearance of appropriate peaks at ∿-7 ppm, and a decrease in intensity of the isotropically shifted resonances of coordinated O-p-C_6H_4Cl ligands. In contrast to the phenolate tetramer system, however, no multiple peaks or new resonances are observed over the range -17 ppm to +1 ppm. Based on the formulation of O-p-C_6H_4Cl/LW as

Figure 24. Proton magnetic resonance spectra (250 MHz) of a solution of $Et_4N/O\text{-}\underline{p}\text{-}C_6H_4Cl$/LW treated sequentially with the indicated amounts of PhSH at 22°C. Peaks from protons of the cation are indicated by Q, solvent by S, and residual water by W. Chemical shifts are in ppm vs. Me_4Si internal standard (TMS).

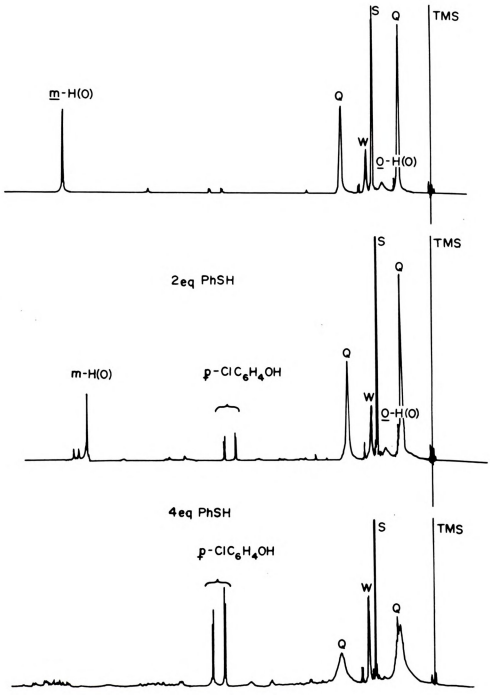

Figure 24

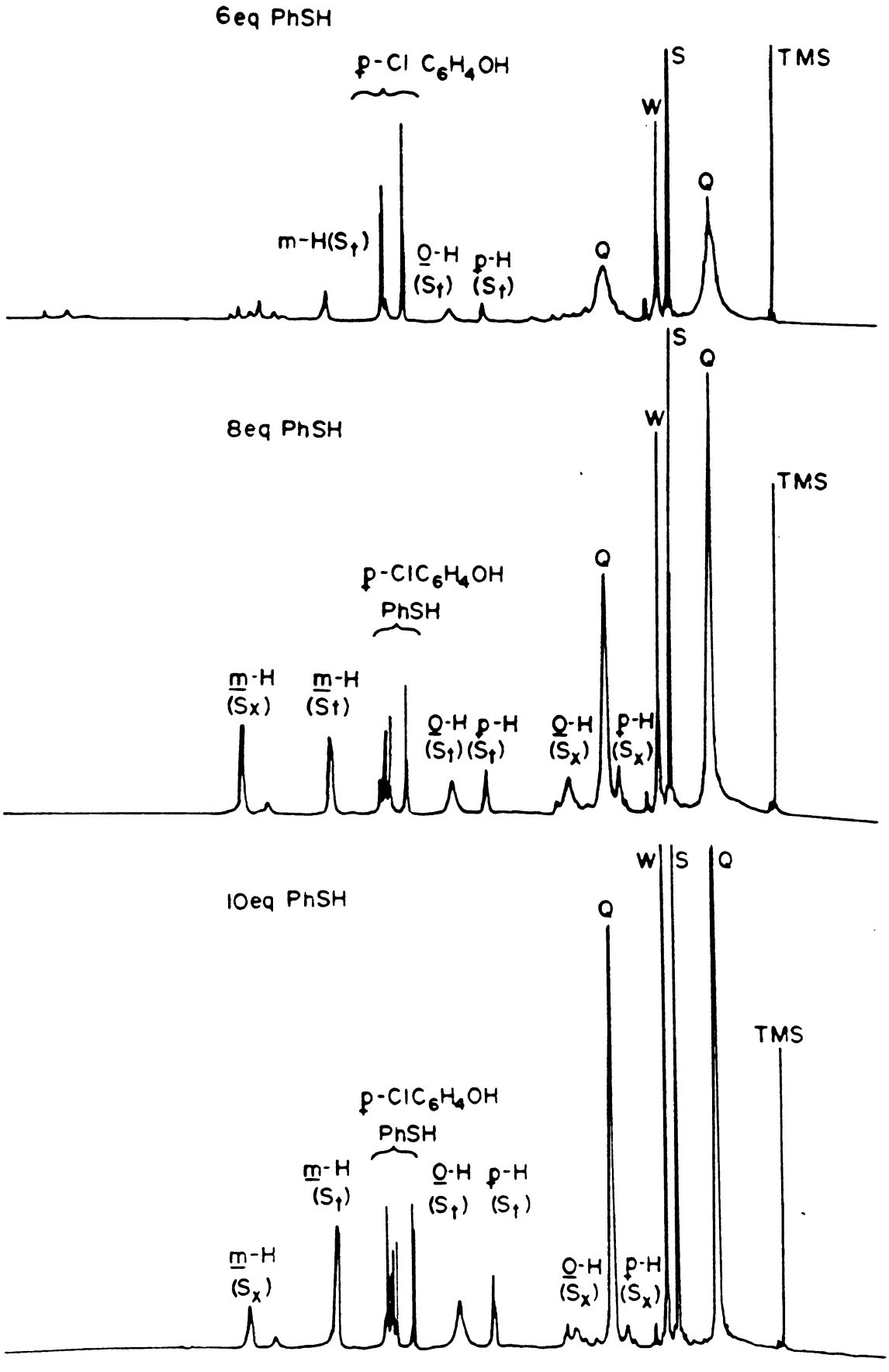
6eq PhSH
p-Cl C6H4OH
S
TMS
W
Q
m-H(St)
o-H (St)
p-H (St)
Q
8eq PhSH
S
Q
W
TMS
p-ClC6H4OH
PhSH
Q
m-H (Sx)
m-H (St)
o-H (St)
p-H (St)
o-H (Sx)
p-H (Sx)
10eq PhSH
W
S
Q
Q
TMS
p-ClC6H4OH
PhSH
m-H (St)
o-H (St)
p-H (St)
m-H (Sx)
o-H (Sx)
p-H (Sx)

Figure 24

$(Et_4N)_2[Fe_4S_4(O\text{-}p\text{-}C_6H_4Cl)_4]$, four equivalents of PhSH, which should quantitatively convert their species to $[Fe_4S_4(SPh)_4]^{2-}$, result in essentially complete extinction of all isotropically shifted resonances in the chemical shift range examined (-17 to +1 ppm). In addition, the cation resonances are greatly broadened with respect to their linewidth at 0 eq. PhSH, which may suggest either a change in the magnetic properties of the species present or aggregation. At 6 eq. PhSH, resonances due to $[Fe_4S_4(SPh)_4]^{2-}$ appear but not as multiple peaks, which suggests no coordinated $O\text{-}p\text{-}C_6H_4Cl$ is present. At 8 eq. PhSH, two sets of isotropically shifted resonances in approximately a 1:1 ratio are apparent. One set clearly corresponds to $[Fe_4S_4(SPh)_4]^{2-}$, and the other set corresponds to no known Fe-S cluster. At the same time, resonances due to free PhSH appear for the first time, indicating that the titration is complete. Two additional equivalents of PhSH result in further reaction to produce substantial quantities of thiophenolate tetramer. Presumably a new Fe-S complex was produced between 6 and 8 equivalents of added PhSH, which subsequently reacted with excess PhSH to yield thiophenolate tetramer. These results argue against the formulation of the LW complexes as Fe_4S_4 moieties and suggest a higher nuclearity, presumably between six and eight.

The results presented in this section provide no real structural information but suggest an antiferromagnetically coupled Fe-S cluster with a nuclearity of 4, 6, 7, or 8 and

a single iron environment very similar to an $[Fe_4S_4]^{2+}$ core and ligated by one phenolate per iron atom. Indeed, most of the evidence seems to su-port an Fe_4S_4 core with terminal ligation different from "authentic" phenolate tetramer. However, one possible structure which would seem to accommodate the observed data is the hexameric formulation $[Fe_6S_6(OAr)_6]^{3-}$ shown below. Very recently, the clusters $[Fe_5S_6Cl_6]^{3-}$ [138] and $[Fe_6S_6I_6]^{2-}$ [139] have been prepared. Structural and physical properties reported for these complexes are consistent with the structure proposed above for the LW complexes. Further interpretation of the data presented above must await an X-ray crystal structure.

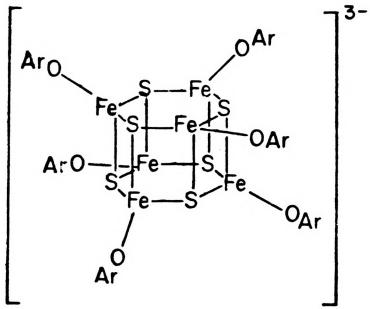

10. Summary

The phenolate substituted Fe_4S_4 clusters can be prepared and isolated in crystalline form as their tetraalkylammonium salts. Coordination of phenoxide ligands to

tetranuclear iron-sulfur clusters in place of arenethiolates gives the expected shift of optical spectral features to shorter wavelengths and has minimal effect on the magnetic properties of the $[Fe_4S_4]^{2+}$ core. Structural results showing somewhat shorter Fe-O bonds than expected, increased ^{57}Fe Mossbauer isomer shifts and isotropic shifts of ligand protons, and negative shifts of first and second reduction potentials all suggest that phenoxide ligands are capable of donating substantial electron density to the $[Fe_4S_4]^{2+}$ core, presumably via a relatively covalent Fe-O bond. This is not, however, reflected in any special stability of the phenoxide species, which are solvolyzed rapidly by substances with acidic protons. They also react with electrophilic reagents and can be converted to the chloro and thiophenolate analogues by addition of PhCOCl and PhSH, respectively. In addition, certain preparations have provided another species of as yet unknown structure that possesses related but distinctly different physical properties.

These results, in particular the effect of phenoxide ligation on cluster redox properties, have certain biological implications. In nonaqueous solvents, phenoxide-ligated tetramers exhibit reduction potentials in the same range as tetramers with simple alkanethiolate ligands[95]. Previous work[123,124] has shown that incorporation of hydrogen-bonding functionalities such as peptide linkages into the

ligands and use of mixed aqueous-organic solvents result in substantial positive shifts of the reduction potentials of thiolate tetramers, bringing them into the same range as is observed for small [4Fe-4S] ferredoxins under comparable conditions. Although the phenoxide tetramers are solvoltically unstable and therefore cannot be examined in aqueous-organic solvent systems, the present results suggest that substitution of a cysteinyl thiol ligand to a [4Fe-4S] center in a protein by tyrosyl phenoxide should have only a minor effect on redox potentials. This is in contrast to other possible oxygen donors such as carboxylate from an aspartate or glutamate residue, for which substantial positive shifts (up to 400 mV) in reduction potentials are expected. Tyrosyl ligation would thus furnish a means of generating a reactive coordination site with minimal perturbation of cluster reduction potentials, possibly providing a site for interaction of a reducible substrate with the [4Fe-4S] core. Finally, the lability of coordinated phenoxide- and alkylthiolate-coordinated [4Fe-4S] clusters would seem to preclude detection of phenoxide for carboxylate ligation by cluster displacement methods[17,125] or by simple optical spectroscopy. Recent crystallographic results on a 7Fe-ferredoxin from Azobacter vinlandii[87] and EXAFS studies on a 3Fe-ferredoxin from Desulfovibrio gigas[88] suggest that one of the ligands to the 3Fe-3S center in each may be an oxygen donor,

tentatively identified as a water molecule in the former. Very recently the first strong evidence for the presence of cluster ligands other than cysteine in an Fe-S protein has been reported for the Rieske protein[140] from Thermus thermophilus.

B. $[Fe_2S_2(OAr)_4]^{2-}$ (Ar = Ph, p-Tol, p-C_6H_4Cl)

1. Synthesis

The phenolate dimer complexes, $(R_4N)_2[Fe_2S_2(OAr)_4]$ (Ar = Ph, p-Tol, p-C_6H_4Cl), can be synthesized by either of two methods. One method involves a direct "spontaneous self-assembly" reaction from simple starting materials, and the second a ligand exchange reaction of a preformed Fe_2S_2 cluster. Addition of one equivalent of tetraalkylammonium chloride to an acetonitrile solution of $FeCl_3$ affords a pale yellow solution, presumably due to formation of $FeCl_4^-$ (produced by Reaction 5). Addition of the appropriate anhydrous sodium phenolate (Reaction 6) causes a color change to bright red corresponding to formation of $[Fe(OAr)_4]^-$ (verified by optical spectra). Addition of Li_2S results in formation of $[Fe_2S_2(OAr)_4]^{2-}$ (Reaction 7), which is isolated as its tetraalkylammonium salt in moderate (~50%) yield after recrystallization. These materials are stable in the solid state and in solution in the absence of oxygen and water; they are extremely soluble in polar aprotic solvents, which makes purification

and isolation in high yields difficult.

$$R_4NCl + FeCl_3 \rightarrow (R_4N)FeCl_4 \quad (5)$$

$$(R_4N)FeCl_4 + 4\ NaOAr \rightarrow (R_4N)[Fe(OAr)_4] \quad (6)$$

$$(R_4N)[Fe(OAr)_4] + Li_2S \rightarrow (R_4N)_2[Fe_2S_2(OAr)_4] \quad (7)$$

Reaction of a slight excess of the appropriate anhydrous sodium phenolate with $[Fe_2S_2Cl_4]^{2-}$ in acetonitrile at ambient temperatures effects full substitution of the terminal chloride ligands with phenolate ligands (Reaction 8).

$$[Fe_2S_2Cl_4]^{2-} + 4\ NaOAr \rightarrow [Fe_2S_2(OAr)_4]^{2-} + 4\ NaCl \quad (8)$$

This method takes advantage of the insolubility of NaCl in acetonitrile to drive the reaction to completion and is analogous to the corresponding method used to prepare $[Fe_4S_4(OAr)_4]^{2-}$ salts (Section III.A.1.). Phenolate dimer salts prepared by this method are of comparable purity and obtained in yields comparable to or greater than those found for the first method of preparation. The first method of preparation is in general the most convenient as it is a "one pot" synthesis, which avoids the necessity of preparing the air-sensitive precursor, $[Fe_2S_2Cl_4]^{2-}$.

A new preparation of $[Fe_2S_2Cl_4]^{2-}$ can be realized by a modification of the first method described above. One equivalent of anhydrous Li_2S is allowed to react with $[FeCl_4]^-$ affording $[Fe_2S_2Cl_4]^{2-}$, is isolated as its tetraalkylammonium salt in ~50% yield after recrystallization. This represents a two fold improvement in the total yield of this complex over the traditional synthetic route: reaction of $[Fe_2S_2(SR)_4]^{2-}$ (50% starting from $FeCl_3$) and acyl chlorides to give $[Fe_2S_2Cl_4]^{2-}$ (50%; total of 25% from $FeCl_3$).

2. X-ray Crystal Structure

The crystal structure of $(Bu_4N)_2[Fe_2S_2(OPh)_4]$ has been solved and consists of discrete cations and anions. At the present level of refinement (R = 12%), the anion exhibits disorder in one of the phenolate ligands coordinated to each iron atom. A schematic representation of the anion showing selected interatomic distances and angles is presented below.

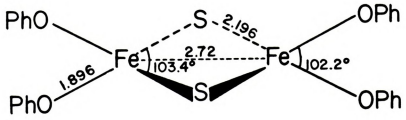

Although the structure has not yet been fully refined, several important aspects of the structure, which should change only slightly upon further refinement, are evident and will be discussed here.

$(Bu_4N)_2[Fe_2S_2(OPh)_4]$ is the fifth compound possessing the $[Fe_2S_2]^{2+}$ core to be structurally characterized. The other complexes, with the general formula $[Fe_2S_2X_4]^{2-}$, include X = S-p-Tol[97], Cl[102] and X_2 = S_2-o-xylyl[97], S_5[126]. Comparative structural data for complexes possessing the same Fe_2S_2 core are given in Table X. Each of the two Fe^{3+} centers in the $[Fe_2S_2(OPh)_4]^{2-}$ dianion is coordinated by two bridging $S^{=}$ ions and by two terminal phenolate ligands in a distorted tetrahedral arrangement. The dimeric structure can be described as resulting from two distorted tetrahedra sharing an S...S edge. The Fe_2S_2 core is planar, with an Fe-Fe distance (2.72 Å) sufficiently short to afford a stabilizing metal-metal interaction and a S-S distance (3.45 Å) far too long for any significant bonding between these two atoms. These results are very similar to corresponding results obtained for the other complexes possessing the $[Fe_2S_2]^{2+}$ core. Indeed, as the results in Table IX show, all interatomic distances and angles pertaining to the Fe_2S_2 core geometry are essentially the same. This provides additional support to the conclusion that the mean dimensions of the Fe_2S_2 core are nearly independent of the nature of the terminal ligands.

Table X. Comparison of Average Bond Distances (Å) and Angles (deg) for Compounds with the $[Fe_2S_2]^{2+}$ Core.

Distance or Angle	$[Fe_2S^*{}_2(S_2\text{-o-xyl})_2]^{2-}$ [a]	$[Fe_2S^*{}_2(S\text{-p-tol})_4]^{2-}$ [a]	$[Fe_2S^*{}_2Cl_4]^{2-}$ [b]	$[Fe_2S^*{}_2(S_5)_2]^{2-}$ [c]	$[Fe_2S^*{}_2(OPh)_4]^{2-}$
Fe...Fe'	2.698	2.691	2.716	2.701	2.72
Fe-S*	2.209	2.201	2.201	2.192	2.196
Fe-X[d]	2.305	2.312	2.252	2.302	1.896
S...S	3.498	3.483	3,463	3.453	3.45
S*-Fe-S*'	104.7	104.6	103.8	104.0	103.4
Fe-S*-Fe'	75.3	75.4	76.2	76.1	76.0
X(1)-Fe-X(2)[d]	106.4	111.2	105.4	-----	102.2

[a] Reference 97.

[b] Reference 102.

[c] Reference 126.

[d] Terminal ligand.

This result is also consistent with corresponding observations regarding $[Fe_4S_4]^{2+}$ cores as described for $[Fe_4S_4(OPh)_4]^{2-}$ in Section III.A.2. These results are also consistent with the magnetic susceptibility data described below.

The major structural difference between $[Fe_2S_2(OPh)_4]^{2-}$ and the other complexes of the Fe_2S_2 family is the presence of Fe-O bonds. The average Fe-O bond distance is 1.896 Å. This is somewhat longer than expected for an Fe^{3+} phenoxide bond, based on the Fe-O distances found for $Fe(OAr)_4^-$ [89] (1.847 (13) Å for Ar = 2,3,5,6-Me_4C_6H, 1.866 (6) Å for Ar = 2,4,6-$Cl_3C_6H_2$) and is closer to that found for the Fe-O bond in $[MoFeS_4(OPh)_2]^{2-}$ [81] (1.897 (13) Å) where the iron atom is formally Fe^{2+}. This may, however, be a result of the disorder in the dianion, and the Fe-O bond length may decrease upon further refinement. For this reason, the chemical significance of this structural feature is difficult to assess. The physical data described below, however, are consistent with a rather strong Fe-O interaction analogous to the results obtained for the $[Fe_4S_4(OAr)_4]^{2-}$ ions presented in Section III.A.

3. Electronic Absorption Spectra

The optical spectra of $[Fe_2S_2(OPh)_4]^{2-}$ and $[Fe_2S_2(SPh)_4]^{2-}$ are shown in Figure 25. Comparative spectral data for the p-Tol and p-C_6H_4Cl analogs are given in Table VIII.

Figure 25. Electronic absorption spectra of the $[Fe_2S_2(OPh)_4]^{2-}$ (——) and $[Fe_2S_2(SPh)_4]^{2-}$ (---) ions in acetonitrile solution at 22°C.

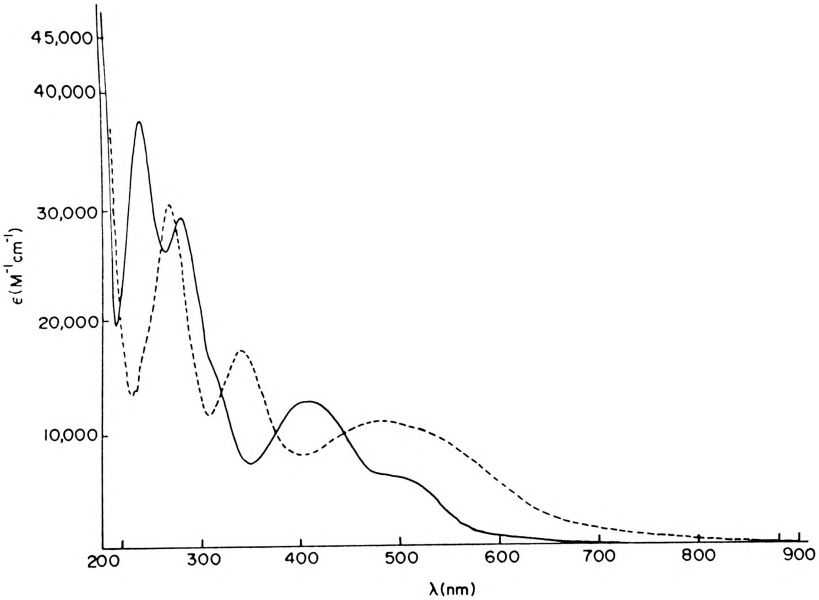
45,000
40,000
30,000
20,000
10,000
ε(M⁻¹cm⁻¹)
200
300
400
500
600
700
800
900
λ(nm)

Figure 25

The spectra presented in Figure 25 clearly show a qualitative similarity. Both have strong absorption maxima in the 400-500 nm range, each with an additional unresolved feature at lower energy. Corresponding bands at 405 nm (OPh) and 490 nm (SPh) are tentatively assigned to terminal ligand-to-metal charge transfer transitions. The large blue shift (~70-80 nm) observed on oxygen substitution is as expected based on simple electronegativity arguments and on results obtained for the phenolate tetramer dianions, but is approximately twice as large as the corresponding blue shifts for the tetramers (~40 nm). There are two differences between the phenolate dimers and tetramers that may cause this difference. First, the formal iron oxidation state is higher in the dimer (Fe^{3+}) versus the tetramer ($Fe^{2.5+}$) and second the dimer has two coordinated phenolates versus one for the tetramer. Corresponding terminal ligand-to-metal charge transfer bands for the phenolate tetramer (410 nm) and dimer (405 nm) are at approximately the same energy, which suggests that phenoxide is capable, presumably through the relatively covalent Fe-O bond, of decreasing the effective charge on iron. Secondly, the difference in the blue shifts obtained upon phenolate substitution of thiophenolate for the tetramers (40 nm) versus the dimers (~85 nm) is consistent with the observation[127] that complexation of Fe^{3+} by successive phenolate groups produces a blue shift in the visible

absorption maximum by approximately 50 nm per phenolate group. Interaction of the iron atoms with an increasing number of p π electrons would be expected to raise the energy of the metal orbitals. This effect seems to be additive for the phenoxide dimers.

The energy of the major band in the phenolate dimers is shifted upon substitution of the p-H for CH_3 and Cl. The order of the shifts is in contrast to those observed for the thiophenolate analogs. In the thiophenolate series, simple inductive effects account for the order Cl (483 nm) < H (490 nm) < CH_3 (502 nm). The electron withdrawing p-Cl group causes a shift to higher energy while the electron donating p-CH_3 group results in a shift to lower energy, as expected. The order of visible maxima for the phenolate dimers, as given in Table VIII, is p-H < p-Cl < p-CH_3. This does not follow the order observed for the thiolate dimers nor does it correlate with the phenol acidity (p-Cl > p-H > p-CH_3), indicating that other effects may be dominant. Since halide substituents in the para position are capable of participating in resonance structures that increase the negative charge at the donor atom, and since such effects are expected to be much greater for phenols than thiophenols (greater overlap of oxygen p orbitals with π system of ring), the observed order may be due in part to dominant electron donating π effects overcoming the normal σ inductive electron-withdrawing effects,

resulting in a net red shift for the p-Cl versus the parent phenolate analog. Resonance effects would be especially important for the deprotonated phenolate anion, which could form quinoid type structures more easily. The trend found here for the phenolate dimers has also been observed by Ackermann and Hesse[127] in the absorbtion maxima due to ligand-to-metal charge transfer of 1:1 iron (III)-phenolate complexes in alcohol solution (p-H (580 nm) < p-Cl (585 nm) < p-CH_3 (610 nm)).

4. Magnetic Susceptibility

The magnetic susceptibility of the complex $(Bu_4N)_2$-$[Fe_2S_2(OPh)_4]$ has been measured at room temperature by the Faraday method. The data were corrected for the diamagnetic contributions due to ligands and cations using Pascals constants[112]. The resulting value for μ_{eff}/Fe of 1.64 BM was obtained. This result is comparable to magnetic moments per iron obtained for $[Fe_2S_2(S_2\text{-o-xylyl})_2]^{2-}$ (1.43 BM)[128] and $[Fe_2S_2Cl_4]^{2-}$ [93] (1.38 BM) and suggests intramolecular antiferromagnetic spin coupling. This result is also consistent with the structural results indicating dimensional invariance of the Fe_2S_2 core as described above.

5. Proton Nuclear Magnetic Resonance

Proton magnetic resonance spectra have been measured for the series of phenoxide complexes $[Fe_2S_2(OAr)_4]^{2-}$, where Ar = Ph, p-Tol, p-C_6H_4Cl in acetonitrile solution at room temperature and as a function of temperature for complexes with Ar = Ph and p-Tol. In addition to resonances due to the cation and residual undeuterated solvent, isotropically shifted resonances due to the phenoxide protons at room temperature are observed; the room temperature shifts are given in Table VIII. Representative 250 MHz ^1H NMR spectra at various temperatures of the dimers with Ar = Ph and p-Tol are shown in Figures 26 and 27, respectively. The temperature dependence of the isotropic shifts is plotted in Figure 28.

At room temperature, the phenoxide protons of $[Fe_2S_2(OPh)_4]^{2-}$ appear at -10.86 ppm and approximately -2.15 ppm. At higher temperatures, a broad signal appears slightly upfield of the cation resonance at approximately -3.0 ppm which is assigned to the ortho proton. The partially obscured resonance at approximately -2.15 ppm, which moves downfield at lower temperatures, disappears upon substitution of the p-H for a CH_3 group and is replaced by a resonance at -6.81 ppm, whose intensity corresponds to three protons. It is therefore assigned to the p-H, and the remaining resonance at -10.86 ppm is assigned to the m-H.

Figure 26. Proton magnetic resonance spectra (250 MHz) of $(Bu_4N)_2[Fe_2S_2(OPh)_4]$ in d_3-MeCN solution at various temperatures. Peaks from protons of the cations are indicated by Q, solvent by S, and unidentified impurities by X. Chemical shifts are in ppm from internal TMS.

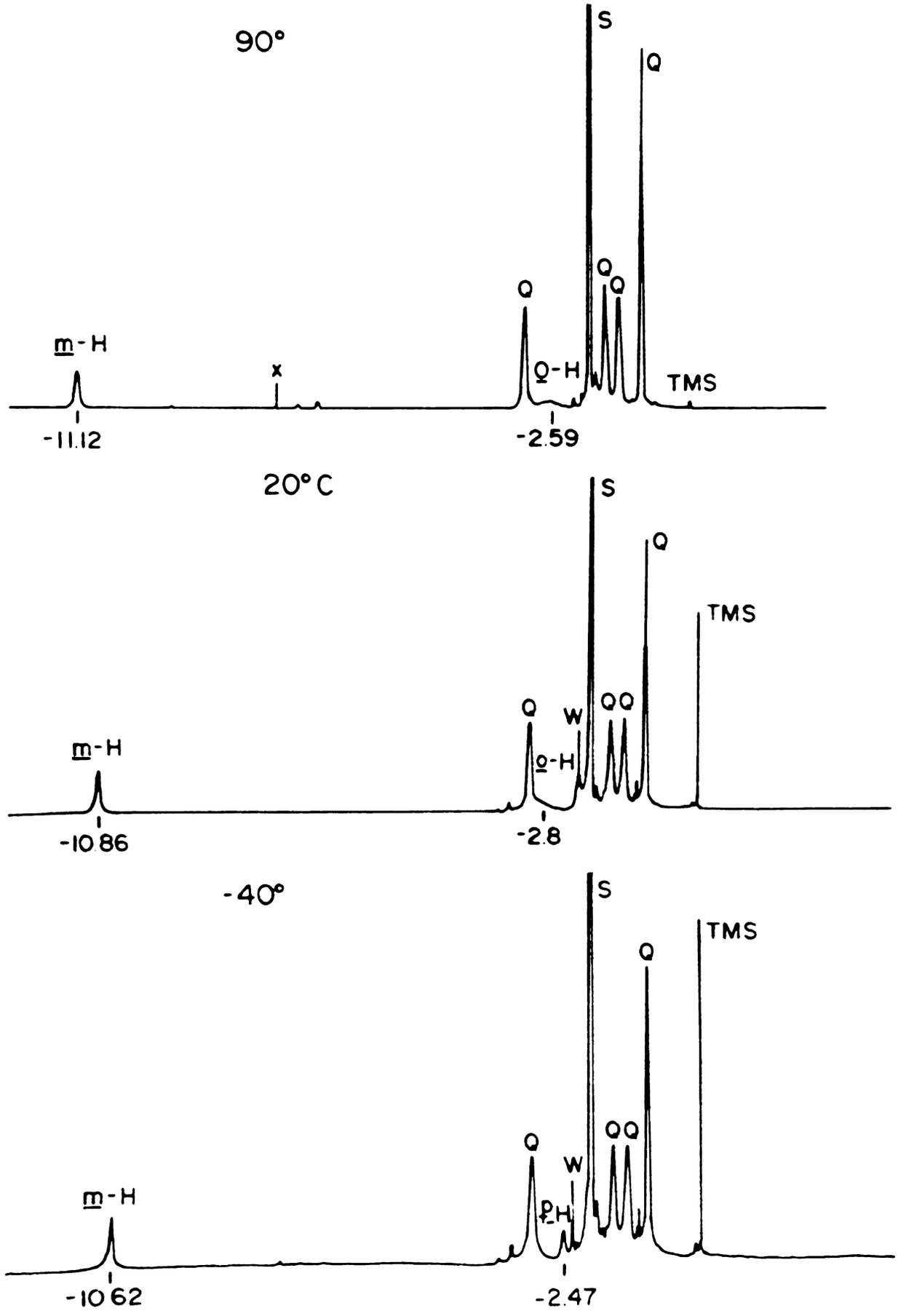
90°
S
Q
Q
Q
Q
m-H
x
o-H
TMS
-11.12
-2.59
20°C
S
Q
TMS
Q
W
QQ
m-H
o-H
-10.86
-2.8
-40°
S
TMS
Q
Q
W
QQ
m-H
p-H
-10.62
-2.47

Figure 26

Figure 27. Proton magnetic resonance spectra (250 MHz) of $(Me_4N)_2[Fe_2S_2(O\text{-}\underline{p}\text{-}Tol)_4]$ in d_3-MeCN solution at various temperatures. Peaks from protons of the cations are indicated by Q, solvent by S, and unidentified impurities by X. Chemical shifts are in ppm from internal TMS.

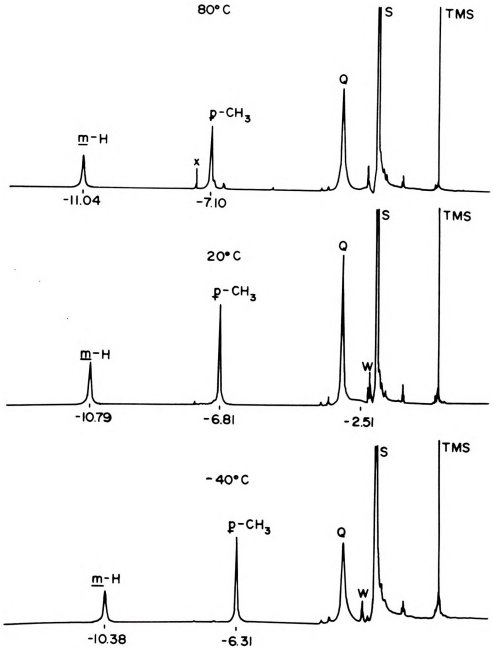
80°C
S
TMS
Q
p-CH3
m-H
x
-11.04
-7.10
20°C
S
TMS
Q
p-CH3
m-H
W
-10.79
-6.81
-2.51
-40°C
S
TMS
p-CH3
Q
m-H
W
-10.38
-6.31

Figure 27

Figure 28. Temperature dependence of isotropically shifted ligand proton resonances of $(Bu_4N)_2[Fe_2S_2(OPh)_4]$ (o) and $(Me_4N)_2[Fe_2S_2(O\text{-}\underline{p}\text{-}Tol)_4]$ (●) in d_3-MeCN.

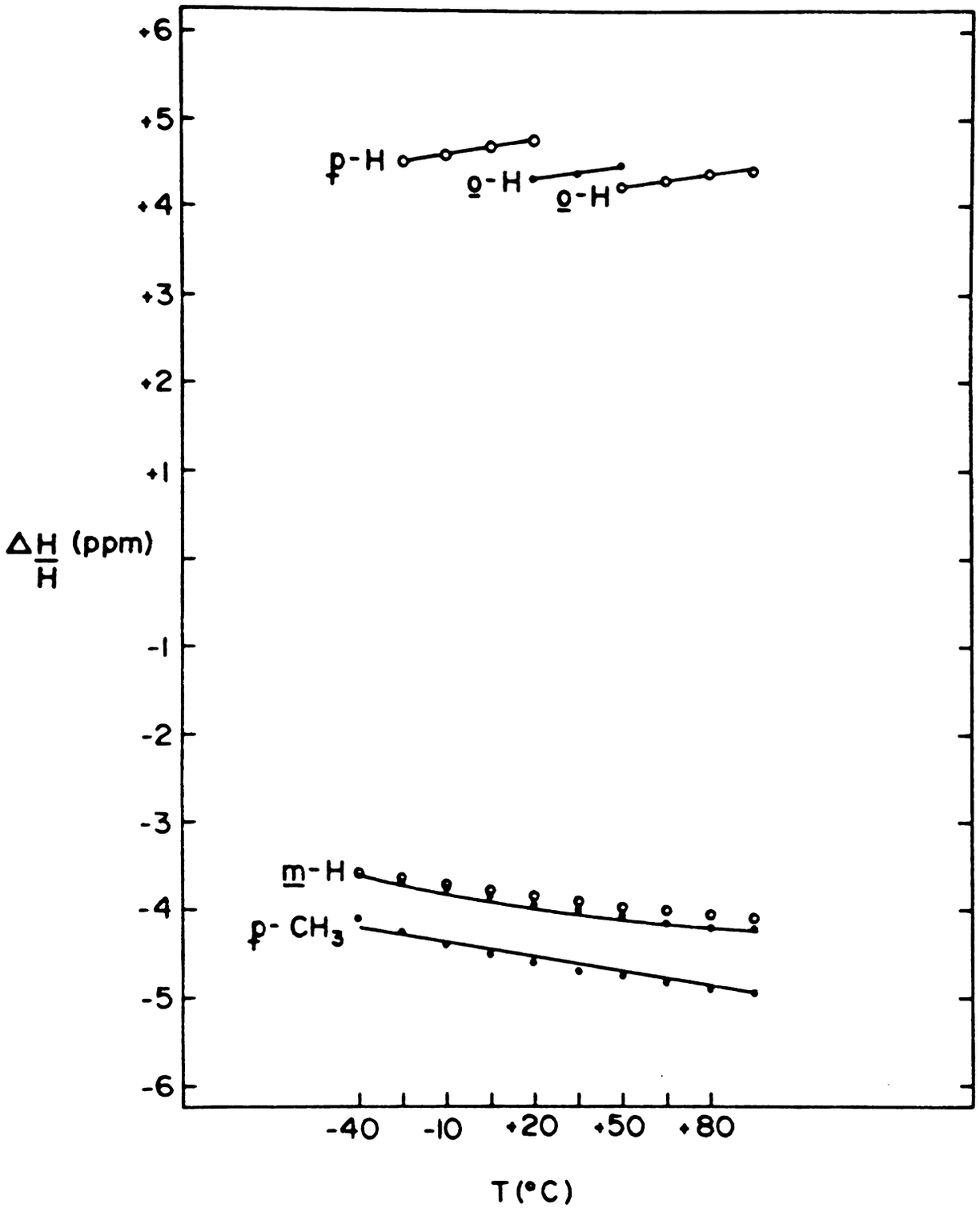

Figure 28

Several features of these spectra suggest that, as with the thiophenolate dimers[96], dominant contact interactions are responsible for the observed isotropic shifts: (i) the alternation of the signs of the shifts as one proceeds around the aromatic ring; (ii) the lack of attenuation of the magnitude of the shifts with increasing distance from the metal center; (iii) the sign reversal of the CH_3 group upon replacement of the p-H. The magnitudes of the shifts relative to those of the meta protons are listed in Table X. The relative shifts for the para protons are slightly less than the corresponding values for $[Fe_2S_2(SPh)_4]^{2-}$ due to a somewhat larger increase in the meta vs the para shifts, but the general trend para > ortho > meta is obeyed. Since the relative shifts should reflect relative spin densities[94] provided the shifts are contact in origin, the data support the conclusion that dipolar interactions are negligible in these systems.

The only significant difference between the NMR spectra of the phenolate dimers and the thiophenolate dimers is that the magnitude of the isotropic shifts is larger for phenolate than for the corresponding thiophenolate analogs. These shift increases are somewhat smaller than those for the tetramer system, where the phenolate shifts are approximately twice as large as the corresponding thiophenolate shifts. These data again indicate more delocalization of unpaired spin density when phenolate replaces thiophenolate.

This behavior is consistent with the structural data indicating a relatively short Fe-O interaction.

The isotropic shifts of the phenyl protons of the phenoxide dimers are temperature dependent. The data plotted in Figure 28 show that the magnitude of the shifts increases with increasing temperature over the entire temperature range. This result provides further evidence for intramolecular antiferromagnetic coupling and parallels the magnetic behavior of $[Fe_2S_2(S_2\text{-}\underline{o}\text{-xylyl})_2]^{2-}$ [128] and $[Fe_2S_2Cl_4]^{2-}$ [93], two structurally characterized dimers for which variable temperature magnetic data is available.

6. ^{57}Fe Mossbauer Spectra

The ^{57}Fe Mossbauer spectrum of a solid sample of $(Bu_4N)_2[Fe_2S_2(OPh)_4]$ diluted with boron nitride was obtained at 4.2 K and zero field. The spectrum is shown in Figure 29. It consists of a single quadrupole doublet with isomer shift γ = 0.37 mm/s, quadrupole splitting ΔE_Q = 0.32 mm/s and linewidth Γ = 0.26 mm/s. The isomer shift is measured relative to Fe metal at room temperature. The spectrum was also measured in a small ($\sim$600 G) applied magnetic field. The spectrum remained essentially unchanged, indicating that a diamagnetic ground state (S = 0) is present, which is consistent with the magnetic data suggesting antiferromagnetic coupling. These results are

Figure 29. ^{57}Fe Mossbauer spectrum of polycrystalline $(Bu_4N)_2[Fe_2S_2(OPh)_4]$ at 4.2 K in zero applied field.

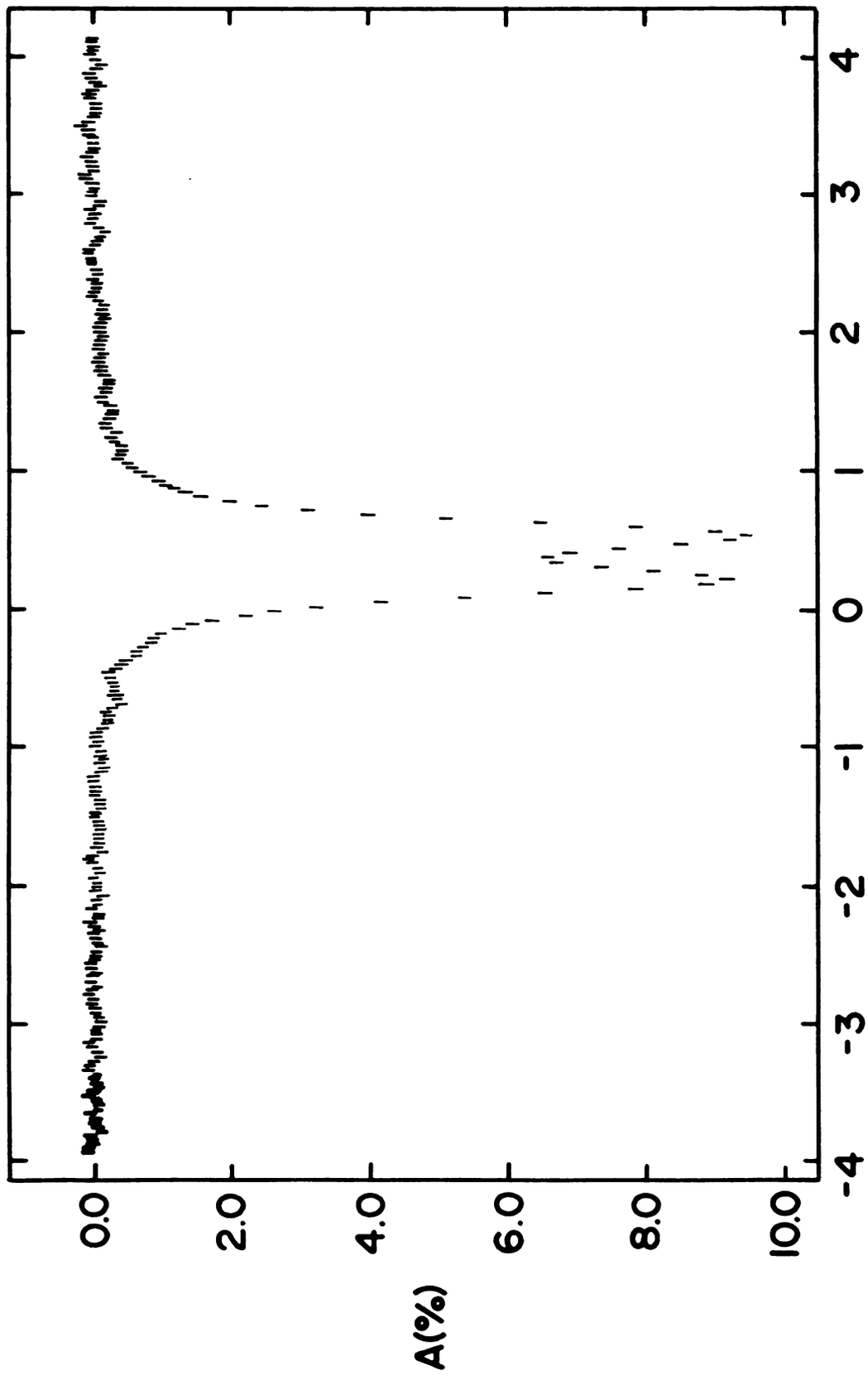

Figure 29

comparable to those obtained for the thiolate dimers, except for the magnitude of the isomer shift, δ. Mossbauer spectra of the complexes $[Fe_2S_2X_4]^{2-}$ [97] where X = SPh and X_2 = S_2-o-xylyl have been obtained, but the isomer shifts were measured relative to Fe metal at 4.2 K. Holm and co-workers[129] have reported a correction factor of +0.12 mm/s in the isomer shift for various reduced tetramers, and a difference of +0.11 mm/s was obtained for the isomer shift of $[Fe_4S_4(SPh)_4]^{2-}$, Section III.A.6. Using a correction of +0.11 mm/s, the thiolate parameters are as follows: δ = 0.28 mm/s, ΔE_Q = 0.36 mm/s (X_2 = S_2-o-xylyl)[97]; δ = 0.28 mm/s, ΔE_Q = 0.32 mm/s (X = SPh)[97]. The increased isomer shift for the phenolate dimer is consistent with increased ferrous character of the iron. This suggests, as before, that phenolate is capable of donating significantly more electron density to iron than thiophenolate, which may be due to a substantial degree of covalency in the Fe-O bonds. This increase in isomer shift for the phenolate vs thiophenolate dimers is approximately twice that found for the corresponding tetramer system and may reflect the presence of two coordinated phenolates per iron versus one per iron in the tetramer. The results obtained for the phenolate dimer are consistent with the structural and magnetic data described above and the electrochemical data described below.

7. Electrochemistry

Electrochemical measurements on the phenoxide complexes $[Fe_2S_2(OAr)_4]^{2-}$ where Ar = Ph, p-Tol, and p-C_6H_4Cl have been performed using three methods: dc polarography (DCP), differential pulse polarography (DPP), and cyclic voltammetry (CV). Measurements were made on 1-2 mM solutions in NMP over the potential range +1.0 to -2.0 V. Each compound exhibits two well-defined cathodic processes corresponding to formation of the tri- and tetraanions. Typical cyclic voltammograms for each compound are presented in Figure 30. All electrochemical data are listed in Table XIX.

Comparison of the data with corresponding data for the $[Fe_2S_2(SAr)_4]^{2-}$ (Ar = Ph, p-Tol, p-C_6H_4Cl)[97] complexes reveals several similarities. First, the thiophenolate analogs also show two cathodic processes over the same potential range. In dc polarography, the diffusion currents are in reasonable agreement with those obtained for the thiophenolate dimers and the phenolate and thiophenolate tetramers measured under similar conditions for a one electron process. Slopes of log $[i/(i_d-i)]$ vs E are usually somewhat less than the theoretical value of 59 mV for a reversible one electron reduction. Peak halfwidths obtained by DPP are in adequate agreement with corresponding values obtained for phenolate tetramers (Table V) for such a process. The slopes (DCP) and peak half-widths (DPP)

Figure 30. Cyclic voltammograms for $(Bu_4N)_2[Fe_2S_2(OPh)_4]$, $(Me_4N)_2[Fe_2S_2(O\text{-}\underline{p}\text{-}Tol)_4]$ and $(Et_4N)_2(O\text{-}\underline{p}\text{-}C_6H_4Cl)_4]$ in NMP at glassy carbon electrode. Scan rates are 100 mV/s.

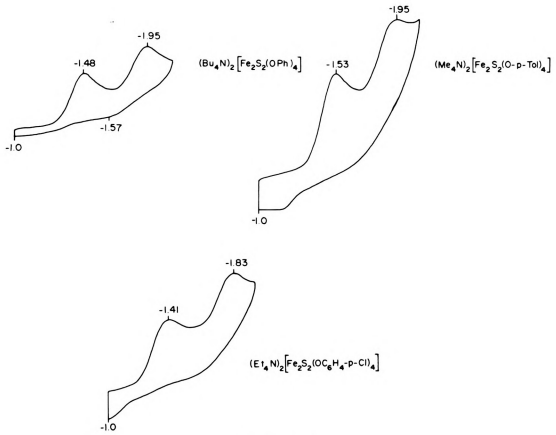
-1.95
-1.48
-1.57
-1.0
$(Bu_4N)_2[Fe_2S_2(OPh)_4]$
-1.95
-1.53
-1.0
$(Me_4N)_2[Fe_2S_2(O\text{-}p\text{-}Tol)_4]$
-1.83
-1.41
-1.0
$(Et_4N)_2[Fe_2S_2(OC_6H_4\text{-}p\text{-}Cl)_4]$

Figure 30

obtained for $[Fe_2S_2(OPh)_4]^{2-}$ are unusually large compared to the p-Tol and p-C_6H_4Cl analogs, suggesting that the reduction process for this compound are less reversible by these criteria. These data show that, as for the thiolate dimers, the electron transfer series $[Fe_2S_2(OAr)_4]^{2-,3-,4-}$ is realized and that the electron transfers are quasireversible by polarographic techniques.

In the CV experiments, two well-developed cathodic peaks with essentially no reverse (anodic) peaks are observed for each phenolate dimer. This result indicates that no 2-/3- or 3-/4- dimer process satisfies the diagnostic criteria for reversible charge transfer. This behavior is very similar to results obtained for the $[Fe_2S_2(SAr)_4]^{2-}$ [97] and $[Fe_2S_2Cl_4]^{2-}$ [93] complexes.

The reduction potentials for the phenolate dimers exhibit variation with substitution of the p-H for CH_3 and Cl. By any method used, the order observed is p-Cl < p-H < p-CH_3 with 20-100 mV negative shifts between members of the series. This trend is also observed for the corresponding arenethiolate dimers, and can be explained by simple inductive effects of the electron releasing CH_3 and electron withdrawing Cl groups. It is, however, somewhat surprising considering the order observed for the shifts in the electronic absorbtion maxima, Section III.B.1.

The most important results obtained from the

electrochemical data are that the same pattern of two one electron reductions typical of all $[Fe_2S_2L_4]^{2-}$ clusters[97,93] is observed, but that the potentials of these reductions are approximately 200 mV more negative than those of the arenethiolate analogs. For reasons explained in Section III.A.7, simple electronegativity arguments would predict the phenolate dimers to be easier to reduce than the thiolate analogs. Again, phenoxide is apparently capable of transferring more electron density to the $[Fe_2S_2]^{2+}$ core than thiophenoxide. This is consistent with a more covalent Fe-O interaction and is reinforced by the Mossbauer and ^1H NMR results. Similar behavior has been observed for the $[MoFeS_4X_2]^{2-}$ [72,81] and the $[Fe_4S_4X_4]^{2-}$ [95] systems where X = SAr and OAr.

8. Ligand Exchange Reactions

The phenoxide dimer complexes are extremely sensitive to water, acidic solvent impurities and strongly donating oxygen solvents, as are the phenoxide tetramers. This behavior necessitates rigorous purification of solvents for use in recrystallizations and solution studies.

The phenolate dimers react with electrophiles such as acyl halides. Treatment with four equivalents of benzoyl chloride in acetonitrile results in rapid quantitative conversion to the corresponding dimeric chloro complex

(Reaction 9), as demonstrated by optical spectra. This reactivity has also been documented for the thiophenolate dimers[93] as well as the phenolate and thiophenolate[101] tetramers and proceeds, presumably, by the same mechanism[93].

$$[Fe_2S_2(OAr)_4]^{2-} + 4PhCOCl \rightarrow [Fe_2S_2Cl_4]^{2-} + PhCO_2Ar \quad (9)$$

Reaction of the phenolate dimers with four equivalents of thiophenol results in immediate formation of the thiophenolate derivative (Reaction 10). This reactivity again is as expected in view of the lability of phenolate ligands and the much greater acidity of thiophenol vs phenol[101].

$$[Fe_2S_2(OAr)_4]^{2-} + 4PhSH \rightarrow [Fe_2S_2(SPh)_4]^{2-} + 4ArOH \quad (10)$$

Previous investigation of the thiolate dimers show that they too undergo facile ligand exchange processes. For example[97], $[Fe_2S_2(S_2\text{-}\underline{o}\text{-xylyl})_2]^{2-}$ complex is smoothly converted to $[Fe_2S_2(SAr)_4]^{2-}$ by treatment with the appropriate arenethiol. In addition, analogous reactivity has been demonstrated for the phenolate tetramers, already discussed. It is apparent that the phenolate dimers undergo facile ligand exchange with retention of the Fe_2S_2 core.

9. Summary

Phenolate substituted binuclear Fe-S clusters can be prepared and isolated in crystalline form as their tetraalkylammonium salts. The optical spectra exhibit the expected blue shift upon oxygen substitution. Structural results show a relatively short Fe-O bond. Magnetic properties remain virtually unchanged upon phenolate substitution while the isotropically shifted phenyl protons in the ^{1}H NMR reflect a substantial increase in unpaired spin density in the aromatic ring. An increased isomer shift in the ^{57}Fe Mossbauer spectra and a substantial negative shift in the reduction potentials suggest that phenolate is transferring more electron density to the $[Fe_2S_2]^{2+}$ core, consistent with the structural and NMR results.

Comparison of corresponding shifts in properties between phenolate and thiophenolate ligated Fe_2S_2 centers with analogous shifts observed for the Fe_4S_4 centers show an interesting trend. The blue shifts in the optical absorption maxima, the isotropic NMR shifts of the phenyl protons, and the negative shifts of the reduction potentials are in each case approximately twice as large for the Fe_2S_2 complexes compared to the Fe_4S_4 complexes. This may reflect coordination of two phenolates to each iron in the dimers compared to one phenolate per iron in the tetramers.

Results obtained for phenolate coordinated Fe_2S_2 clusters

suggest that substitution of a cysteinyl thiol ligand to an Fe_2S_2 core in a protein by tyrosyl phenolate should have only a minor effect on cluster redox properties. This observation is entirely consistent with results obtained for the phenoxide tetramers, and indicates that tyrosyl ligation could provide a reactive coordination site with minimal change in cluster reduction potentials.

Phenolate coordination to Fe^{3+} has been implicated in a variety of metalloproteins and enzymes[130] including transferrins[131], purple phosphatases[132] and uteroferrin[133], catechol dioxygenases[134] and certain heme proteins[130]. Tetrahedral phenolate coordination of Fe^{3+} has not been reported for any of the biological systems cited above. In addition, only one other synthetic four coordinate Fe^{3+} complex with mondentate phenolate coordination has been reported[89]. However, a 2Fe-2S center has been identified[135] in a protein containing no cysteine amino acid residues, but only tyrosine, serine, glutamic and aspartic acid moieties, strong evidence for non-cysteine coordination has been reported for the Rieske center[140] from Thermus thermophilus.

C. $[Mo_2Fe_6S_8(SEt)_3(OPh)_6]^{3-}$

1. Synthesis

The phenolate double cubane complex $[Mo_2Fe_6S_8(SEt)_3(OPh)_6]^{3-}$ can be prepared by reaction of $[Mo_2Fe_6S_8(SEt)_9]^{3-}$

with a large excess of PhOH (Reaction 11). This reaction is completely analogous to the reaction of $[Fe_4S_4(SR)_4]^{2-}$ with excess phenol (Reaction 1, Section III.A.1) and represents a ligand exchange equilibria which is driven to completion by removal of the volatile EtSH in vacuo. The resulting product is isolated as its tetraalkylammonium salt in 50-60% yields after recrystallization.

$$[Mo_2Fe_6S_8(SEt)_9]^{3-} + \text{xs PhOH} \rightarrow$$

$$[Mo_2Fe_6S_8(SEt)_3(OPh)_6]^{3-} + 6EtSH \qquad (11)$$

Isolation and recrystallization are made difficult because of the extremely high solubility in polar organic solvents. Once prepared and isolated, however, the complex is stable in the absence of oxygen and water. A schematic view of the proposed structure is shown below.

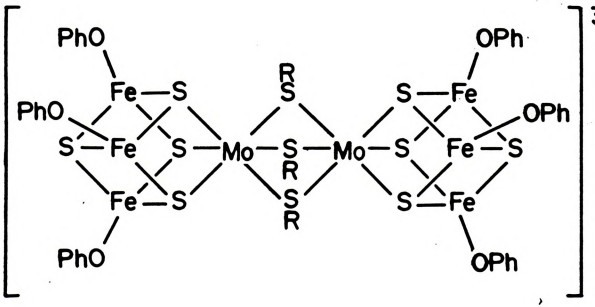

2. Electronic Absorption Spectra

The electronic absorption spectra for $[Mo_2Fe_6S_8(SEt)_9]^{3-}$ and $[Mo_2Fe_6S_8(SEt)_3(OPh)_6]^{3-}$ are presented in Figure 31. Spectral data are presented in Table VIII. Comparison of the spectra show the elimination of the original bands at 281 nm and 391 nm and replacement with bands at 233 nm, 270 nm, and 400 nm. Similar spectral changes are observed for the reaction of greater than six equivalents of PhSH with $[Mo_2Fe_6S_8(SEt)_9]^{3-}$ to yield the $[Mo_2Fe_6S_8(SEt)_3(SPh)_6]^{3-}$ ion[136], which exhibits prominant shoulders at ∿346 nm and ∿418 nm, and has recently been isolated as its tetraethylammonium salt. Apparently corresponding bands at∿400 nm (OPh) and ∿418 nm (SPh) are tentatively assigned to terminal ligand-to-metal charge transfer transitions. The observed blue shift in this band is again expected based on electronegativity arguments already discussed in Section III.A.3. The magnitude of the shift (∿20 nm) is somewhat less than expected based on results of the Fe_4S_4 system (∿40 nm), which possesses a structurally similar core and one terminal ligand to each iron.

3. Magnetic Susceptibility

The room temperature magnetic susceptibility of $(Et_3NCH_2Ph)_3[Mo_2Fe_6S_8(SEt)_3(OPh)_6]$ has been measured by

Figure 31. Electronic spectra of the $[Mo_2Fe_6S_8(SEt)_3(OPh)_6]^{3-}$ (——) and $[Mo_2Fe_6S_8(SEt)_9]^{3-}$ (---) ions in MeCN at 22°C.

Figure 31

the Faraday method. After correction for the diamagnetic contribution of the ligands and cations using Pascal's constants[112], an effective magnetic moment, μ_{eff}, of 5.74 BM for the cluster was obtained, suggesting the presence of intramolecular antiferromagnetic coupling. This result is virtually identical to that measured for $(Et_3NCH_2Ph)_3[Mo_2Fe_6S_8(SEt)_9]$[51] (5.73 BM) and $(Bu_4N)_3$-$[Mo_2Fe_6S_8(SPh)_9]$[58] (5.70 BM) and corresponds to a spin only value of S = 5/2 at room temperature. A recent mathematical model[66] which has satisfactorally simulated the variable temperature susceptibility data for representative double cubane complexes shows the ground magnetic state to be S = 1, with thermal population of higher excited states resulting in the observed magnetic moments at higher temperatures. These results suggest that the magnetic properties of the double cubane clusters, as with the Fe-S tetramers and dimers, are not sensitive to the nature of the terminal ligand.

4. Proton Nuclear Magnetic Resonance

Proton magnetic resonance spectra of $(Et_3NCH_2Ph)_3$-$[Mo_2Fe_6S_8(SEt)_3(OPh)_6]$ have been measured as a function of temperature in acetonitrile solution. In addition to the resonances due to the ctaions and residual undeuterated solvent, isotropically shifted resonances due to the phenyl protons and bridging ethanethiolate groups are observed.

Representative 250 MHz spectra at two temperatures are shown in Figure 32, while spectral data are collected in Table VIII. Plots of isotropic shifts versus temperature are displayed in Figure 33. As in the usual convention, resonances downfield of TMS are negative and isotropic shifts are measured relative to the diamagnetic ligands.

Assignments were made based on the well demonstrated spectra of $[Mo_2Fe_6S_8(SPh)_9]^{3-}$,[51,58] and $[Mo_2Fe_6S_8(SEt)_3(SPh)_6]^{3-}$ [136] and are shown in Figure 32. No resonances attributable to μ-OPh groups were detected. The data suggest that, for reasons already discussed in Section III.A.5, contact interactions are responsible for the isotropic shifts of the phenyl protons. Analysis of the isotropic shifts of bridging groups for a series of double cubane complexes[51,58] indicate that there is an appreciable dipolar contribution. In $[Mo_2Fe_6S_8(SEt)_3(OPh)_6]^{3-}$, resonances for the bridging methylene protons have approximately the same shift (-16.4 ppm) as those for $[Mo_2Fe_6S_8X_6]^{3-}$ where X = Cl (-15.49 ppm)[136], SPh (-14.49)[136], SEt (-15.0)[51] and it is assumed that dipolar interactions are also in effect here.

Comparison of the magnitudes of the isotropic shifts of the phenyl protons of the phenolate complex (Table VII) with those of the thiophenolate analog (-6.6 ppm (m-H), +10.9 ppm (p-H)[136] shows that the general trend of substantially larger shifts for phenolate vs thiophenolate

Figure 32. Proton magnetic resonance spectra (250 MHz) of $(Et_3NCH_2Ph)_3[Mo_2Fe_6S_8(SEt)_3(OPh)_6]$ in d_3-MeCN. Peaks from protons of the cations are indicated by Q, solvent by S, and unidentified impurities by X. Chemical shifts are in ppm from internal TMS.

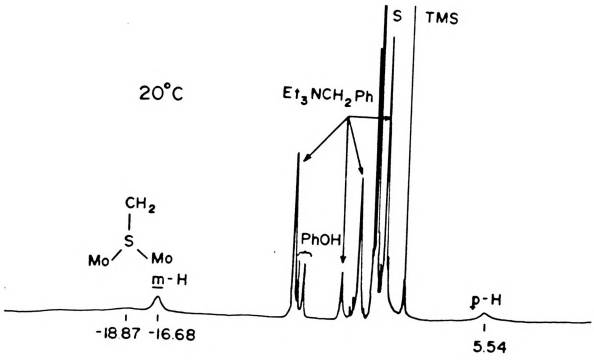
20°C
S
TMS
Et3NCH2Ph
CH2
S
Mo
Mo
PhOH
m-H
p-H
-18.87
-16.68
5.54

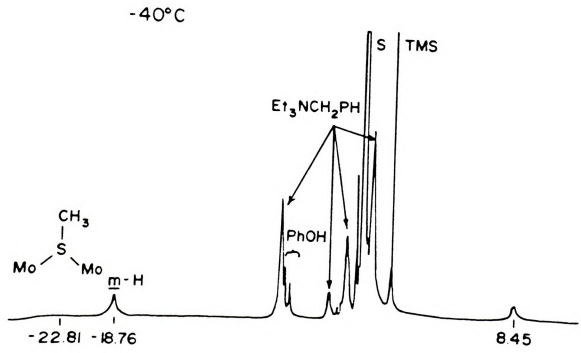
-40°C
S
TMS
Et3NCH2PH
CH3
S
Mo
Mo
PhOH
m-H
-22.81
-18.76
8.45

Figure 32

Figure 33. Temperature dependence of isotropically shifted ligand proton resonances of $(Et_3NCH_2Ph)_3$-$[Mo_2Fe_6S_8(SEt)_3(OPh)_6]$ in d_3-MeCN.

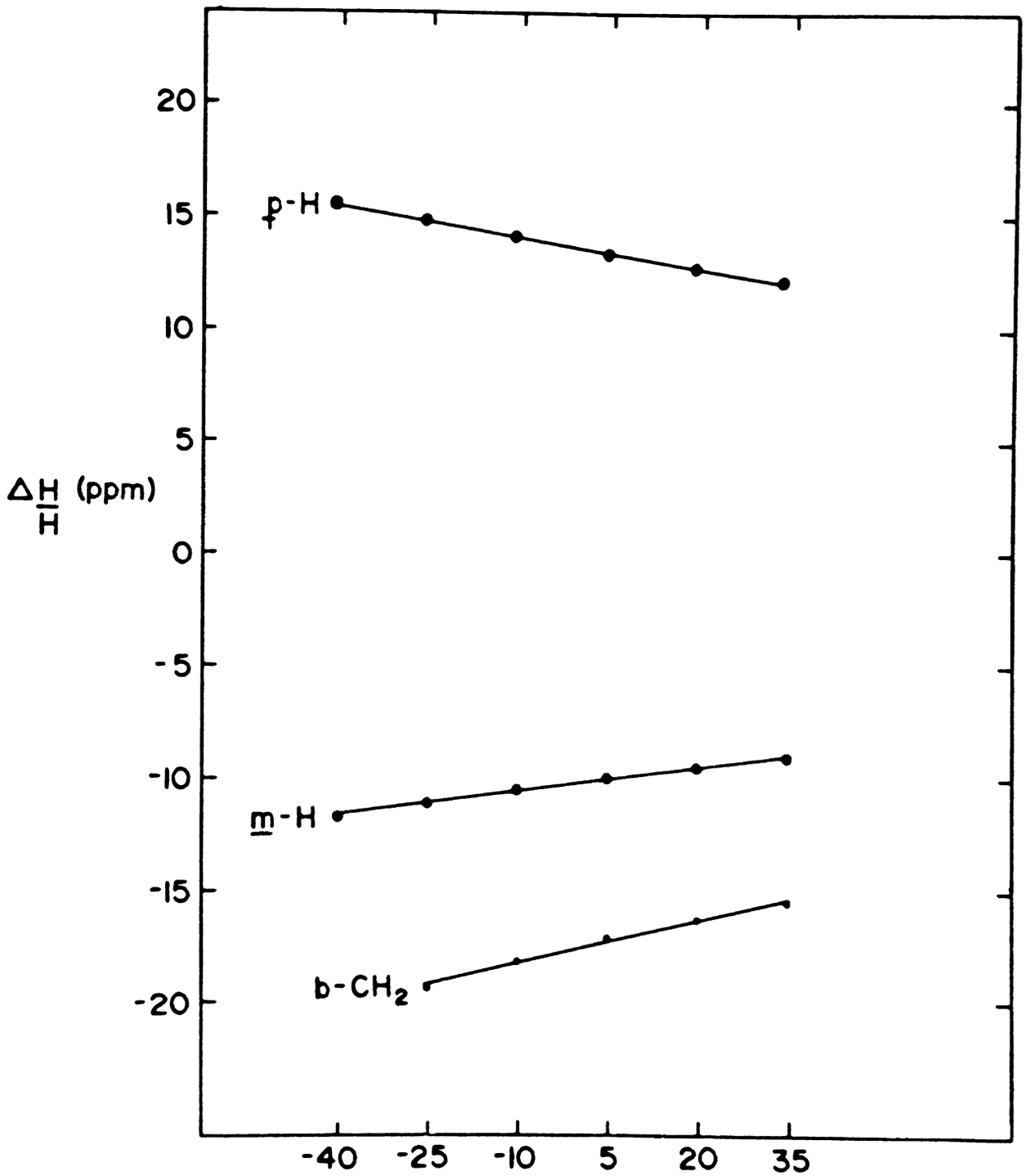

Figure 33

analogs established for the phenolate tetramers and dimers is followed for the double cubanes. These results once again suggest that phenolate is capable of more electron density to the metal center than thiophenolate, and are consistent with the electrochemical results discussed below.

The temperature dependence of the observed isotropic shifts for the phenolate protons plotted in Figure 33 shows that the magnitudes of the shifts increase with decreasing temperature. This behavior parallels that obtained for the terminal thiophenolates of $[Mo_2Fe_6S_8(SPh)_9]^{3-}$,[58] and is also consistent with the temperature dependence of the magnetic susceptibility of several double cubane complexes[51,66] of the same type. These results are again consistent with intramolecular antiferromagnetic coupling.

5. Electrochemistry

The electrochemical behavior of $[Mo_2Fe_6S_8(SEt)_3(OPh)_6]^{3-}$ has been examined by differential pulse polarography and cyclic voltammetry. Measurements were performed on 1 m$\underline{M}$ solutions in acetonitrile over the potential range +1.0 to -2.0 V. The complex exhibited two well defined quasireversable one electron reductions corresponding to sequential formation of the 4- and 5- ions. A typical cyclic voltammogram and differential pulse polarogram are

shown in Figure 34. Electrochemical data are provided in Table XIX.

Examination of the cyclic voltammetric results suggest that while reduction of the complex is not strictly electrochemically reversible (Shown by $|E_p - E_p| > 59$ mV), it does approximate chemical reversibility, as shown by the value of $i_{pc}/i_{pa} \sim 1$. Peak half-widths obtained by DPP measurements, although somewhat larger than the theoretical value of 90 mV for a reversible one electron process, are in reasonable agreement with values obtained for the quasi-reversible one electron reductions of the phenolate and thiophenolate tetramers under similar conditions.

Comparison of the corresponding reduction potentials for $[Mo_2Fe_6S_8(SEt)_3X_6]^{3-}$ where X = SPh (E_1 = -1.01 V, E_2 = -1.19 V)[136]; OPh (Table VIII); Cl (E_1 = -0.83 V, E_2 = -1.01 V)[136] show the same order of decreasing ease of reduction, Cl < SPh < OPh established for the Fe-S tetramer and dimer series. The shift of approximately -120 mV for each of the two reductions on substitution of phenolate for thiophenolate represents further evidence of the ability of phenolates to donate more electron density to the metal sulfur center than thiophenolates, therefore rendering them more difficult to reduce. Similar results have also been obtained for the $[MoFeS_4X_2]^{2-}$ system where X = SAr[72], OAr[81].

Figure 34. Cyclic voltammogram and differential pulsed polarogram for $(Et_3NCH_2Ph)_3[Mo_2Fe_6S_8(SEt)_3(OPh)_6]$ in MeCN. Scan rates are 100 mV/s (CV) and 5 mV/s (DPP).

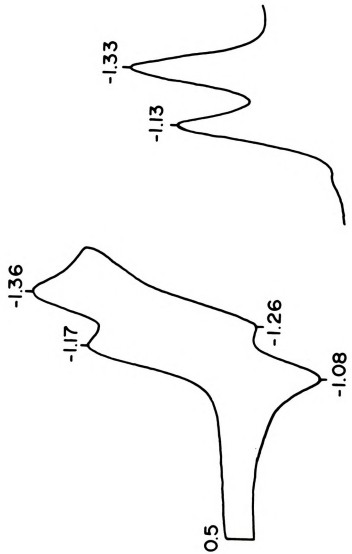

Figure 34

6. Ligand Exchange Reactions

The phenolate double cubane cluster is extraordinarily sensitive to water, acidic solvent impurities and strongly donating solvents, as are the phenolate Fe-S clusters. They also undergo reactions with electrophiles. Reaction with benzoyl chloride smoothly converts the phenolate complex to the corresponding chloro cluster[136,65] in quantitative yield as shown by optical spectra (Reaction 12).

$$[Mo_2Fe_6S_8(SEt)_3(OPh)_6]^{3-} + 6\ PhCOCl \downarrow [Mo_2Fe_6S_8(SEt)_3Cl_6]^{3-} + 6\ PhCO_2Ph \qquad (12)$$

Reaction with thiophenol quantitatively converts the phenolate complex to the thiophenolate analog[136] (Reaction 13).

$$[Mo_2Fe_6S_8(SEt)_3(OPh)_6]^{3-} + 6\ PhSH \downarrow [Mo_2Fe_6S_8(SEt)_3(SPh)_6]^{3-} + 6\ PhOH \qquad (13)$$

Of the two atoms potentially susceptible to attack by electrophiles, the sulfur atoms of the bridging ethanethiolates and the oxygen atoms of the terminal phenolate groups, only the terminal phenolates are reactive under

the conditions examined. This parallels the reactivity of the entirely thiolate ligated double cubanes[136,65] containing both terminal and bridging thiolate ligands, where bridge integrity was preserved in all cases. The observed ligand exchange reactivity is entirely expected based on the evident lability of phenolate ligands and the analogous reactivity of the phenolate Fe-S clusters.

7. Summary

Reaction of phenol with an alkyl thiolate ligated double cubane complex effects phenolate substitution at the terminal positions; the product can be isolated as its benzyltriethylammonium salt. The phenolate cluster possesses unaltered magnetic properties, blue shifted optical spectra, and undergoes analogous ligand exchange reactions with electrophiles as expected for terminal phenolate substitution. Increased isotropic proton NMR shifts, and large negative shifts in corresponding first and second reduction potentials are consistent with increased donation of electron density to the $[MoFe_3S_4]^{3+}$ cores for phenolate vs thiophenolate terminal ligands to iron. Similar behavior has been observed for the Fe-S tetramers and dimers and for the molybdenum-iron dimer systems.

Several chemical and physiochemical studies of FeMo-co[44,84-86], including iron K-edge EXAFS, have suggested that oxygen donor ligands are bound to the iron atoms

within the FeMo-cofactor. Also, FeMo-co can be extracted from the MoFe-protein without addition of thiols which are necessary for cluster displacement of typical Fe-S centers. The results obtained for the $[Mo_2Fe_6S_8(SEt)_3(OPh)_6]^{3-}$ ion indicate that phenoxide is a more labile ligand than ethanethiolate. In addition, electrochemical results indicate that $[Mo_2Fe_6S_8(SEt)_3(OPh)_6]^{3-}$ exhibits reduction potentials in the same range as $[Mo_2Fe_6S_8(SEt)_9]^{3-}$. These results suggest that substitution of a cysteinyl thiolate ligand by a tyrosyl phenolate ligand to iron in FeMo-co should provide a more labile coordination site without significantly changing cluster reduction potentials.
To date, the phenolate double cubane, $[Mo_2Fe_6S_8(SEt)_3(OPh)_6]^{3-}$, and the phenolate dimer $[MoFeS_4(OPh)_2]^{2-}$ are the only examples of synthetic MoFeS clusters possessing oxygen ligation to iron.

IV. CONCLUSIONS

The tetrameric iron-sulfur clusters $[Fe_4S_4(OAr)_4]^{2-}$ (Ar = Ph, p-Tol) have been prepared by two types of ligand exchange reactions and isolated as their tetraalkylammonium salts. The X-ray crystal structure of $(Et_4N)_2[Fe_4S_4(OPh)_4]$ has been determined and shows an Fe-O bond length somewhat shorter than expected. A variety of physical measurements including optical and ^{57}Fe Mossbauer spectroscopy and proton NMR spectrometry have been performed on these complexes and compared to corresponding results obtained for the $[Fe_4S_4(SAr)_4]^{2-}$ complexes. The optical spectra of the phenolate tetramers exhibit blue shifts of 40 nm vs corresponding features in the arenethiolate analogs. Proton magnetic resonance spectra indicate that the isotropic shifts of the phenoxide protons are contact in origin and that their magnitudes are approximately twice as large as those of the thiophenolate tetramers. The Mossbauer spectrum of $[Fe_4S_4(OPh)_4]^{2-}$ has been obtained and shows increased ferrous character of the iron atoms upon oxygen substitution. Electrochemical results show approximately 100 mV negative shifts in reduction potentials upon oxygen substitution. Taken together, these results suggest that phenoxide ligands are capable

of donating substantial electron density to the $[Fe_4S_4]^{2+}$ core, presumably through a relatively covalent Fe-O bond. These complexes are also reactive toward electrophiles such as PhCOCl and PhSH and can be smoothly converted to the chloro and thiophenolate tetramers by these reagents, respectively. In addition, certain preparations of phenolate tetramers yield a complex of as yet unknown structure possessing related but distinctly different physical properties; it is probably a higher nuclearity cluster, possibly a hexane.

The dinuclear iron-sulfur clusters $[Fe_2S_2(OAr)_4]^{2-}$ (Ar = Ph, p-Tol, p-C_6H_4Cl) have been prepared by two methods: direct synthesis, and by ligand exchange reactions involving $[Fe_2S_2Cl_4]^{2-}$. They are isolated in pure, crystalline form as their tetraalkylammonium salts. Preliminary X-ray crystallographic results indicate a relatively short Fe-O bond. Optical spectra of these complexes exhibit the expected blue shifts upon oxygen substitution and unaltered magnetic properties. Increased isotopic proton NMR shifts, ^{57}Fe Mossbauer isomer shifts and negative shifts in the reduction potentials compared to results obtained for the corresponding arenethiolate complexes suggest that phenoxide ligands donate substantial electron density to the $[Fe_2S_2]^{2+}$ core. The phenoxide dimers undergo ligand exchange reactions by treatment with electrophiles such as PhCOCl and PhSH, which yield $[Fe_2S_2Cl_4]^{2-}$ and $[Fe_2S_2(SPh)_4]^{2-}$, respectively.

The phenoxide substituted "double cubane" complex $[Mo_2Fe_6S_8(SEt)_3(OPh)_6]^{3-}$ has been prepared by reaction of $[Mo_2Fe_6S_8(SEt)_9]^{2-}$ with PhOH. The phenoxide cluster exhibits the expected blue shifts in the optical spectra and unaltered magnetic properties. Increased isotropic shifts of the phenyl protons in the NMR spectra and negative shifts in the reduction potentials are consistent with increased donation of electron density to the $MoFe_3S_4$ cores for phenoxide vs thiophenoxide terminal ligands to iron. This complex undergoes ligand exchange reactions with electrophiles as expected for terminal phenolate substitution.

To date, terminal phenoxide substitution to iron has been achieved for the one-, two-, and four-iron Fe-S synthetic analogs and for the molybdenum-iron-sulfur dimer and "double cubane" complexes. A schematic representation of these complexes is shown in Figure 35. Results obtained for the complexes described in this work, together with results obtained for $[Fe(OAr)_4]^{1-}$ and $[MoFeS_4(OAr)_2]^{2-}$, reveal several apparently general trends for terminal phenoxide substitution to iron when compared to results obtraind for the corresponding arenethiolate complexes. These include: i) unaltered magnetic properties, ii) approximately a two fold increase in the isotropic shifts of the phenyl protons; iii) blue shifts of 20-80 nm in corresponding optical absorption bands; iv) an approximately 0.04

Figure 35. Schematic of known Fe-S and Mo-Fe-S clusters with phenoxide ligands to iron.

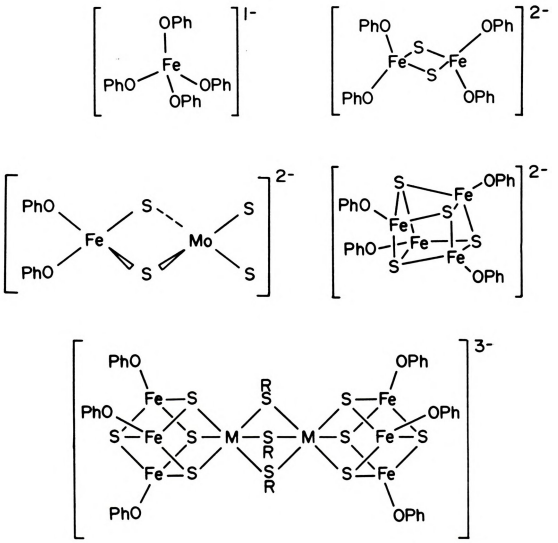
OPh
Fe
PhO
OPh
OPh
1-
PhO
OPh
Fe
S
Fe
S
PhO
OPh
2-
PhO
S
S
Fe
Mo
PhO
S
S
2-
S
OPh
Fe
PhO
Fe
S
Fe
PhO
S
Fe
S
OPh
2-
PhO
OPh
Fe
S
R
S
S
Fe
PhO
OPh
S
Fe
S
M
S
R
M
S
Fe
S
Fe
S
S
R
S
Fe
PhO
OPh
3-

Figure 35

to 0.1 mm/s increase in the ^{57}Fe Mossbauer isomer shift, δ; v) approximately 100-200 mV negative shifts in corresponding electrochemical reduction potentials. Finally, these trends suggest that substitution of a cysteinyl thiolate ligand to an Fe-S center by a tyrosyl phenoxide in a protein, or to iron atoms within FeMo-co in the MoFe protein of nitrogenase, would provide a means to a reactive coordination site without significantly altering the redox potentials of the cluster.

REFERENCES

REFERENCES

1. Ibers, J. A. and Holm, R. H. Science 1980, 209, 223.

2. Holm, R. H. and Ibers, J. A. in Iron-Sulfur Proteins, Vol. 3, W. Lovenberg, Ed., Academic Press, New York, NY, 1977. Ch. 7.

3. a) Averill, B. A. and Orme-Johnson, W. H., in Metal Ions in Biological Systems, Vol. 7, "Iron in Model and Natural Compounds," H. Sigel, Ed., Marcel Decker, Inc., New York, NY, 1978, Ch. 4. b) Beinert, H; Emptage, M. H.; Dryer, J.-L.; Scott, R. A.; Hahn, J. E.; Hodgson, K. O.; Thomson, A. J. Proc. Natl. Acad. Sci. U.S.A. 1983, 80, 393.

4. Holm, R. H. Acc. Chem. Res. 1977, 10, 427.

5. Berg, J. M. and Holm, R. H. in Iron-Sulfur Proteins, T. G. Spiro, Ed., Wiley-Interscience, New York, NY, 1982, Ch. 1.

6. Carnahan, J. E.; Mortenson, L. E.; Mower, H. F.; Castle, J. E. Biochim. Biophys. Acta 1960, 44, 520.

7. Averill, B. A. Structure and Bonding 1983, 53, 59.

8. Orme-Johnson, W. H.; Davis, L. C. in Iron-Sulfur Proteins, Vol. 3, W. Lovenberg, ed., Academic Press, New York, NY, 1977. Ch.

9. Hageman, R. V.; Burris, R. H. Proc. Natl. Acad. Sci. USA 1978, 75, 2699.

10. Orme-Johnson, W. H.; Davis, L. C.; Henzl, M. T.; Averill, B. A.; Orme-Johnson, N. R.; Munck. E.; Zimmerman, R. in Recent Developments in Nitrogen Fixation Newton, W. P.; Postgate, J. R.; Rodrigue, N.; eds.; Academic Press, New York, NY, 1977, pp. 131-178.

11. Tso, M.-Y.W.; Burris, R. H. Biochim. Biophys. Acta. 1973, 309, 263.

12. Hageman, R. V.; Orme-Johnson, W. H.; Burris, R. H. Biochemistry 1980, 19, 2333.

13. Zimmerman, R.; Munck, E.; Brill, W. J.; Shah, V. K.; Henzl, M. T.; Rawlings, J.; Orme-Johnson, W. H. Biochim. Biophys. Acta 1978, 537, 185.

14. Huynh, B. H.; Henzl, M. T.; Christner, J. A.; Zimmerman, R.; Orme-Johnson, W. H.; Munck, E. Biochim. Biophys. Acta 1980, 623, 124.

ac

15. Orme-Johnson, W. H.; Lindahl, P.; Meade, J.; Warren, W.; Nelson, M.; Groh, S.; Orme-Johnson, N. R.; Munck, E.; Huynh, B. H.; Emptage, M.; Rawlings, J.; Smith, J.; Roberts, J.; Hoffmann, B.; Mims, W. B. In Current Perspectives in Nitrogen Fixation, Gibson, A. H.; Newton, W. E., Eds.; Australian Academy of Science, Canberra: 1981, pp. 79-83.

16. Nelson, M. J.; Lindahl, P. A.; Orme-Johnson, W. H. In Advances in Inorganic Biochemistry, Eichorn, G.; Marzilli, L., Ed.; Elsevier: New York, 1982, in press.

17. Wong, G. B.; Kurtz, D. M., Jr.; Holm, R. H.; Mortenson, L. E.; Upchurch, R. G. J. Am. Chem. Soc. 1979, 101, 3078.

18. Kurtz, D. M., Jr.; McMillan, R. S.; Burgess, B. K.; Mortenson, L. E.; Holm, R. H. Proc. Natl. Acad. Sci. USA 1979, 76, 4986.

19. Orme-Johnson, W. H.; Davis, L. C.; Henzl, M. T.; Averill, B. A.; Orme-Johnson, N. R.; Munck, E.; Zimmerman, R. In Recent Developments in Nitrogen Fixation, Newton, W.; Postgate, J. R.; Rodriguez-Barrueco, C., Eds.; Academic Press; New York, 1977, pp. 131-178.

20. Rawlings, J.; Shah, V. K.; Chisnell, J. R.; Brill, W. J.; Zimmerman, R.; Munck, E.; Orme-Johnson, W. H. J. Biol. Chem. 1978, 253, 1001.

21. Munck, E.; Rhodes, H.; Orme-Johnson, W. H.; Davis, L. C.; Brill, W. J.; Shah, V. K. Biochim. Biophys. Acta 1975, 400, 32.

22. Smith, B. E.; Lang, G. Biochem. J. 1974, 137, 169.

23. Smith, B. E.; O'Donnel, M. J.; Lang, G.; Spartalian, K. Biochem. J. 1980, 191, 449.

24. Johnson, M. K.; Thomson, A. J.; Robinson, A. E.; Smith, B. E. Biochim. Biophys. Acta 1981, 671, 61.

25. Smith, J. P.; Emptage, M. H.; Orme-Johnson, W. H. J. Biol. Chem. 1982, 257, 2310.

26. Stephens, P. J.; McKenna, C. E.; Smith, B. E.; Nguyen, H. T.; McKenna, M.-C.; Thomson, A. J.; Devlin, F.; Jones, J. B. Proc. Natl. Acad. Sci. U.S.A. 1979, 76, 2585.

27. Cotton, F. A.; Wilkinson, G. in Advanced Inorganic Chemistry: A Comprehensive Text, John Wiley and Sons, New York, 1980, pp. 759.

28. Johnson, R. W.; Holm, R. H. J. Am. Chem. Soc. 1978, 100, 5338.

29. Kanatzidis, M. G.; Ryan, M.; Coucouvanis, D.; Simpoulos, A.; Kostikas, A. Inorg. Chem. 1983, 22, 1979.

30. Johnson, R. E.; Papaefthymiou, G. C.; Frankel, R. B.; Holm, R. H. J. Am. Chem. Soc. 1983, 105, 7280.

31. Shah, V. K.; Brill, W. J. Proc. Natl. Acad. Sci. USA 1977, 74, 3249.

32. a) Burgess, B. K.; Jacobs, D. R.; Stiefel, E. I. Biochim. Biophys. Acta 1980, 614, 196. b) Nelson, M. J.; Levy, M. A.; Orme-Johnson, W. H. Proc. Natl. Acad. Sci. USA 1983, 80, 147.

33. Burgess, B. K. In Nitrogen Fixation: Chemical/Bio-Chemical/Genetics Interface, Muller, A.; Newton, W. E., Ed.; Plenum: New York, 1982.

34. Shah, V. K.; Brill, W. J. Proc. Natl. Acad. Sci. USA 1981, 78, 3438.

35. Palmer, G.; Multani, J. S.; Cretney, W. C.; Zumft, W. G.; Mortenson, L. E. Arch. Biochem. Biophys. 1972, 153, 325.

36. Huynh, B. H.; Munck. E.; Orme-Johnson, W. H. Biochim. Biophys. Acta 1979, 527, 192.

37. a) Hofmann, B. M.; Venters, R. A.; Roberts, J. E.; Nelson, M.; Orme-Johnson, W. H. J. Am. Chem. Soc. 1982, 104, 4711. b) Hoffman, B. M.; Roberts, J. E.; Orme-Johnson, W. H. J. Am. Chem. Soc. 1982, 104, 861.

38. Cramer, S. P.; Hodgson, K. O.; Gillum, W. O.; Mortenson, L. E. J. Am. Chem. Soc. 1978, 100, 3398.

39. Cramer, S. P. Gillum, W. O.; Hodgson, K. O.; Mortenson, L. E.; Stiefel, E. I.; Chisnell, J. R.; Brill, W. J.; Shah, V. K. J. Am. Chem. Soc. 1978, 100, 3814.

40. Wolff, T. E.; Berg, J. M.; Warrick, C.; Hodgson, K. O.; Holm, R. H. J. Am. Chem. Soc. 1978, 100, 4630.

41. Teo, B.-K.; Antonio, M. R.; Averill, B. A. J. Am. Chem. Soc. 1983, 105, 3751.

42. Antonio, M. R.; Teo, B. K.; Cleland, W. E.; Averill, B. A. J. Am. Chem. Soc. 1983, 105, 3477.

43. Teo, B.-K.; Antonio, M. R.; Tiekelmann, R. H.; Silvis, H. C.; Averill, B. A. J. Am. Chem. Soc. 1982, 104, 6126.

44. Antonio, M. R.; Teo, B.-K.; Orme-Johnson, W. H.; Nelson, M. J.; Groh, S. E.; Lindahl, P. A.; Kauzlarich, S. M.; Averill, B. A. J. Am. Chem. Soc. 1982, 104, 4703.

45. Shah, V. K.; Chisnell, J. R.; Brill, W. J. Biochim. Biophys. Res. Commun. 1978, 81, 232.

46. Newton, W. E. in Kirk-Othmer: Encyclopedia of Chemical Technology, Vol. 15, 3rd Edn.; John Wiley and Sons: New York, 1981, pp. 942-968.

47. Mortenson, L. E.; Thornley, R. N. F. Ann. Rev. Biochem. 1979, 48, 387.

48. Holm, R. H. Chem. Soc. Rev. 1981, 10, 455.

49. Wolff, T. E.; Berg, J. M.; Hodgson, K. O.; Frankel, R. B.; Holm, R. H. J. Am. Chem. Soc. 1979, 101, 4140.

50. Wolff, T. E.; Berg, J. M.; Power, P. P.; Hodgson, K. O.; Holm, R. H.; Frankel, R. B. J. Am. Chem. Soc. 1979, 101, 5454.

51. Wolff, T. E.; Power, P. P.; Frankel, R. B.; Holm, R. H. J. Am. Chem. Soc. 1980, 102, 4694.

52. Wolff, T. E.; Berg, J. M.; Power, P. P.; Hodgson, K. O.; Holm, R. H. Inorg. Chem. 1980, 19, 430.

53. Christou, G.; Garner, C. D.; Mabbs, F. E. Inorg. Chim. Acta 1978, 28, L189.

54. Christou, G.; Garner, C. D.; Mabbs, F. E.; King, T. J. J. Chem. Soc. Chem. Commun. 1978, 740.

55. Acott, S. R.; Christou, G.; Garner, C. D.; King, T.J.; Mabbs, F. E.; Miller, R. M. Inorg. Chim. Acta 1979, 35, L337.

56. Christou, G.; Garner, C. D.; Miller, R. M. J. Inorg. Biochem. 1979, 11, 349.

57. Christou, G.; Garner, C. D.; Mabbs, F. E.; Drew, M. G. B. J. Chem. Soc., Chem. Commun. 1979, 91.

58. Christou, G.; Garner, C. D. J. Chem. Soc., Dalton Trans. 1980, 2354.

59. Christou, G.; Garner, C. D.; Miller, R. M.; Johnson, C. E.; Rush, J. D. J. Chem. Soc., Dalton Trans. 1980, 2363.

60. Christou, G.; Mascharak, P. K.; Armstrong, W. H.; Papaefthymiou, G. C.; Frankel, R. B.; Holm, R. H. J. Am. Chem. Soc. 1982, 104, 2820.

62. Wolff, T. E.; Berg, J. M.; Holm, R. H. Inorg. Chem. 1981, 20, 174.

63. Armstrong, W. H.; Holm, R. H. J. Am. Chem. Soc. 1981, 103, 6246.

64. Palermo, R. E.; Power, P. P.; Holm, R. H. Inorg. Chem. 1981, 20, 173.

65. Christou, G.; Garner, C. D. J. Chem. Soc. Chem. Commun. 1983, 613.

66. Christou, G.; Collison, D.; Garner, C. D.; Mabbs, F. E.; Petrouleas, V. Inorg. Nucl. Chem. Lett. 1981, 17, 137.

67. Armstrong, W. H.; Mascharak, P. K.; Holm, R. H. J. Am. Chem. Soc. 1982, 104, 4373.

68. Armstrong, W. H.; Mascharak, P. K.; Holm, R. H. Inorg. Chem. 1982, 21, 1699.

69. Mascharak, P. K.; Armstrong, W. H.; Mizobe, Y.; Holm, R. H. J. Am. Chem. Soc. 1983, 105, 475.

70. Palermo, R. E.; Holm, R. H. J. Am. Chem. Soc. 1983, 105, 4310.

71. Coucouvanis, D.; Simhon, E. D.; Swenson, D.; Baenziger, N. C. J. Chem. Soc., Chem. Commun. 1979, 361.

72. Tieckelmann, R. H.; Silvis, H. C.; Kent, T. A.; Huynh, B. H.; Waszczak, J. V.; Teo, B.-K.; Averill, B. A. J. Am. Chem. Soc. 1980, 102, 5550.

73. Coucouvanis, D.; Baenziger, N. C.; Simhon, E. D.; Stremple, P.; Swenson, D.; Simopoulos, A.; Kostikas, A.; Petrouleas, V.; Papaefthymiou, V. J. Am. Chem. Soc. 1980, 102, 1732.

74. Muller, A.; Tolle, H.-G.; Bogge, H. Z. Anorg. Allg. Chem. 1980, 471, 115.

75. Tieckelmann, R. H.; Averill, B. A. Inorg. Chim. Acta 1980, 46, L35.

76. Muller, A.; Sarkar, S.; Dommrose, A.-M.; Filgueira, R. Z. Naturforsch., Teil., B. 1980, 35, 1592.

77. McDonald, J. W.; Friesen, G. D.; Newton, W. E. Inorg. Chim. Acta 1980, 46, L79.

78. Coucouvanis, D.; Simhon, E. D.; Baenziger, N. C. J. Am. Chem. Soc. 1980, 102, 6644.

79. Dahlstrom, P. L.; Kumar, S.; Zubieta, J. J. Chem. Soc., Chem. Commun. 1981, 411.

80. Coucouvanis, D.; Simhon, E. D.; Stremple, P.; Baenziger, N. C. Inorg. Chim. Acta 1981, 53, L135.

81. Silvis, H. C.; Averill, B. A. Inorg. Chim. Acta 1981, 54, L57.

82. Coucouvanis, D.; Stremple, P.; Simhon, E. D.; Swenson, D.; Baenziger, N. C.; Draganjac, M.; Chan, L. T.; Simopoulos, A.; Papaefthymiou, V. Inorg. Chem. 1983, 22, 293.

83. Coucouvanis, D. Acc. Chem. Res. 1981, 14, 201.

84. Burgess, B. K.; Stiefel, E. I.; Newton, W. E. J. Biol. Chem. 1980, 255, 353.

85. Burgess, B. K.; Yang, S.-S.; You, C.-B.; Li, J.-G.; Friesen, G. D.; Pan, W.-H.; Stiefel, E. I.; Newton, W. E. in Current Perspectives in Nitrogen Fixation, Gibson, A. H.; Newton, W. E., Ed.; Australian Academy of Science: Canberra, 1981; pp. 71-74.

86. Newton, W. E.; Burgess, B. K.; Stiefel, E. I. in Molybdenum Chemistry of Biological Significance, Newton, W. E.; Otsuka, S., Ed.; Plenum Press: New York, 1980; pp. 191.

87. Ghosh, D.; Furey, W., Jr.; O'Donnell, S.; Stout, C. D. J. Biol. Chem. 1981, 256, 4185.

88. Antonio, M. R.; Averill, B. A.; Moura, I.; Moura, J. J. G.; Orme-Johnson, W. H.; Teo, B.-K.; Xavier, A. V. J. Biol. Chem. 1982, 257, 6646.

89. Koch, S. A.; Millar, M. J. Am. Chem. Soc. 1982, 104, 5255.

90. a) Cleland, W. E.; Averill, B. A. Inorg. Chim. Acta 1981, 56, L9 b) Cleland, W. E.; Holtman, D. A.; Sabat, M.; Ibers, J. A.; DeFotis, G. C.; Averill, B. A. J. Am. Chem. Soc. 1983, 105, 6021.

91. Averill, B. A.; Herskovitz, T.; Holm, R. H.; Ibers, J. A. J. Am. Chem. Soc. 1973, 95, 3523.

92. Christou, G.; Garner, C. D. J. Chem. Soc., Dalton Trans. 1979, 1093.

93. Wong, G. B.; Bobrick, M. A.; Holm, R. H. Inorg. Chem. 1978, 17, 1093.

94. Holm, R. H.; Phillips, W. D.; Averill, B. A.; Mayerle, J. J.; Herskovitz, T. J. Am. Chem. Soc. 1974, 96, 2109.

95. DePamphilis, B. V.; Averill, B. A.; Herskovitz, T.; Que, L., Jr.; Holm, R. H. J. Am. Chem. Soc. 1974, 96, 4159.

96. Reynolds, J. G.; Holm, R. H. Inorg. Chem. 1980, 19, 3257.

97. Mayerle, J. J.; Denmark, S. E.; DePamphilis, B. V.; Ibers, J. A.; Holm, R. H. J. Am. Chem. Soc. 1975, 97, 1032.

98. Ryan, J. L. Inorg. Synth., Vol. XV, pp 231.

99. Kruss, G. Justus Liebigs Ann. Chem. 1884, 225, 6.

100. Emptage, M. H.; Zimmerman, R.; Que, Jr., L.; Munck, E. Hamilton, W. D.; Orme-Johnson, W. H. Biochim. Biophys. Acta 1977, 495, 12.

101. Que, L., Jr.; Bobrik, M. A.; Ibers, J. A.; Holm, R. H. J. Am. Chem. Soc. 1974, 96, 4168.

102. Bobrik, M. A.; Hodgson, K. O.; Holm, R. H. Inorg. Chem. 1977, 16, 1851.

103. Gerloch, M.; Mabbs, F. E. J. Chem. Soc. A. 1967, 1598.

104. a) Coggon, P.; McPhail, A. T.; Mabbs, F. E.; McLachlan, V. N. J. Chem. Soc. A. 1971, 1014. b) Gerloch, M.; McKenzie, E. D.; Towl, A. D. C. J. Chem. Soc. A. 1969, 2580.

105. a) Anderson, B. F.; Buckingham, D. A.; Robertson, G. R.; Webb, J. Nature (London) 1976, 262, 7222. b) Raymond, K. N.; Isied, S. S.; Brown, L. D.; Fronczek, F. F.; Nibert, J. H. J. Am. Chem. Soc. 1976, 98, 1767.

106. Beattie, J. K.; Moore, C. J. Inorg. Chem. 1982, 21, 1292.

107. Heistand, R. H.; Roe, A. L.; Que, L., Jr. Inorg. Chem. 1982, 21, 676.

108. Geurtz, P. J. M.; Gosselink, J. W.; Van Der Avoird, A.; Baerends, E. J.; Snijders, J. G. Chem. Phys. 1980, 46, 133.

109. Aizman, A.; Case, D. A. J. Am. Chem. Soc. 104, 3269.

110. Yang, C. Y.; Johnson, K. H.; Holm, R. H.; Norman, J. G. J. Am. Chem. Soc. 1975, 97, 6596.

111. Thomson, A. J. J. Chem. Soc. Dalton Trans. 1981, 1180.

112. Figis, B. N.; Lewis, J., In Technique of Inorganic Chemistry, Vol. IV, Jonassen, H. B. and Weissberger, Ed., Interscience, New York, NY, 1965, pp. 137-248.

113. Laskowski, E. J.; Frankel, R. B.; Gillum, W. O.; Papaefthymiou, G. C.; Renaud, J.; Ibers, James A.; Holm, R. H. J. Am. Chem. Soc. 1978, 100, 5322.

114. Herskowitz, T.; Averill, B. A.; Holm, R. H.; Ibers, J. A.; Phillips, W. D.; Weiher, J. F.; Proc Natl. Acad. Sci. USA 1972, 69, 2437.

115. Hatfield, W. E.; In "Theory and Applications of Molecular Paramagnetism", Boudreux, E. A. and Mulay, L. N., Eds.; Wiley-Interscience: New York, NY, 1976, Chapter 7.

116. Antanaitis, B. C.; Moss, T. H. Biochim. Biophys. Acta 1975, 405, 262.

117. Papaefthymiou, G. C.; Laskowski, E. J.; Frosta-Pessoa, S.; Frankel, R. B.; Holm, R. H. Inorg. Chem. 1982, 21, 1723.

118. Horrocks, Jr., W. D.; In "NMR of Paramagnetic Molecules: Principles and Applications", LaMar, G. N.; Horrocks, Jr., W. D.; Holm, R. H., Ed.; Academic Press: New York, 1973; Chapter 4.

119. Frankel, R. B.; Averill, B. A.; Holm, F. H. J. Phys. (Orsay, Fr.) 1974, 35, C6-107.

120. Van Tamelen, E. E.; Gladysz, J. A.; Brulet, C. R.; J. Am. Chem. Soc. 1974, 96, 3020.

121. Johnson, R. W.; Holm, R. H. J. Am. Chem. Soc. 1978, 100, 5338.

122. Dukes, G. R.; Holm, R. H. J. Am. Chem. Soc. 1975, 97, 528.

123. Que, L., Jr.; Anglin, J. R.; Bobrick, M. A.; Davison, A.; Holm, R. H. J. Am. Chem. Soc. 1974, 96, 6042.

124. Hill, C. L.; Renaud, J.; Holm, R. H.; Mortenson, L. E. J. Am. Chem. Soc. 1977, 99, 2549.

125. Averill, B. A.; Bale, J. R.; Orme-Johnson, W. H. J. Am. Chem. Soc. 1978, 100, 3034.

126. Coucouvanis, D.; Swenson, D.; Stremple, P.; Baenziger, N. C. J. Am. Chem. Soc. 1979, 101, 3392.

127. Ackermann, G.; Hesse, D. Z. Anorg. Allg. Chem. 1970, 375, 77.

128. Gillum, W. O.; Frankel, R. B.; Foner, S.; Holm, R. H. Inorg. Chem. 1976, 15, 1095.

129. Laskowski, E. J.; Reynolds, J. G.; Frankel, R. B.; Foner, S.; Papaefthymiou, G. C.; Holm, R. H. J. Am. Chem. Soc. 1979, 101, 6562.

130. Que, L., Jr.; Coord. Chem. Revs. 1983, 50, 73.

131. Aisen, P.; Listowsky, I. Ann. Rev. Biochem. 1980, 49, 357.

132. Davis, J. C.; Averill, B. A. Proc. Natl. Acad. Sci. USA, 1982, 79, 4623.

133. Antanaitis, B. C.; Strekas, T.; Aisen, P. J. Biol. Chem., 1982, 257, 3766.

134. Que, L., Jr.; Epstein, R. M. Biochemistry 1981, 20, 2545.

135. Hawkins, C. J.; Parry, D. L.; Wood, B. J. Inorg. Chim. Acta 1983, 78, L29.

136. Palermo, R. E.; Power, P. P.; Holm, R. H. Inorg. Chem. 1982, 21, 173.

137. Reynolds, J. G.; Laskowski, E. J.; Holm, R. H. J. Am. Chem. Soc. 1978, 100, 5315.

138. Kanatzidis, M. G.; Dunham, W. R.; Hagen, W. R.; Coucouvanis, D.; J. Chem. Soc. Chem. Commum. 1984, 356.

139. Saak, W.; Henkel, G.; Pohl, S. Angew. Chem. Int. Ed. Eng. 1984, 23.

140. Fee, J. A.; Findling, K. L.; Yoshida, T.; Hille, R.; Tarr, G. E.; Hearshen, D. O.; Dunham, W. R.; Day, E. P.; Kent, T. A.; Münck, E. J. Biol. Chem. 1984, 259, 124.